RSC Advances

ROYAL SOCIETY OF CHEMISTRY

www.rsc.org/advances

Noble metal ions in CeO_2 and TiO_2: Synthesis, structure and catalytic properties

Parthasarathi Bera[a,*] and M. S. Hegde[b]

[a]*Surface Engineering Division, CSIR–National Aerospace Laboratories, Bangalore 560017, India*

[b]*Solid State and Structural Chemistry Unit, Indian Institute of Science, Bangalore 560012, India*

Abstract

In past four decades, CeO_2 has been recognized as an attractive material in the area of auto exhaust catalysis because of its unique redox properties. In presence of CeO_2, catalytic activity of noble metals supported on Al_2O_3 gets enhanced due to higher dispersion of noble metals in their ionic form. In last several years, we have been exploring an entirely new approach of dispersing noble metal ions on CeO_2 and TiO_2 matrices for redox catalysis. In this article, dispersing of noble metal ions by solution combustion as well as other methods over CeO_2 and TiO_2 resulting mainly in $Ce_{1-x}M_xO_{2-\delta}$, $Ce_{1-x-y}Ti_xM_yO_{2-\delta}$, $Ce_{1-x-y}Sn_xM_yO_{2-\delta}$, $Ce_{1-x-y}Fe_xM_yO_{2-\delta}$, $Ce_{1-x-y}Zr_xM_yO_{2-\delta}$ and $Ti_{1-x}M_xO_{2-\delta}$ (M = Pd, Pt, Rh and Ru) catalysts, structure of these materials, their catalytic properties toward different types of catalysis, structure–property relation and mechanism of catalytic reactions are reviewed. In these catalysts, noble metal ions are incorporated into substrate matrix to a certain limit in a solid solution form. Lower valent noble metal ion substitution in CeO_2 and TiO_2 creates noble metal ionic sites and oxide ion vacancies that act as adsorption sites for redox catalysis. It has been demonstrated that these new generation noble metal ionic catalysts (NMIC) have been found to be catalytically more active than conventional respective nano crystalline noble metal catalysts dispersed on oxide supports.

---

*Corresponding author; Tel: +91–80–25086359, Fax: +91–80–25210113

E mails: partho@nal.res.in (P. Bera)

1. Introduction

Catalysis has widespread applications from environment clean up to manufacturing various chemicals, energy production, food processing and biological processes. Production of most of the useful commercial bulk and fine chemicals involves catalysis.[1–7] The science and technology of heterogeneous catalysis is one of the rapidly moving frontiers in the area of catalysis as well as chemical sciences. Synthesis of ammonia, sulfuric acid and nitric acid, production of hydrogen, controlling of exhaust emission, ammoxidation, methanol synthesis and many other important reactions of present days are associated with heterogeneous catalysis. Metals, metal clusters, alloys, oxides, sulfides, solid acids and bases have been used as catalysts for several catalytic reactions since early days of heterogeneous catalysis.[1] Among these catalysts, supported and unsupported metals have been regarded as efficient catalysts for their usefulness in different catalytic reactions. Extensive research and investigations like metal–support interaction, structure–catalytic property relation, metal dispersion, redispersion, synergistic effect and other relevant aspects have been carried out over these catalysts since decades.

Since early days of catalysis it has been established that metals are in general, active sites for adsorption of reactant molecules and subsequent catalysis and hence, most catalysts contain nanocrystalline metals especially noble metals dispersed on supports like Al_2O_3 or SiO_2.[1,8,9] However, in these catalysts, noble metal atoms present on the surfaces of the metal nanoparticles in their zero valent state serve as active sites for both oxidizing and reducing molecules. But, only 1/4 or 1/5 of the total number of noble metals are utilized for adsorption and subsequent catalytic conversion in 4–6 nm metal

particles. For example, if 5 nm Pt particle is considered, then total number of Pt atoms in a 5 nm cubic Pt metal crystal is 8365 taking four atoms per unit cell of Pt (fcc) metal. Again, total metal atoms on 6 surfaces of 5 nm Pt metal cube are 1962 with two atoms per unit cell surface. Pt metal particles are anchored on a solid substrate surface. Therefore, five faces of the Pt metal crystal with 1635 surface atoms are exposed. This indicates that 1/5th of total number of Pt atoms are available for the adsorption and catalysis when reactant molecules are exposed on the catalyst surface and 4/5th number of atoms inside the metal nanocrystal are not available for adsorption or they are wasted. If all Pt atoms are utilized, then reaction rate would be higher by 5 times and thus, catalytic activity increases with increase in metal dispersion. However, atomic dispersion of Pt and other noble metals on traditional supports like Al_2O_3 and SiO_2 is difficult because metal atoms sinter into metal particles due to metal–metal bonding. Can there be alternate ways to utilize all the Pt atoms present in the catalyst? One possible way to keep the Pt metal atoms apart is to convert Pt atoms (Pt^0) into Pt ions (Pt^{2+}) and keep them separated by O^{2-} ions. Pt^{2+} ions cannot come closer to form Pt crystal. If Pt^{2+} ions act as adsorption centers as good as Pt atoms, in principle all the metal atoms become available for adsorption.

Auto exhaust catalysts are mainly dispersed noble metals such as Pt, Pd and Rh on oxide supports like Al_2O_3 in the form of nanocrystalline metal particles.[10] Huge increase in the dispersion of noble metals has been observed with the addition of CeO_2 to Al_2O_3 leading to increase in oxygen storage capacity (OSC) and auto exhaust catalytic activity.[10–18] Even though oxidized Pt, Pd and Rh are found on Al_2O_3/CeO_2 surface, reasons for higher dispersion of noble metals in the form of ions in presence of CeO_2

have not been understood. In early 1990s, Sayle and coworkers have demonstrated the segregation of noble metal ions such as Pd^{2+}, Pt^{2+} and Rh^{3+} at the surface of CeO_2 with oxygen vacancies by computer simulation studies.[19] Theoretically, noble metal ions can be stable in CeO_2 matrix that leads to the formation of defects on the surface. Therefore, complete dispersion of noble metals can be achieved in terms of ions within reducible oxide supports like CeO_2 and TiO_2. In this regard, entirely new generation catalysts that can be useful for multipurpose applications in different catalytic reactions have been developed in our laboratory in last 15 years. It has been found that increase in the dispersion of noble metals is possible through oxidation of noble metals into their ions which are dispersed on the reducible oxide surface simultaneously reducing the oxide support.[20–24] In other words, direct substitution of noble metal ions in reducible supports like CeO_2 and TiO_2 results in uniform solid catalysts in the form of their solid solutions. Thus, a new idea in heterogeneous catalysis has been conceptualized where dispersed metal ions act as catalytically active sites for heterogeneous catalysis. In last several years, significant works on these types of ionically dispersed catalysts have been done by other groups. Research works on supported gold catalysts by Corma and Gates groups have demonstrated that gold is mainly present in its ionic form in these catalysts. They have reviewed the significance of cationic gold in different matrices regarding several organic reactions and CO oxidation.[25,26] Flytzani-Stephanopoulos and Gates have discussed key findings of cationic noble metals as catalytic sites on solid supports.[27]

Noble metal oxides such as PtO, PtO_2, PdO and Rh_2O_3 are known and therefore, it should be possible to synthesize solid solution between CeO_2 or TiO_2 and noble metal oxides. Nobel metal loading for several catalytic reactions is only to the extent of 1–2

at.% and hence, substitution of only 1–2 at.% noble metal ion in CeO_2 is sufficient to develop a catalyst. The underlying principle of doping aliovalent metal ions into CeO_2 or TiO_2 lattice is to retain their parent structures. In this sense, new-age advanced catalysts such as $Ce_{1-x}M_xO_{2-\delta}$ (M = Pd, Pt, Rh, Cu, Ag and Au), $Ce_{1-x-y}A_xM_yO_{2-\delta}$ (A = Ti, Zr, Sn and Fe; M = Pt and Pd) and $Ti_{1-x}M_xO_{2-\delta}$ (M = Pd, Pt, Rh and Ru) retaining their parent fluorite and anatase structures have been prepared in our laboratory employing solution combustion method.[20–23] Thus, synthesis of these single phase oxides is a new concept which is the basis of metal ion catalysts. In these catalysts, noble metal ions and corresponding oxide ion vacancies are supposed to be the active sites. Since, the adsorption sites in these catalysts are noble metal ions such as Pd^{2+}, Pt^{2+}, Rh^{3+} and Ru^{4+}, we have named these materials as noble metal ionic catalysts (NMIC). In last several years, we have been studying several exhaust catalytic reactions such as NO reduction, CO and hydrocarbon oxidation, selective catalytic reduction of NO, three-way catalytic reaction, water gas shift (WGS) reaction, preferential oxidation of CO (CO–PROX), H_2 + O_2 recombination reaction, hydrogenation and Heck reaction over these noble metal ionic catalysts and it has been demonstrated that these catalysts are much more active for several catalytic reactions compared to other conventional supported metal catalysts. In this review, at first, we mainly discuss about background, synthesis and characterization of these noble metal ionic catalysts (NMIC). Then we emphasize on our detailed work related to exhaust catalysis comparing activities with the several catalysts reported in the literature. Afterwards, we write about our studies on water gas shift reaction, CO–PROX reaction, H_2 + O_2 reaction, hydrogenation, dehydrogenation, Heck reaction and unique reaction mechanism over these catalysts. Metal–support interaction and synergistic effect

for the interaction which lead to the superiority of these catalysts over conventional catalysts would also be discussed. We would also focus on our density functional theory (DFT) studies for high oxygen storage capacity (OSC) and catalytic properties of several CeO_2 and TiO_2 based materials. Finally, we conclude our review focusing with future prospects of these noble metal ionic catalysts.

2. Synthesis of noble metal ionic catalysts

2.1. Conventional preparation methods of catalysts

Dispersion of metals over suitable supports is one of the important issues for higher catalytic activities. Dispersed noble metals and transition metal ions on a particular support are the active sites for adsorption of CO, NO, hydrocarbon and oxygen. In this sense, method of catalyst preparation can influence the dispersion characteristics of metals on the supports and their catalytic behavior. The main objective of the preparation of a supported metal catalyst is to get maximum dispersion of catalytically active species over support material from its precursor at a particular concentration. The catalysts for fundamental studies are usually prepared by coprecipitation, sol-gel, deposition, impregnation, ion exchange, anchoring-grafting and spreading-wetting methods.[28,29] In general, dispersion of active components is carried out over the oxide support in a single step preparation such as coprecipitation, sol-gel processes, whereas dispersion has been done over independently prepared oxide support by impregnation, deposition, incipient wetness methods. Some of these preparation procedures are briefly described below.

(a) Coprecipitation–This involves the reaction between a solution of two or more metal salts in presence of a base such as hydroxide, alkali carbonate and bicarbonate. For

example, Ni/Al_2O_3 catalyst is prepared from $Ni(NO_3)_2$ and $AlCl_3$ in presence of $NaHCO_3$.[29]

(b) Sol-gel–This process describes the transition of a system from liquid, mostly colloidal into a solid or gel phase. This is based on the polymerization of molecular precursors such as metal alkoxides. Hydrolysis and condensation of these alkoxides lead to the formation of oxopolymers which are then transformed into a homogeneous oxide network. Pd/SiO_2, Pt/SiO_2 and Pd/Al_2O_3 catalysts are prepared by this method.[30]

(c) Deposition–It describes the addition of catalytically active component to a separately produced support. It is of two types.

(i) Deposition-precipitation–A precipitating agent is added to a suspension of the support in an active metal salt solution. Accordingly, active metal species is adsorbed onto the surface of the support. Ni/Al_2O_3 catalyst is prepared by the slow addition of NaOH to a suspension of Al_2O_3 in $NiCl_2$ solution. This process is used to synthesize nickel supported on silica, alumina, magnesia, titania, thoria, ceria, zinc oxide and chromium oxide.[31] This process is also used for the preparation of $Pd(OH)_2/C$, $Rh(OH)_3/C$ and $Ru(OH)_3/C$.

(ii) Deposition-reduction–Addition of a reducing agent to a suspension of the support in a solution of the active metal salt provides supported reduced metal catalysts. Pd/C and Pt/C can be prepared by this method. Generally, hydrogen, formaldehyde, hydrazine and borohydride are used as the reducing agents.[29]

(d) Impregnation–It consists of introducing a precursor solution into the pore space of the support that is filled with the same solvent as the precursor solution. Here, the concentration gradient is the driving force. It is also called wet or diffusional impregnation. Rh/TiO_2, Rh/Al_2O_3, Pt/C and Ru/MgO are prepared by this method.[29]

(e) Incipient wetness–This is one kind of impregnation process. In this process, precursor solution is introduced into contact with the previously dried support. It is also called dry or pore volume impregnation. It is an exothermic process and it depends on capillary pressure developed in the pores and rate of impregnation process. Ni/Al_2O_3, Pt/SiO_2, Pt/Al_2O_3, Ni/SiO_2, Ni/C, Ru/SiO_2, Rh/SiO_2 and Ru/C are prepared by this method.[29]

(f) Ion exchange–In this method, an ion in an electrostatic interaction with the surface of a support is replaced by another ionic species. For examples, zeolites, clays, silicates are cation exchangers, whereas hydrotalcites are anion exchangers. The overall charge of a zeolite is negative that is distributed over oxygen atom and this charge is neutralized by various cations like Na^+, K^+.[29]

(g) Microemulsion–It is a physical mixture of two immiscible liquid along with a surfactant. Reverse micelles formed can act as micro reactors. These reactors are utilized for synthesis of nanoparticles. Nanocrystalline CeO_2 was prepared by water-in-oil micro-emulsion methods.[32] CeO_2–ZrO_2 ultrafine particles were also prepared by the micro-emulsion method.[33]

(h) Mechanical milling–It is a solid to solid synthetic method. Mechanical milling has been used extensively to synthesize CeO_2–MO_x (M = Zr, Hf, Tb, Cu and Mn) mixed oxide catalysts.[34,35] The feature of this method is to obtain powder small crystallite size of a few nanometers with high concentration of lattice defects. Mechanical alloying has also been applied to prepare mixed oxide containing CeO_2 to enhance the catalysis. High-energy mechanical alloying of pure CeO_2 and ZrO_2 at room temperature results in the formation of a single phase fluorite structured solid solution of $Ce_{1-x}Zr_xO_2$ in all the examined composition ranges.

Generally, most of the above conventional preparation methods are quite involved and require long processing time. The steps of post preparation include washing, drying, H_2 reduction and removal of Cl^- ions by heating in steam.

2.2. Solution combustion method

In last several years, there has been a trend of novel chemical routes of synthesis which leads to ultra-fine and high surface area catalysts for heterogeneous catalysis. The solution combustion method has been found to be unique for obtaining nanocrystalline oxide materials.[36,37] Generally, combustion is a chemical reaction that is accompanied by heat and light. Many exothermic non-catalytic, solid-solid or solid-gas reactions liberate enough heat so that they can self-propagate after being ignited. The reactions, ignited locally by an external energy source with short term service, may propagate throughout the sample at a certain rate and occur in a narrow zone which separates the starting substances and reactions. In the literature, a variety of names have been given for redox reactions employed for the synthesis of different materials. Some of the fashionable names are furnaceless or fire synthesis, self-propagating chemical decomposition (SCD), self-propagating high temperature synthesis (SHS) and combustion method. Merzhanov has introduced the process of SHS where he has employed metals and organic fuels to produce oxides, carbides and sulfides.[38] Patil and coworkers have developed solution combustion method involving metal salts, mainly nitrates and organic fuels.[39,40] Metal salts are easily available and therefore, this method provides a better alternative for the synthesis of variety of complex oxides. Thus, solution combustion method becomes attractive to prepare high surface area oxides.

The solution combustion method involves rapid heating at a particular temperature of an aqueous redox mixture containing stoichiometric amounts of corresponding metal salts and hydrazine based fuels and the product is formed within 5 min. Redox compounds or mixtures containing hydrazide groups have been found useful for the solution combustion synthesis of oxide materials. An ideal fuel should be water soluble and have low ignition temperature (< 500 ^{o}C). It should be compatible with transition metal nitrate so that the combustion can be controlled, smooth and does not lead to explosion. The merits of solution combustion technique are: (a) being a solution process, it has all the advantages of wet chemical process such as control of stoichiometry, doping of desired amount of impurity ions and forming nano size particles (b) low temperature initiated process, (c) highly exothermic due to redox reaction, (d) self propagating, (e) transient high temperature, (f) production of huge amount of gases, (g) simple, fast and economical and (h) formation of high surface area, voluminous and homogeneous product. Using this method a variety of oxide materials such as α-Al_2O_3, ZnO, Y_2O_3, CeO_2, γ-Fe_2O_3, Cr_2O_3, $MgFe_2O_4$, $MnFe_2O_4$, $CoFe_2O_4$, $PbTiO_3$, $PbZrO_3$ and $BaFe_{12}O_{19}$ have been prepared. The solution combustion method not only yields nanosize TiO_2, ZrO_2 and hexaferrites but it also yields metastable phases like γ-Fe_2O_3, t-ZrO_2 and anatase TiO_2. Several supported, unsupported and doped oxide catalysts have been synthesized by this method. In a recent review, González-Cortés and Imbert have discussed current approaches and future possibilities for developing advanced solid catalysts from solution combustion synthesis.[41] Fig. 1 shows a typical sequence of the formation of a catalyst by solution combustion process.

Substitution of noble metal ions in CeO_2 achieved for the first time by solution combustion method was an accidental discovery.[20] When an aqueous solution containing stoichiometric amounts of $Al(NO_3)_3$, H_2PtCl_6 and urea (CON_2H_4) is heated rapidly at 500 ^oC, the solution boils, froths and burns with flame temperature of 1500 ^oC yielding nano size Pt metal particles dispersed on α-Al_2O_3.[42] In contrast, Pt metal particles are not formed when the similar attempt has been made to disperse 1–2 at.% Pt metal on CeO_2 by the combustion of ceric ammonium nitrate [$(NH_4)_2Ce(NO_3)_6$], chloroplatinic acid (H_2PtCl_6) and oxalyl dihydrazide ($C_2H_6N_4O_2$, ODH) heated at 350 ^oC. Instead of nano size Pt metal particles dispersed on CeO_2, 25–30 nm $Ce_{1-x}Pt_xO_{2-\delta}$ nanocrystallites have been formed where Pt has been observed to be present in +2 and +4 oxidation states. A typical reaction for the preparation of $Ce_{1-x}Pt_xO_{2-x}$ catalyst is given below:

$$5(1-x)\ (NH_4)_2Ce(NO_3)_6 + 5x\ H_2PtCl_6 + 12(1-x)\ C_2H_6N_4O_2 \rightarrow$$

$$5\ Ce_{1-x}Pt_xO_{2-x} + 24(1-x)\ CO_2 + 44(1-x)\ N_2 + (56-66x)\ H_2O + 10x\ HCl.$$

Similarly, Pd, Rh, Ag and Au substituted $Ce_{1-x}M_xO_{2-\delta}$ catalysts have been prepared by this method using $PdCl_2$, $RhCl_3$, $AgNO_3$ and $HAuCl_4$ as respective metal precursors.[20,43–46] $Ce_{1-x-y}Ti_xM_yO_{2-\delta}$ (M = Pt and Pd), $Ce_{1-x-y}Sn_xPd_yO_{2-\delta}$, $Ce_{1-x-y}Fe_xPd_yO_{2-\delta}$, $Ce_{1-x-y}Zr_xPd_yO_{2-\delta}$ and $Ce_{1-x-y}Hf_xPd_yO_{2-\delta}$ catalysts have also been prepared with the combustion mixture of $(NH_4)_2Ce(NO_3)_6$, $TiO(NO_3)_2$ or SnC_2O_4 or $Fe(NO_3)_3$ or $ZrO(NO_3)_3$ or $Hf(NO_3)_4$, H_2PtCl_6, $PdCl_2$ and $C_2H_5NO_2$.[47–52]

Combustion of $TiO(NO_3)_2$, noble metal salts and glycine ($C_2H_5NO_2$) fuel has been employed for the preparation of noble metal ion doped TiO_2 catalysts in the form of $Ti_{1-x}M_xO_{2-x}$ (M = Pd, Pt, Rh and Rh) solid solution.[53–56] A typical reaction for the preparation of $Ti_{1-x}Pd_xO_{2-x}$ catalyst is given below:

$$9(1-x)\ TiO(NO_3)_2 + 10(1-x)\ C_2H_5NO_2 + 9x\ PdCl_2 \rightarrow$$

$$9\ Ti_{1-x}Pd_xO_{2-x} + 20(1-x)\ CO_2 + 14(1-x)\ N_2 + (25-34x)\ H_2O + 18\ HCl.$$

2.3. Hydrothermal method

The term 'hydrothermal' is of geological origin. Many materials including zeolites were formed in the earth crust under high temperature and high pressure. Hydrothermal method has been introduced by Barrer to synthesize zeolites.[57] Hydrothermal method utilizes water under pressure and temperature above its boiling point as a means of speeding up the reaction between solids. Under hydrothermal condition, reaction occurs at relatively low temperature (~150–200 ^{o}C) which otherwise needs much higher temperature. Since hydrothermal reaction must be carried out in a closed vessel the temperature–pressure relationship is very important. Among all these preparation methods, hydrothermal synthesis always offers an extra merit in preparing highly crystallized nanomaterials with controlled shape, size and orientation. In this method, metal salts are dissolved in water and mixed with structure directing reagents, generally, amines that form a gel. Gel is taken in a vessel called hydrothermal bomb which is a thick walled steel vessel with a hermetic seal. Inside the vessel, containers made of teflon is filled with the gel to the extent of 75%. The pressure vessel is closed and heated in an oven to 200 °C for 24 to 48 h. Nanostructural CeO_2 and TiO_2 were prepared via alkaline hydrothermal route.[58,59] Hydrothermal method is one of the most popular techniques to prepare metal doped CeO_2 materials such as $Ce_{1-x}M_xO_{2-\delta}$ (M = Ca and Sm).[60] Several $Ce_{1-x}M_xO_{2-\delta}$ (M = Zr, Ti, Pr, Y, Fe, Cr and Ru) catalysts have been prepared by hydrothermal method in our laboratory.[61–63]

2.4. Sonochemical Method

Ultrasound radiation is being used mostly for diagnosis of diseases, whereas focused ultrasound radiation has been used to burn cancer cells. The ultrasonic radiation is utilized to break the chemical bonds to produce nanoparticles. Gedanken has pioneered the sonochemical method to prepare a number of oxides nanomaterials such as CeO_2, ZnO and RVO_4 (R = La, Ce, Nd, Sm, Eu and Gd).[64–66] Ceria nanoparticles embedded in poly methyl methacrylate (PMMA) were also synthesized using sonochemical method.[67] Pt-supported TiO_2@C core-shell composites were synthesized by sonochemical route for methanol electrooxidation application.[68] This method is especially suitable to make Fe and noble metal ion substituted CeO_2 and TiO_2 catalysts. In our laboratory, $Ce_{1-x}Pt_xO_{2-\delta}$, $Ce_{1-x}Fe_xO_{2-\delta}$ and $Ce_{1-x-y}Fe_xPd_yO_{2-\delta}$ catalysts have been synthesized by sonochemical method.[69,70]

Noble as well as transition metal ions have been substituted into CeO_2 and TiO_2 matrices by solution combustion, hydrothermal and sonochemical methods successfully. Table 1 summarizes metal ions substituted CeO_2 and TiO_2 materials synthesized in our laboratory.[20,43–56,61–63,69–75]

3. Structure of $Ce_{1-x}M_xO_{2-\delta}$ and $Ti_{1-x}M_xO_{2-\delta}$ based catalysts

Several physical characterization techniques such as X-ray diffraction (XRD), transmission electron microscopy (TEM), X-ray photoelectron spectroscopy (XPS) and X-ray absorption fine structure spectroscopy (XAFS) have been employed to study the crystal structure, morphology, electronic structure, local structure and oxide ion vacancies of the $Ce_{1-x}M_xO_{2-\delta}$ and $Ti_{1-x}M_xO_{2-\delta}$ based catalysts. Main findings of these studies are discussed in the following subsections.

3.1. XRD studies

High resolution XRD data (Rigaku-2000, PANalytical X'Pert PRO) demonstrate that CeO_2 crystallizes in fluorite structure in all CeO_2 based catalysts where Ce^{4+} ions are cubic close packed with all tetrahedral sites occupied by oxygen. There are no impurity peaks related to any platinum oxides in $Ce_{0.99}Pt_{0.01}O_{2-\delta}$ catalyst. However, a small broad hump at $2\theta = 39^o$ due to Pt(111) could be observed in the diffraction pattern indicating the presence of trace amount of Pt in the catalyst. Comparing the intensity ratio of Pt(111) in $Ce_{0.99}Pt_{0.01}O_{2-\delta}$ with that in 1% Pt + CeO_2 physical mixture it has been evaluated that at least 92 at.% of the platinum taken in the preparation of $Ce_{0.99}Pt_{0.01}O_{2-\delta}$ is incorporated into CeO_2 lattice.[71,72] Total oxygen content in $Ce_{0.99}Pt_{0.01}O_{2-\delta}$ is 1.883 and that in pure CeO_2 is 1.934 and a decrease in lattice parameter is observed in $Ce_{0.99}Pt_{0.01}O_{2-\delta}$ compared to pure CeO_2. Similarly, diffraction lines are indexed to fluorite structure in $Ce_{0.99}Pd_{0.01}O_{2-\delta}$ and $Ce_{0.98}Pd_{0.02}O_{2-\delta}$ and lines corresponding to Pd or PdO are not observed in their XRD patterns. Even a slow scan in Pd(111) region ($2\theta \approx 40 \pm 5^o$) does not show any indication of Pd metal peak.[43] On the other hand, 1% Pd/CeO_2 catalyst prepared by impregnation method shows diffraction lines due to Pd metal. Lattice parameter decreases from 5.4113(2) Å in pure CeO_2 to 5.4107(3) Å in $Ce_{0.98}Pd_{0.02}O_{2-\delta}$ confirming the substitution of Pd^{2+} ions (0.84 Å) for Ce^{4+} ions (0.99 Å) in CeO_2. In $Ce_{0.99}Rh_{0.01}O_{2-\delta}$ catalyst, diffraction lines corresponding to Rh metal, Rh_2O_3 and RhO_2 are not detected. Total oxygen content in $Ce_{0.99}Rh_{0.01}O_{2-\delta}$ catalyst is 1.87, whereas it is 1.934 for pure CeO_2.[44] Therefore, a decrease in oxygen content in the catalyst compared with pure CeO_2 signifies the creation of oxide ion vacancy. Thus, detailed XRD studies demonstrate the formation of $Ce_{1-x}M_xO_{2-\delta}$ (M = Pd, Rh, Pt, Ru, Cu, Ag and Au), $Ce_{1-x-y}Ti_xM_yO_{2-\delta}$ (M = Pd and Pt), $Ce_{1-x-y}Sn_xPd_yO_{2-\delta}$, $Ce_{1-x-y}Fe_xPd_yO_{2-\delta}$ and

$Ce_{1-x-y}Zr_xPd_yO_{2-\delta}$ solid solution phases.[43–52,63,69–75] Similarly, solution combustion synthesized $Ti_{1-x}M_xO_{2-\delta}$ (M = Pd, Rh, Ru and Pt) catalysts crystallize in anatase structure.[53–56] All catalysts show broad lines in their XRD patterns. A rutile contribution has been observed to the extent of 10% only for $Ti_{1-x}Ru_xO_{2-\delta}$. No diffraction lines due to noble metals or their oxides are observed in $Ti_{1-x}M_xO_{2-\delta}$. Rietveld refinement of these catalysts reveals a slight increase in cell volume for $Ti_{1-x}Pt_xO_{2-\delta}$ due to slight increase in ionic radius of Pt, however, there is almost no change in cell volume as well as cell parameters for Pd^{2+}, Rh^{3+} and Ru^{4+} ion doped TiO_2. The particle sizes measured from Scherrer formula are in the range of 10–15 nm for the four catalysts. Typical Rietveld refined XRD patterns of $Ce_{0.99}Pt_{0.01}O_{2-\delta}$ and $Ti_{0.98}Pd_{0.02}O_{2-\delta}$ are shown in Fig. 2.

XRD patterns of hydrothermally prepared $Ce_{1-x}M_xO_{2-\delta}$ (M = Zr, Ti, Pr, Y, Fe and Cr) catalysts are indexed to fluorite structure and there are no traces of respective oxides in their patterns.[61,62] Similarly, diffraction lines associated with RuO_2 and Ru metal are not observed in XRD patterns of $Ce_{1-x}Ru_xO_{2-\delta}$ ($0 \leq x \leq 0.1$) prepared by hydrothermal method and they show fluorite structure.[63] Ru and RuO_2 impurity peaks are observed in XRD pattern of $Ce_{1-x}Ru_xO_{2-\delta}$ prepared with $x = 0.15$. Thus, only up to 10% Ru^{4+} ion can be substituted for Ce^{4+} in CeO_2 by this method.

Diffraction lines related to Pt and Pd metals or PtO_2 and PdO impurities are not observed in the XRD patterns of $Ce_{1-x}M_xO_{2-\delta}$ (M = Pt and Pd; x = 0.02, 0.05 and 0.10) synthesized by sonochemical method where all the peaks are indexed to cubic fluorite lattice indicating the substitution of Pt^{2+} and Pd^{2+} ions into CeO_2 lattice to certain extent.[70]

Li and coworkers have demonstrated the absence of Pd metal up to 2.5 wt.% metal loading in the XRD pattern of mesoporous Pd/CeO_2.[76] Pt metal is not found in combustion synthesized 1 at.% Pt/CeO_2 as shown by Tang et al.[77] Diffraction peaks related to Pd metal are not observed in sol-gel synthesized 1 at.% Pd/CeO_2 in the work done by Wang and coworkers.[78] Pt metal or any of its oxides are absent in the XRD pattern of solution combustion synthesized 2 at.% Pt/CeO_2 as showed by Bisht and coauthors.[79] Pd metal is not seen in the XRD pattern of 1 wt.% $Pd/CeO_2{-}SiO_2$ catalyst.[80] Misch et al. have demonstrated the formation of single phase $Ce_{1-x}Pd_xO_{2-\delta}$ (x = 0.025, 0.05, 0.075, 0.1) solid solution with fluorite structure.[81]

3.2. TEM studies

High resolution TEM (FEI Technai 20) images of noble metal ion substituted CeO_2 and TiO_2 catalysts have been recorded to understand their morphology and lattice fringes. CeO_2 based catalysts show cubic morphology of CeO_2 crystallites with average sizes of 5–30 nm. Noble metal particles are not be observed on the surface of CeO_2 crystallites. A HRTEM image and electron diffraction (ED) pattern of solution combustion synthesized $Ce_{0.73}Ti_{0.25}Pd_{0.02}O_{2-\delta}$ is displayed in top panel of Fig. 3. The fringes spacing at ~3.12 Å correspond to (111) layers of $Ce_{0.75}Ti_{0.25}O_2$. The ED pattern clearly demonstrates the crystalline nature of the catalyst and it is indexed into fluorite structure. No lattice fringe in the HRTEM image or ring in ED pattern due to Pd metal particles at 2.25 Å are observed. In contrast, Pd(111) ring is visible as indicated by arrow in ED pattern of 2% $Pd/Ce_{0.75}Ti_{0.25}O_2$ prepared by impregnation method shown in Fig. 3C of top panel. Absence of diffraction ring due to Pd metal in the solution combustion synthesized material shows substitution of Pd in the lattice leading to $Ce_{0.73}Ti_{0.25}Pd_{0.02}O_{2-\delta}$ solid

solution.[48] The average particle size of CeO_2 crystallites obtained from low magnification image is ~20 nm. Similarly, lattice fringes with 3.2 Å of (111) plane of $Ce_{0.85}Ti_{0.15}O_2$ has been observed in a high resolution image of Pt ion substituted $Ce_{0.85}Ti_{0.15}O_2$ and fringes related to Pt metal particles at 2.30 Å are absent. Energy dispersive X-ray spectroscopy (EDXS) confirms the presence of 1% Pt in the catalyst and Pt ion substitution in $Ce_{0.85}Ti_{0.15}O_2$.[47] Lattice fringes in the HRTEM image of $Ce_{0.89}Fe_{0.1}Pd_{0.01}O_{2-\delta}$ are 3.1 Å corresponding to its (111) plane.[51] On the other hand, large number of nano size fine Pt metal particles can be dispersed on α-Al_2O_3 by solution combustion method.[42,71]

HRTEM image and corresponding ED pattern of $Ti_{0.97}Pd_{0.03}O_{2-\delta}$ catalyst are shown in bottom panel of Fig. 3. Lattice fringes in $Ti_{0.97}Pd_{0.03}O_{2-\delta}$ catalyst shown in Fig. 3 (b) of bottom panel correspond to (101) planes of TiO_2. Lattice fringes due to PdO or Pd metals are not detected in the high resolution lattice images from $Ti_{0.97}Pd_{0.03}O_{2-\delta}$ catalyst. EDX spectrum of this image show the presence of Pd. ED pattern is indexed to polycrystalline TiO_2 in anatase structure in both catalysts and there is no signature of Pd metal or PdO phases in their ED patterns.[55] Therefore, absence of Pd or PdO in $Ti_{0.97}Pd_{0.03}O_{2-\delta}$ in TEM image and presence of Pd in EDX spectrum confirm the substitution of Pd^{2+} ion in TiO_2 lattice. In an another study, Pd metal diffraction line is observed in the ED pattern of 1% Pd/TiO_2 prepared by impregnation.[54] The particle sizes measured from the image are in the range of 8–15 nm that agrees well with the XRD studies. Other noble metal doped TiO_2 catalysts show similar kind of characteristics.

HRTEM image of $Ce_{0.9}Ru_{0.1}O_{2-\delta}$ synthesized by hydrothermal method shows the absence of isolated RuO_2 and Ru metal and average crystallites size is 10 nm. Ring type ED pattern is indexed to fluorite structure.[63]

3.3. XPS studies

Oxidation states of Pt, Pd, Rh, Ru, Cu, Ag, Au, Ce and Ti present in the CeO_2 and TiO_2 based catalysts studied here can be obtained from XPS (ESCA-3 Mark II, Thermo Fisher Scientific). Typical Pt4f and Rh3d core level spectra in reference compounds and CeO_2 based catalysts are shown in Fig. 4. In $Ce_{0.99}Pt_{0.01}O_{2-\delta}$ and $Ce_{0.83}Ti_{0.15}Pt_{0.02}O_{2-\delta}$ catalysts, Pt is present in both +2 and +4 oxidation states along with small amount of Pt metal.[20,71,72,47] XPS of Pt4f core level peaks of Pt metal, PtO_2, $Ce_{0.99}Pt_{0.01}O_{2-\delta}$ and $Ce_{0.83}Ti_{0.15}Pt_{0.02}O_{2-\delta}$ are displayed in left panel of Fig. 4. Rh is in +3 oxidation state in $Ce_{1-x}Rh_xO_{2-\delta}$ catalyst as observed in Rh3d core level spectra.[44] In right panel of Fig. 4, Rh3d core level spectra in Rh, Rh_2O_3, $RhCl_3$ and $Ce_{1-x}Rh_xO_{2-\delta}$ are displayed. Similarly, Core level $Pd3d_{5/2}$ peak is observed at 337.6 eV in $Ce_{0.98}Pd_{0.02}O_{2-\delta}$ which is 2.4 and 0.9 eV higher than Pd metal and PdO.[43] Binding energies of Pd3d peaks in $Ce_{0.98}Pd_{0.02}O_{2-\delta}$ are close to Pd3d peaks of $PdCl_2$ and $Pd(NO_3)_2$ clearly indicating that Pd^{2+} ions are much more ionic in CeO_2 matrix than PdO. Pd is observed to be in high binding energy region in $Ce_{0.98}Pd_{0.02}O_{2-\delta}$. Pd is also observed to be in +2 state in $Ce_{0.73}Ti_{0.25}Pd_{0.02}O_{2-\delta}$, $Ce_{0.78}Sn_{0.2}Pd_{0.02}O_{2-\delta}$, $Ce_{0.89}Fe_{0.1}Pd_{0.01}O_{2-\delta}$ and $Ce_{0.73}Zr_{0.25}Pd_{0.02}O_{2-\delta}$.[48–52] Therefore, XPS of $Ce_{1-x}Pd_xO_{2-\delta}$ based catalysts indicate that Pd is present in highly ionic Pd^{2+} state. Similarly, XPS results demonstrate that Cu in $Ce_{1-x}Cu_xO_{2-\delta}$, Ag in $Ce_{1-x}Ag_xO_{2-\delta}$ and Au in $Ce_{1-x}Au_xO_{2-\delta}$ are fully dispersed in +2, +1 and +3 oxidation states, respectively.[74,75,45,46] XP spectra of Ce3d with characteristic satellites in all catalysts show that Ce is mainly present in +4 oxidation state. Ru in $Ce_{1-x}Ru_xO_{2-\delta}$ prepared by hydrothermal method, Pt and Pd in $Ce_{1-x}M_xO_{2-\delta}$ (M = Pt and Pd) and Pd doped $Ce_{1-x}Fe_xO_{2-\delta}$ prepared by sonochemical method are in oxidized state.[63,69,70]

Pd metal and highly ionic Pd^{2+} species are observed in Pd/CeO_2 prepared by wet impregnation method.[76] $Pd3d_{5/2}$ core level peaks observed at 336.5 and 338.0 eV in Pd/CeO_2 catalysts prepared by coprecipitation method correspond to PdO_x and highly ionic Pd^{2+} species of $Ce_{1-x}Pd_xO_{2-\delta}$ solid solution.[82] Li and coworkers have demonstrated $Pd3d_{5/2}$ core level peak at 336.7 eV in coprecipitated $PdCeO_x$ solid solution.[83] XPS studies have showed that Pt, Pd and Ru are in their ionic states in $M/Ce_{0.72}Zr_{0.18}Pr_{0.1}O_2$ (M = Pt, Pd and Ru) catalysts.[84] There are several recent reports where Pt and Pd are present in their ionic states in CeO_2 matrix.[85–89] $Pt4f_{7/2}$ core level peaks are observed at 71.3, 72.3 and 73.9 eV in 3.7 wt.% Pt-Ce(La)O_x catalyst synthesized by coprecipitation method.[90] Combustion synthesized Pt/CeO_2 catalyst contains Pt^0, Pt^{2+} and Pt^{4+} species as demonstrated by XPS.[77] Presence of Pt^0, Pt^{2+} and Pt^{4+} species are found in Pt/CeO_2 catalysts prepared by deposition–reduction method.[91] Ru is in +4 oxidation state in Ru/CeO_2 catalysts.[92,93] Au^0, Au^+ and Au^{3+} species are present in 4.7 wt.% Au-Ce(La)O_x and 1% Au/CeO_2 prepared by coprecipitation and photoreduction methods.[90,94] Au is in Au^0, Au^+ and Au^{3+} oxidation states in 2.8 wt.% Au/CeO_2 obtained from deposition–precipitation method.[95] $Ag3d_{5/2}$ core level peaks at 368.3 and 367.8 eV observed in Ag/CeO_2 catalyst prepared by impregnation method are attributed to Ag^0 and Ag^+ species.[96]

XPS studies of $Ti_{0.99}M_{0.01}O_{1.99}$ (M = Pd, Pt, Rh and Ru) catalysts also show the ionic nature of substituted noble metals in TiO_2 matrix.[54] Core level XPS of Pd3d in $Ti_{0.99}Pd_{0.01}O_{1.99}$, Pt4f in $Ti_{0.99}Pt_{0.01}O_{1.99}$, Rh3d in $Ti_{0.99}Rh_{0.01}O_{1.99}$ and Ru3p in $Ti_{0.99}Ru_{0.01}O_{1.99}$ are presented in Fig. 5. $Pd3d_{5/2}$ peak at 337.2 eV is attributed to Pd^{2+} ion substitution in TiO_2 support. As Pd3d peaks in $Ti_{0.99}Pd_{0.01}O_{1.99}$ are observed at higher

binding energies compared to PdO suggesting that Pd^{2+} ions in TiO_2 is in more ionic state than Pd^{2+} in PdO. Pt4f in $Ti_{0.99}Pt_{0.01}O_{1.99}$ shows a broad spectrum of mixed valence state of Pt^{2+} and Pt^{4+}. $Rh3d_{5/2}$ at 310.0 eV indicates clearly Rh is in +3 oxidation state in $Ti_{0.99}Pt_{0.01}O_{1.99}$. $Ru3p_{3/2}$ peak observed at 463 eV indicates that Ru is in +4 state in $Ti_{0.99}Ru_{0.01}O_{1.99}$ and peak position is similar to RuO_2. In all cases, core level $Ti2p_{3/2,1/2}$ peaks are observed at 459.0 and 464.0 eV indicating Ti is in +4 oxidation state.

Stabilization of noble metal ions in CeO_2 or TiO_2 can be substantiated from the relative positions of metal valence levels with respect to valence levels of CeO_2 and TiO_2. Typical valence band XPS of CeO_2, $Ce_{0.98}Pd_{0.02}O_{1.98}$, Pd metal, PdO, TiO_2 and $Ti_{0.97}Pd_{0.03}O_{2-\delta}$ are shown in Fig. 6. The valence band of CeO_2 consists of the O2p band spread over ~3–9 eV that is shown in left panel of Fig. 6. Empty Ce4f level is located at ~2 eV below the Fermi level (E_F) where binding energy is referenced to zero. Pt, Pd, and Rh metals have high electron density at the E_F and the valence bands of these metals extend even up to 6 eV below E_F. When these metals are oxidized, M^{n+}d bands shift to higher binding energies with the effect that the M^{n+}d bands are located at about 2.5–3.5 eV below E_F as in PdO in the figure. In $Ce_{1-x}M_xO_{2-\delta}$, the M^{n+}d band lies between Ce4f and O2p bands and hence, Ce in the compound remains mostly in the +4 state. When metal ion in $Ce_{1-x}M_xO_{2-\delta}$ is reduced to metal in the lattice, the metal valence band is shifted towards the E_F which is above the empty Ce4f band. Hence, electron transfer from metal to Ce^{4+} ion ($M^0 + 2\ Ce^{4+}4f^0 \rightarrow M^{2+} + 2\ Ce^{3+}4f^1$) becomes facile and the noble metals remain ionic in CeO_2.[21] For example, the difference of valence band XPS of CeO_2 and $Ce_{0.98}Pd_{0.02}O_{1.98}$ shows a small density of states at ~3.2 eV from E_F. This density of states corresponds to $Pd^{2+}4d^8$ occupied state that is higher than that of Ce4f level.[51]

Similarly, Pt^{2+} and Pd^{2+} ions get stabilized in TiO_2, because Pt^{2+}5d and Pd^{2+}4d bands are situated below Ti^{3+}3d (0.9 eV) and above O2p bands.[21,53,97] Right panel of Fig. 6 shows the band positions of TiO_2 and $Ti_{0.97}Pd_{0.03}O_{2-\delta}$.

3.4. XAFS studies

Substitution of metal ions into CeO_2 lattice has been confirmed by XAFS studies (SPring-8, Japan). XAFS analysis shows unique Ce–Pd, Ce–Rh and Ce–Pt distances at 3.31, 3.16 and 3.28 Å, respectively, whereas Ce–Ce distance is observed at 3.84 Å demonstrating the substitution of Pd^{2+}, Rh^{3+} and Pt^{2+} ions into CeO_2 lattice.[43,44,72] Similar type of distances related to Ce–Pt and Ce–Pd interactions are also observed in $Ce_{1-x-y}Ti_xPt_yO_{2-\delta}$, $Ce_{1-x-y}Ti_xPd_yO_{2-\delta}$ and $Ce_{1-x-y}Sn_xPd_yO_{2-\delta}$ catalysts.[98,50] It is important to mention that these unique interactions are not found in either CeO_2 or noble metals or their oxides such as PdO, Rh_2O_3 and PtO_2. Typical XAFS of Pt and Rh ion substituted CeO_2 catalysts along with Pt metal, PtO_2, Rh metal and Rh_2O_3 are shown in Fig. 7. Lower coordination numbers around metal ions compared to Ce ion indicate the oxide ion vacancy due to lower valent metal ion substitution.

3.5 DRIFTS studies

DRIFTS technique has been used to understand the interaction of CO and NO with noble metal ionic catalysts such as $Ce_{0.98}Pd_{0.02}O_{2-\delta}$ and $Ce_{0.73}Sn_{0.25}Pd_{0.02}O_{2-\delta}$ and nature of Pd species present on their surface by doing CO and NO adsorption. Adsorption studies are also carried out with Pd/Al_2O_3 where Pd is in metallic state. It has been demonstrated that CO and NO are molecularly adsorbed on Pd/Al_2O_3, whereas NO gets dissociatively adsorbed on $Ce_{0.98}Pd_{0.02}O_{2-\delta}$ and $Ce_{0.73}Sn_{0.25}Pd_{0.02}O_{2-\delta}$ catalysts.[99] In contrast, linear $Pd^{\delta+}$–CO adsorption band along with bridging CO band has been observed over CeO_2

based catalysts when CO is adsorbed first, whereas band related to Pd^{2+}–CO interaction is noticed on preadsorbed NO catalysts. As CO is a reducing molecule partial surface reduction of Pd^{2+} occurs when only CO is adsorbed on the $Ce_{0.98}Pd_{0.02}O_{2-\delta}$ and $Ce_{0.73}Sn_{0.25}Pd_{0.02}O_{2-\delta}$ catalysts. But, Pd^{2+} remains intact after CO adsorption in presence of oxidizing molecule like NO indicating the presence of Pd^{2+} species on the surface. Again, Pd^{2+}–NO band is observed when only NO is adsorbed on their surface. Therefore, CO and NO adsorption studies demonstrate that Pd is in +2 oxidation state in $Ce_{0.98}Pd_{0.02}O_{2-\delta}$ and $Ce_{0.73}Sn_{0.25}Pd_{0.02}O_{2-\delta}$ catalysts. Typical DRIFT spectra of (a) NO adsorption and (b) followed by CO adsorption over $Ce_{0.98}Pd_{0.02}O_{2-\delta}$ are shown in Fig. 8. Similarly, Pt^{2+}–CO band has been observed when CO is passed over $Ce_{0.99}Pt_{0.01}O_{2-\delta}$ catalyst.[70] In a recent study, Cu^{2+}–CO band is observed to be present in $Ce_{0.93}Cu_{0.07}O_{2-\delta}$ and $Ce_{1-x-y}M_xCu_yO_{2-\delta}$ (M = Zr, Hf and Th) catalysts with CO exposure.[100]

Based on the extensive characterization studies employing XRD, TEM, XPS, XAFS and DRIFTS it has been demonstrated that noble metals are ionically dispersed over CeO_2 based catalysts and noble metal ions are incorporated into the CeO_2 matrix in the form of $Ce_{1-x}M_xO_{2-\delta}$ solid solution phase in combustion synthesized M/CeO_2 catalysts. In addition to this, oxide ion vacancies are created due to aliovalent ionic substitutions for Ce^{4+}, there seems to be additional oxide ion vacancies to the extent of 3.5% in nano CeO_2. Similarly, $Ti_{1-x}M_xO_{2-\delta}$ type of solid solution phase has been formed in M/TiO_2 catalysts by substituting noble metal ions into TiO_2 matrix.

4. Exhaust catalysis

Energy for the modern civilization comes from the burning of fossil fuels such as coal, natural gas and oil. Most of the fossil fuels constitute carbon, nitrogen, hydrogen and to

some extent sulfur containing compounds. The energy stored in the fossil fuels, biomass, industrial and domestic waste is released mostly by complete as well as partial combustion of these constituents. Partial combustion leads to emission of nitrogen oxides (NO_x), carbon monoxide (CO), sulfur oxides (SO_x), NH_3 and unburned hydrocarbons (HC) to the atmosphere which are the main reasons for environmental pollution. These pollutants are emitted everyday from the exhausts of mobile and stationary sources and have harmful effects on earth's atmosphere, ecological system and also on human health.[22,101,102] Emissions from automobiles and aeroplanes are the mobile sources, whereas industrial processes, power plants, combustion of waste and biomass and domestic burning are the stationary sources. In the early 1950s, air pollution and automobiles were first correlated by California scientists who established that huge traffics were to blame for the smoggy skies over Los Angeles area.[103–107] Over the years, international concerns for the environmental pollution caused by polluting sources have been increasing as it becomes a global environmental issue. Consequently, several developed and developing countries have enacted legislation for the control of pollutant gases in the exhaust stream of automobiles. Each of these countries has set particular emission standards by law for different kinds of vehicles according to their own country's situation. Emission standards set specific limits to the amount of pollutants that can be released into the environment. It is a limit that sets threshold amounts above which different types of emission control technology must be necessary. Standards generally regulate the emissions of NO_x, CO, HCs, SO_x and particulate matters (PM) or soot. Therefore, controlling these pollutants to get clean environment of the world is an important issue in present days.

There are several technologies for controlling pollutants from exhaust emission. Among available technologies one of the best ways of controlling exhaust emission can be to reduce or convert these pollutant gases by using catalyst at the source itself. Therefore, the conversion of environmentally unacceptable gases such as NO_x, CO and HC to N_2, CO_2 and H_2O using catalysts is a challenging task and hence, this area of heterogeneous catalysis has immensely been developing in last four decades. Within this context, environmental catalysis related to auto exhaust has received much more attention as exhausts from automobiles have significant contribution to the global environment pollution. Extensive studies on the scientific research and technological development in this area have been carried out in last several years. A number of reviews, articles and books regarding various aspects of exhaust catalysis have been published to update the status of catalytic science and technological development in this area from time to time.[108–115]

4.1. Reactions involved in exhaust catalysis

In last several years, enormous efforts have been put to advance the scientific and technological development for the controlling of exhaust emission. Catalytic converter has been found to be the best way to control exhaust emission from automobiles among all the types of technologies developed so far.[116] Catalytic converter is a device that usually reduces the toxicity of exhaust emission. A catalyst housed inside a catalytic converter performs chemical reactions by which combustion by-products of pollutants are converted to less-pollutant or benign substances. Since 1981 three-way catalytic converters have been used in vehicle emission control systems of roadgoing vehicles in North America and many other countries. The catalyst used in a three-way catalytic

converter is called three-way catalyst (TWC). A TWC has three simultaneous tasks, namely (i) reduction of NO_x to nitrogen and oxygen, (ii) oxidation of CO to CO_2 and (iii) oxidation of unburned hydrocarbons to CO_2 and H_2O, provided that air to fuel (A/F) ratio is constantly kept in the exhaust stream at the stoichiometric point (14.7) where concentrations of oxidizing and reducing gases are equal.

The essential requirement for the catalyst employed in the present-days catalytic converters for gasoline engine is to carry out the high conversion of NO_x, CO and HCs present in the auto exhaust gases to inert and harmless N_2, CO_2 and H_2O. The overall catalytic reactions which are important for controlling auto exhaust emissions are given by the following stoichiometric equations:

a) reduction reactions

$$2\ NO + 2\ CO \rightarrow N_2 + 2\ CO_2$$

$$2\ NO + 2\ H_2 \rightarrow N_2 + 2\ H_2O$$

$$(2x + \frac{y}{2})\ NO + C_xH_y \rightarrow (x + \frac{y}{4})\ N_2 + x\ CO_2 + \frac{y}{2}\ H_2O$$

b) oxidation reactions

$$2\ CO + O_2 \rightarrow 2\ CO_2$$

$$2\ H_2 + O_2 \rightarrow 2\ H_2O$$

$$C_xH_y + (x + \frac{y}{4})\ O_2 \rightarrow x\ CO_2 + \frac{y}{2}\ H_2O$$

c) three-way catalytic reaction

$$2\ NO + 4\ CO + 2\ C_xH_y + (2x + \frac{y}{2} + 1)\ O_2 \rightarrow N_2 + (2x + 4)\ CO_2 + y\ H_2O$$

d) decomposition reaction

$$2\ NO \rightarrow N_2 + O_2$$

e) selective catalytic reduction

$$4\ NO + 4\ NH_3 + O_2 \rightarrow 4\ N_2 + 6\ H_2O$$

$$2\ NO + 2\ C_xH_y + (2x + \frac{y}{2})\ O_2 \rightarrow N_2 + (2x + 1)\ CO_2 + y\ H_2O$$

$$6\ NO_2 + 8\ NH_3 \rightarrow 7\ N_2 + 12\ H_2O$$

f) secondary reactions with NO

$$2\ NO + CO \rightarrow N_2O + CO_2$$

$$2\ NO + H_2 \rightarrow N_2O + H_2O$$

$$2\ NO + 5\ H_2 \rightarrow 2\ NH_3 + 2\ H_2O$$

$$4\ NH_3 + 5\ O_2 \rightarrow 4\ NO + 6\ H_2O$$

$$4\ NH_3 + 4\ NO + O_2 \rightarrow 4\ N_2O + 6\ H_2O$$

$$2\ NH_3 + 2\ O_2 \rightarrow N_2O + 3\ H_2O$$

$$2\ NO + O_2 \rightarrow 2\ NO_2$$

g) secondary reactions with SO_2

$$2\ SO_2 + O_2 \rightarrow 2\ SO_3$$

$$SO_2 + 3\ H_2 \rightarrow H_2S + 2\ H_2O.$$

All the above reactions required some heat or temperature on the catalyst surface for the reaction to occur. In case of auto exhaust catalysis, when automobile first starts, both the engine and catalyst are cold. After start up, heat of combustion is transferred from the engine and the exhaust piping begins to heat up. Finally, a temperature is reached within the catalyst that initiates the catalytic reactions. This light-off temperature depends on the chemistry of the catalyst.

4.2. Importance of OSC in auto exhaust catalysis and role of CeO_2

In early 1980s, discovery of catalytic converter with three way catalyst (TWC) has been considered as a major breakthrough in the development of device for the controlling of auto exhaust emission. Pollutant gases like CO, HC and NO_x are converted into benign CO_2, H_2O and N_2 simultaneously and efficiently over TWCs with constant A/F stoichiometric ratio (14.7) in the exhaust. High efficiency of conversion is achieved over TWC in a very narrow A/F window that requires a highly efficient control of exhaust composition, particularly in terms of residual oxygen concentration. Strong deviations or oscillations of A/F from the stoichiometric value lead to widening of operating window resulting in an average poor performance of TWC. For widening the operating window of the TWC, the exhaust gas composition on the catalyst must be controlled by storing oxygen in the oxygen-rich condition and by releasing oxygen in the oxygen-lean condition. This can be achieved by adding oxygen storage material in TWC which shows high oxygen storage capacity (OSC). In this sense, OSC is defined as the extent of reversibly exchanged oxygen of an oxygen storage material under rich and lean fluctuation of exhaust gas composition. This oxygen storage material readily undergoes reduction-oxidation cycles that provide oxygen for CO and HC oxidation in rich region and the reduced state can remove oxygen from gas phase when the exhaust gas runs into lean region. Thus, an oxygen storage material not only widens A/F ratio window, but also promotes oxidation activity. Therefore, materials for TWC applications should have redox behavior capable to release/uptake rapidly as much oxygen as possible leading to have high OSC. Utilization of lattice oxygen from reducible oxides under reducing condition and thereafter replenishment of oxygen under oxidizing atmosphere has played a critical role in various oxidation reactions. Therefore, a reducible oxide with redox

characteristics can act as both oxidizing and reducing agent to various reactants depending on the reaction condition. In this regard, CeO_2 has been found as an efficient oxygen storage material for the wide application in TWCs according to the following reversible reactions:

$$CeO_2 \rightarrow CeO_{2-\delta} + \delta/2\ O_2$$

$$CeO_{2-\delta} + \delta/2\ O_2 \rightarrow CeO_2$$

where first reaction is related to oxygen-lean region and second one is for oxygen-rich region and value for δ is in between 0 and 0.25. However, experimentally achieved δ is ~0.05 in the temperature range up to 600 ^oC.

To understand the reducibility of oxygen species as well as the metal-support interaction in CeO_2 and related materials, H_2-TPR is extensively employed where the volume of H_2 consumed by the reduction of an oxide is measured. OSC of CeO_2 for oxidation/reduction reaction was first time estimated in a H_2-TPR experiment on CeO_2 by Yao and Yao.[13] Simple mechanism of OSC from H_2-TPR can be written as follows:

$$CeO_2 + \delta\ H_2 \rightarrow CeO_{2-\delta} + \delta\ H_2O$$

$$CeO_{2-\delta} + \delta/2\ O_2 \rightarrow CeO_2.$$

H_2-TPR of CeO_2 shows primarily two peaks at approximately 500 ^oC and 825 ^oC.[13, 103,117,118] The low temperature peak is due to the reduction of most easily reducible surface oxygen of CeO_2 while removal of bulk oxygen is suggested as the cause of high temperature at 825 ^oC. The first peak is dependent on the surface area and responsible for higher catalytic activity at lower temperature. Thus, unique redox property of CeO_2 has made it a special component of three-ways catalysts, since it can store oxygen during lean

(net oxidizing, excess of O_2) conditions and release it during rich (net reducing, deficient of O_2) conditions as given below:[119]

$$CeO_2 + \delta\ CO \rightarrow CeO_{2-\delta} + \delta\ CO_2$$

$$CeO_2 + C_xH_y \rightarrow CeO_{2-(2x+1/2y)} + x\ CO_2 + 1/2y\ H_2O$$

$$CeO_2 + \delta\ H_2 \rightarrow CeO_{2-\delta} + \delta\ H_2O$$

$$CeO_{2-\delta} + \delta\ NO \rightarrow CeO_2 + \delta/2\ N_2$$

$$CeO_{2-\delta} + \delta\ H_2O \rightarrow CeO_2 + \delta\ H_2$$

$$CeO_{2-\delta} + 1/2\ \delta O_2 \rightarrow CeO_2.$$

It has also been observed that substitution of isovalent cations like Hf^{4+}, Pr^{4+} and Tb^{4+} into CeO_2 lattice forming $Ce_{1-x}M_xO_{2-\delta}$ solid solution enhances the OSC.[117,118] Nonreducible ZrO_2 does not show redox properties as there is no peak in their respective H_2-TPR profiles, whereas significant OSC have been observed in $Ce_{1-x}Zr_xO_2$ samples.[117,118] Higher OSC has also been noticed when precious metals are doped with CeO_2.[117] In general, high surface area, oxygen vacancy and movement of oxide ions from tetrahedral sites to vacant octahedral sites are the possibilities for enhancing the OSC. It is important to note that $Ce_{1-x}Zr_xO_2$ and such oxygen storage materials are not the catalysts themselves for real applications. Noble metals such as Pt, Pd Rh, bimetallic Pt–Rh are dispersed mostly in the form of nanocrystalline metal particles on such OSC materials and they are used as catalysts.

4.3. Conventional catalysts for exhaust catalysis

In auto exhaust catalysis, high efficiency of the conversions of NO_x, CO and hydrocarbons can be achieved over a TWC in a very narrow A/F window that requires a highly efficient control of exhaust composition, particularly in terms of residual oxygen

concentration. This has been achieved by adding oxygen storage material in TWC which shows high OSC. Therefore, formulating suitable catalysts for TWC is a challenging task in auto exhaust catalysis. Within this context, studies on individual reactions for controlling exhaust emission such as NO reduction, CO and hydrocarbon oxidation and SCR of NO by NH_3, CO and hydrocarbons in presence of O_2 are also important. Hence, extensive research works have been going on in the last several decades to find out efficient catalysts for these reactions.

Generally, in early years of exhaust catalysis, metal, alloy and metal oxide catalysts were used for catalytic reactions to control exhaust emission especially NO_x removal.[119] Basic studies on metal catalysts involve single crystal or polycrystalline forms of bulk metal such as powder, wire, foil or ribbons. Prominent metals used are Pt, Pd, Rh, Ru and Ir.[120–123] CuO, Fe_2O_3, TiO_2, V_2O_5, MoO_3, WO_3, Cr_2O_3 and Al_2O_3 are employed as oxide catalysts.[124] Transition metal ion exchanged zeolites have also been developed for exhaust catalysis.[125] Copper is one of the promising elements which has the ability to increase the SCR activity of NO with NH_3. Cu^{2+} ion exchanged Y zeolite, mordenite, ZSM-5 and MFI-ferrisilicate have been found to be effective SCR catalysts for NO.[119,126,127] Other metal ions such as Fe^{3+}, Co^{2+}, Ce^{4+} and Ag^{+} exchanged zeolites also show good SCR activity for NO.[119,128–130] Noble metal exchanged zeolites are active for the removal of NO.[131] The catalytic reduction of NO, oxidation of CO and hydrocarbons have also been carried out over pure and cation substituted perovskite oxides such as $LaFeO_3$, $LaCoO_3$, $LaMnO_3$, $Ln_{1-x}Pb_xMnO_3$ (Ln = La, Pr and Nd), $LaMn_{1-x}Cu_xO_3$ and $La_{1-x}Sr_xMnO_3$.[132–134] They have different cationic sites in the crystal structure which are highly amenable to substitution. Usually metals of high oxidation

states can be stabilized in perovskite structure. Similarly, a large number of spinels AB_2O_4 (A = Mg^{2+}, Co^{2+}, Ni^{2+}, Cu^{2+} and Zn^{2+} and B = Al^{3+}, Cr^{3+}, Mn^{3+}, Fe^{3+} and Co^{3+}) are also employed for NO reduction and CO and hydrocarbon oxidation.[119,135]

In early 1980s, supported metal catalysts have come in the scenario of auto exhaust catalysis.[136–138] Metal catalysts with low metal loadings are usually dispersed on the surface of a support. Highly dispersed catalysts provide a maximum surface area. As metal loading increases the crystallites come closer together causing larger particle size. Generally, the more expensive noble metal catalysts have low metal loadings and are highly dispersed, whereas catalysts containing less expensive base metals have higher metal loadings, usually 20–40 % by weight or atom. Supports like Al_2O_3, SiO_2, TiO_2, CeO_2, ZrO_2, SnO_2, WO_3 and MgO are used for the dispersion of metals. In this sense, in search of suitable material to satisfy several requirements for exhaust catalysis, CeO_2 has emerged as a unique and active oxide support in last several years. However, a catalyst in the rigorous automotive exhaust condition should have (a) intrinsic reactivity, (b) poison resistance ability and (c) durability and it soon has become apparent that the base metal oxides of Ni, Co, Mn or Cr do not have these properties. In particular, modern days automotive exhaust catalysts revolve around three noble metals such as Pt, Pd and Rh that have been dispersed, stabilized, promoted, alloyed and segregated in sophisticated ways to fulfill the required performance and γ-Al_2O_3 has been found to be the main support along with CeO_2 additive. It is observed that addition of CeO_2 increases the activity of Al_2O_3 catalyst towards three-way catalytic activities. The promoting effect of CeO_2 is largely attributed to the enhancement of metal dispersions, OSC, increase in oxygen mobility due to oxide ion defects and thermal stability. CeO_2 is able to act as an

efficient oxygen storage material by releasing/storing oxygen because of its capability to undergo effective reduction and reoxidation under fuel-rich (A/F < 14.7) and fuel-lean (A/F > 14.7) conditions. The reversible oxygen storage/release feature coupled with chemical stability in adverse conditions is a unique feature that offers CeO_2 as a prime material in TWC design.[117,136,139]

4.4. Noble metal ionic catalysts for exhaust catalysis

From fundamental basis of TWC it is necessary to develop such kind of materials that can provide unique OSC as well as active sites for redox type of exhaust catalytic reactions, because both the properties are correlated. Realizing the importance of CeO_2 as oxygen storage material as well as active catalyst support for redox type exhaust catalytic reactions, we have synthesized $Ce_{1-x}M_xO_{2-\delta}$ (M = Pd, Pt, Rh, Ru, Cu, Ag and Au), $Ce_{1-x-y}A_xM_yO_{2-\delta}$ (A = Ti, Zr, Sn and Fe; M = Pt and Pd) and $Ti_{1-x}M_xO_{2-\delta}$ (M = Pd, Pt, Rh and Ru) catalysts by solution combustion, hydrothermal and sonochemical methods where metal ions act as active sites for adsorption as well as reaction. Promoting action of CeO_2 and TiO_2, metal-support interaction, high OSC, hydrogen spillover and synergistic interaction are attributed to the interaction of M^{n+}/M^0, Ce^{4+}/Ce^{3+} and Ti^{4+}/Ti^{3+} redox couples in the noble metal ion substituted reducible oxides.[21] In the following sections we discuss about several aspects of exhaust catalysis over these novel materials.

4.4.1. OSC of CeO_2 and TiO_2 based materials

To understand the OSC, reducibility of oxygen species and metal–support interaction in CeO_2 and TiO_2 and related materials, H_2–TPR and CO–TPR are extensively employed where the volume of H_2 or CO consumed by the reduction of an oxide is measured. Pure CeO_2, TiO_2, PdO, Rh_2O_3, CuO and SnO_2 show H_2 uptake peaks at higher temperatures in

comparison with metal substituted CeO_2. ZrO_2 does not show redox properties as there is no peak in its H_2-TPR profile, whereas significant OSC have been observed in $Ce_{1-x}Zr_xO_2$ samples. For specific example, H_2-TPR profiles of CeO_2, Pt doped CeO_2 and $Ce_{1-x}Ti_xO_{2-\delta}$ compounds are shown in Fig. 9. There are three regions of H_2 uptake. First one extends from −50 to 120 °C, the second region extends from ~120 to 300 °C and the third region is above 300 °C. The low-temperature region corresponds to hydrogen uptake related to Pt species in the compound.[47] The second and third regions of the H_2 uptake are attributed to the reduction of Ti^{4+} and Ce^{4+} state, respectively. Reduction of both Ti^{4+} and Ce^{4+} ions occurs at a lower temperature upon Pt substitution and the extent of reduction of Ce^{4+} increases. The H_2 uptake curve for $Ce_{0.99}Pt_{0.01}O_{2-\delta}$ is also given for comparison in the figure. The H_2/Pt molar ratio in the first region of 1 at.% $Pt/Ce_{0.85}Ti_{0.15}O_2$ is 12.0, which is 3 times higher than that observed over $Ce_{0.99}Pt_{0.01}O_{2-\delta}$. The ratio is 7.5 under first region for 1 at.% $Pt/Ce_{0.85}Ti_{0.15}O_2$. H_2 uptake starts at ~30 ^oC in $Ce_{0.98}Pd_{0.02}O_{2-\delta}$ with a hydrogen adsorption peak at ~65 ^oC and a small peak at 450 ^oC due to CeO_2 reduction is observed. Taking the low temperature H_2 peak at 65 ^oC, the ratio of H/Pd is four in $Ce_{0.98}Pd_{0.02}O_{2-\delta}$. In the case of $Ce_{0.73}Ti_{0.25}Pd_{0.02}O_{2-\delta}$, H/Pd ratio is 17.[48] Hydrogen consumption peak around 100 °C $Ce_{1-x}Rh_xO_{2-\delta}$ is attributed to reduction of Rh^{3+} species and second broad centered at ~270 °C corresponding to reduction of CeO_2.[44] Thus, $Ce_{1-x}M_xO_{2-\delta}$, $Ce_{1-x-y}Ti_xM_yO_{2-\delta}$, $Ce_{1-x-y}Sn_xM_yO_{2-\delta}$, $Ce_{1-x-y}Fe_xM_yO_{2-\delta}$ and $Ce_{1-x-y}Zr_xM_yO_{2-\delta}$ (M = Pd, Pt, Rh and Ru) catalysts have been observed to show high oxygen storage capacities.[44,47,49–52,62,63,70] There is one sharp peak at low temperature and a broad peak at higher temperature region in all the substituted TiO_2 catalysts.[54] Unsubstituted TiO_2 shows very little H_2-uptake and the reduction starts above 400 °C. So,

the higher temperature broad peak for the substituted catalysts is attributed to the reduction of TiO_2. On the other hand, low temperature peak corresponds to the reduction of Pd^{2+} and Pt^{2+} ions in TiO_2. Oxygen storage capacities of $Ti_{0.97}Pd_{0.03}O_{2-\delta}$ and $Ti_{0.97}Pt^{2+}_{0.03}O_{1.97}$ and $Ti_{0.97}Pt^{4+}_{0.03}O_{1.97}$ are 5100, 2010 and 2315 μmol g^{-1}, respectively.[55,56] Oxygen storage capacities of a large number of CeO_2 and TiO_2 based materials studied in our laboratory are summarized in Table 2.[44,47,49–52,55,56,62,63,70,140,141]

4.4.2. Exhaust catalysis over noble metal ionic catalysts

Noble metal ionic catalysts have been examined for various important catalytic reactions like CO oxidation, NO reduction by NH_3 and CO, hydrocarbon oxidation, three-way catalytic reaction, water-gas shift reaction (WGSR), preferential oxidation of CO (CO–PROX), H_2–O_2 recombination, hydrogenation and Heck reaction that are discussed in the following sections. It has been observed that catalytic activities of noble metal ionic catalysts toward these reactions are much higher than supported noble metal catalysts.

4.4.2.1. CO oxidation by O_2

Among Pt^{2+}, Pd^{2+} and Rh^{3+} ions, Pd^{2+} ion substituted CeO_2 or $Ce_{1-x}Ti_xO_2$ or TiO_2 show the highest rate of CO conversion and lowest activation energy toward CO oxidation. Within this context, it is important to note that Pd is the cheapest among noble metals. It has also been observed that activation energy decreases with increase in the effective charge on Pd^{2+} ion in these oxides.[52] It has to be noted that rates with metal ionic catalysts are higher by 20–30 times compared with the same amount of metal impregnated catalysts. Pt and Pd ion substituted $Ce_{1-x}Ti_xO_2$, $Ce_{1-x}Sn_xO_2$ and $Ce_{1-x}Fe_xO_2$ catalysts show very high CO conversion.[47–50] In top panel of Fig. 10, CO conversion over

different Pt^{2+} substituted catalysts is presented. $Ti_{0.99}Pt_{0.01}O_{2-\delta}$ catalyst is observed to show lowest temperature 100% CO conversion. Complete conversions of CO to CO_2 are achieved below 105 and 135 ^oC over hydrothermally prepared $Ce_{0.9}Ru_{0.1}O_{2-\delta}$ and $Ce_{0.95}Ru_{0.05}O_{2-\delta}$ catalysts, respectively in presence of feed oxygen.[63] In another type of experiment, CO gets oxidized to CO_2 by extracting activated lattice oxygen in the absence of feed oxygen. On exposure to oxygen, the lattice oxygen is replenished. This means that the feed oxygen gets adsorbed and incorporated in the oxide ion vacancy indicating the presence of two independent sites on the catalyst that adsorb reducing and oxidizing molecules respectively.[48,49,63] $Ce_{0.65}Fe_{0.33}Pd_{0.02}O_{2-\delta}$ catalyst prepared by sonochemical method shows very low temperature CO oxidation with activation energy of 38 kJ mol^{-1}.[70] Low temperature CO oxidation over $Ti_{1-x}Pd_xO_{2-x}$ catalysts has been demonstrated by our group.[142] It is important to note that CO oxidation over Pt/Al_2O_3 and Pd/Al_2O_3 synthesized by solution combustion method occurs at higher temperature compared to CeO_2 and TiO_2 based catalysts.[42]

In recent times, there are reports about CO oxidation activities of supported ionic noble metals and it has been found that these oxidized noble metals are more active compared to noble metals. Grass and coauthors have demonstrated the formation thin active RhO_x over layer on polymer stabilized Rh nanoparticles that is responsible for low temperature CO oxidation.[143] Active RhO_x phased dispersed on CeO_2 has been found to be highly active for CO oxidation as reported by Ligthart et al.[144] Manuel and coworkers have shown that oxidized Rh species (Rh^{x+}) on $Ce_{0.75}Zr_{0.25}O_2$ exhibits a significant 25 times higher turnover rate in CO oxidation than corresponding zero valent one (Rh^0).[145] Here, $Ce_{0.75}Zr_{0.25}O_2$ support is to stabilize Rh atom as ions. Comparison of CO oxidation

over $Rh^{x+}/Ce_{0.75}Zr_{0.25}O_2$ and $Rh^0/Ce_{0.75}Zr_{0.25}O_2$ is displayed in bottom panel of Fig. 10. Solution combustion synthesized Au/CeO_2 catalyst where Au is in +3 oxidation state shows very high CO oxidation rate at low temperature.[46] Carrettin et al. have demonstrated the stabilization of Au^{3+} in nanocrystalline CeO_2 that shows very high CO oxidation acivity.[146] Strong interaction between ionic gold and CeO_2 is attributed to exceptionally high CO oxidation rate over Au/CeO_2 catalyst prepared by deposition-precipitation method.[147] In Table 3, comparison of CO conversion rates and activation energies (E_a) for CO + O_2 reaction over noble metal ion substituted CeO_2 and TiO_2 catalysts with supported nano metal catalysts are presented.[47–49,51,55,56,63,70,82,84,87,142,148–153]

4.4.2.2. NO Reduction by CO

High activity for NO + CO reaction with 100% N_2 selectivity has been observed over $Ce_{0.98}Pd_{0.02}O_{2-\delta}$.[154,155] Decomposition rate of adsorbed NO is faster over this catalyst that leads to higher N_2 selectivity. For NO + CO + O_2 reaction N_2 selectivity of 100% is seen at higher temperatures over this catalyst. $Ce_{0.98}Pd_{0.02}O_{2-\delta}$ shows low temperature NO reduction by CO in relation to $Ce_{0.98}Pt_{0.02}O_{2-\delta}$ and $Ce_{0.98}Rh_{0.02}O_{2-\delta}$ catalysts.[155] N_2 selectivity is highest in $Ce_{0.98}Pd_{0.02}O_{2-\delta}$ among all these three catalysts in the temperature range of 125−350 ^oC, But N_2 selectivities are more or less same over all catalysts at higher temperature (>300 ^oC). Complete NO reduction by CO occurs over $Ce_{0.99}Pt_{0.01}O_{2-\delta}$ and $Ce_{0.84}Ti_{0.15}Pt_{0.01}O_{2-\delta}$ at 180 ^oC.[47] 100% N_2 selectivity is observed at 240 ^oC for NO reduction by CO over $Ce_{0.73}Ti_{0.25}Pd_{0.02}O_{2-\delta}$ catalyst.[48] $Ce_{0.78}Sn_{0.2}Pd_{0.02}O_{2-\delta}$ exhibits 70% N_2 selectivity at 200 ^oC, whereas 100% N_2 selectivity is obtained at 245 ^oC over this catalyst.[49] Complete NO conversion into N_2 is observed at 200 and 250 ^oC over $Ce_{0.95}Ru_{0.05}O_{2-\delta}$ and $Ce_{0.9}Ru_{0.1}O_{2-\delta}$, respectively where N_2O formation occurs at low

temperature.[63] NO reduction by CO over $Ti_{0.99}Pd_{0.01}O_{1.99}$ catalyst shows high rates of NO conversion for NO + CO reaction with high N_2 selectivity. Rate of N_2O reduction by CO is very high over this catalyst.[137] N_2 selectivity is 80% or more at all temperatures over this catalyst for NO + CO + O_2 reaction. However, it is important to mention that complete NO reduction by CO over 1% Pt/Al_2O_3 and 1% Pd/Al_2O_3 catalysts are seen at 400 and 350 ^oC, respectively.[42] Comparison of NO conversion rates, activation energies and N_2 selectivities for NO + CO reaction over noble metal ion substituted CeO_2 and TiO_2 catalysts with supported nano metal catalysts are presented in Table 4.[47–49,51,63,142,154,156–161]

4.4.2.3. NO Reduction by H_2

NO can also be reduced by H_2 which is also present in the mobile and stationary sources. 100% N_2 selectivity and high reaction rates at low temperature are observed over $Ce_{0.98}Pd_{0.02}O_{1.98}$ catalyst, thereby making it a superior to other existing catalysts reported in literature.[162] Temperature of 100% NO conversions are observed at 160, 180 and 370 ^oC over $Ce_{0.89}Fe_{0.1}Pd_{0.02}O_{2-\delta}$, $Ce_{0.99}Pd_{0.01}O_{2-\delta}$ and $Ce_{0.9}Fe_{0.1}O_{2-\delta}$, respectively.[51] Solution combustion synthesized $Ti_{0.99}M_{0.01}O_{2-\delta}$ (M = Pd, Pt, Rh and Ru) catalysts have been tested for NO + H_2 reaction.[54] The rate of NO reduction by H_2 follows the order: $Ti_{0.99}Pt_{0.01}O_{2-\delta} > Ti_{0.99}Pd_{0.01}O_{2-\delta} > Ti_{0.99}Rh_{0.01}O_{2-\delta} > Ti_{0.99}Ru_{0.01}O_{2-\delta}$. Formation of lowest amount of N_2O occurs over $Ti_{0.99}Pd_{0.01}O_{2-\delta}$ and no NH_3 formation is traced during the reaction, whereas a significant amount of N_2O and NH_3 formation could be seen over $Ti_{0.99}Pt_{0.01}O_{2-\delta}$ catalyst. The experimental observations demonstrate that $Ti_{0.99}Pd_{0.01}O_{2-\delta}$ is the best catalyst among the four catalysts investigated. In presence of excess O_2, N_2

selectivity increases over $Ti_{0.99}Pd_{0.01}O_{2-\delta}$ catalyst during NO + H_2 + O_2 reaction (lean condition).

4.4.2.4. Selective Catalytic Reduction (SCR) of NO by NH_3

SCR of NO by NH_3 has been used extensively to clean up emission from stationary exhausts. Good SCR catalysts should show low temperature activity, high N_2 selectivity and wide SCR window. A series of metal ion substituted TiO_2 catalysts have been synthesized by solution combustion method and their SCR activities have been tested to understand the structure-property relationship and reaction mechanism. SCR reaction occurs at the lowest temperature over $Ti_{0.9}Mn_{0.1}O_{2-\delta}$ among $Ti_{0.9}M_{0.1}O_{2-\delta}$ (M = Cr, Mn, Fe, Co and Cu) catalysts, but N_2 selectivity is found to be highest over $Ti_{0.9}Fe_{0.1}O_{2-\delta}$.[163] In this sense, $Ti_{0.9}Mn_{0.05}Fe_{0.05}O_{2-\delta}$ catalyst where both Mn and Fe are substituted in TiO_2 have been synthesized to optimize low temperature SCR activity and N_2 selectivity. Indeed, SCR reaction occurs at low temperature with a high N_2 selectivity over this catalyst. SCR activities over $Ti_{0.9}Mn_{0.1}O_{2-\delta}$, $Ti_{0.9}Fe_{0.1}O_{2-\delta}$ and $Ti_{0.89}Mn_{0.1}Pd_{0.01}O_{2-\delta}$ have also been carried out to understand the role of base metal and noble metal ionic catalysts.[164] From H_2-TPR and SCR activity studies it has been observed that more reducible catalyst shows better NH_3 oxidation and poor SCR activity. NO reduction follows the order: $Ti_{0.9}Mn_{0.1}O_{2-\delta}$ > $Ti_{0.89}Mn_{0.1}Pd_{0.01}O_{2-\delta}$ > $Ti_{0.9}Fe_{0.1}O_{2-\delta}$ and the ammonia oxidation follows the reverse order that agrees well with the reducibility of the catalyst. $Ti_{0.89}Mn_{0.1}Pd_{0.01}O_{2-\delta}$ catalyst where a base metal and a noble metal are substituted in TiO_2 does not show any synergetic effect. Therefore, the catalyst should have less reducibility in order to achieve better SCR activity. Thus, noble metal ion (Pd^{2+})

substituted TiO_2 which has better reducibility than the base metal ion (Mn^{3+}) substituted TiO_2 performs poorly for SCR.

4.4.2.5. NO Reduction over NMIC Coated on Cordierite Monolith

In recent years, monolith supports with honeycomb structure are attractive alternative carriers for catalysts in heterogeneous catalysis and have been extensively used as catalyst supports inside the catalytic converters for removal of exhaust gas in the automobile industry.[165–167] In general, monolith is first coated with high surface area oxide like γ-Al_2O_3 and the process is called washcoating. Catalyst active phase is dispersed over the monolith support after washcoating. Several methods for washcoating and coating of catalyst active phase on monoliths have been in the literature.[168,169] Due to advances in monolith technology, simple catalyst mounting methods, flexibility in reactor design, low pressure drop and high heat and mass transfer rates monolithic support dominates the entire automotive market as the preferred catalyst support. Ceramic monolith materials are leaders in the market among different monolith supports and the preferred material is cordierite.

Noble metal ionic catalysts are coated on cordierite monoliths by a single-step solution combustion method and three-way catalytic reactions have been carried out over these catalysts. The coating process involves growing of γ-Al_2O_3 on cordierite by solution combustion method and then further growing of active catalyst phase containing noble metal ionic catalysts on γ-Al_2O_3 coated cordierite again by the same method. Due to closeness of unit cell lattice parameters of cordierite and γ-Al_2O_3 as well as γ-Al_2O_3 and $Ce_{1-x}M_xO_{2-\delta}$, polycrystalline γ-Al_2O_3 on cordierites and $Ce_{0.98}Pd_{0.02}O_{2-\delta}$, $Ce_{0.98}Pt_{0.02}O_{2-\delta}$

and $Ce_{0.9}Cu_{0.1}O_{2-\delta}$ over γ-Al_2O_3 coated cordierites have been grown by solution combustion method following the idea of epitaxial growth.[170,171]

It has been observed that $Ce_{0.98}Pd_{0.02}O_{2-\delta}$ coated on cordierite shows much more catalytic activity toward CO oxidation, NO reduction and three-way catalysis in comparison with $Ce_{0.98}Pt_{0.02}O_{2-\delta}$ and $Ce_{0.9}Cu_{0.1}O_{2-\delta}$ coated cordierite catalysts. Within this context, details investigation on $Ce_{0.98}Pd_{0.02}O_{2-\delta}$ coated cordierite catalyst has been carried out. 100% CO and NO conversions is achieved around 80 and 200 ^oC for CO + O_2 and NO + CO reactions, respectively at a space velocity of 880 h^{-1}. At the same space velocity, three-way catalytic reaction over $Ce_{0.98}Pd_{0.02}O_{2-\delta}$ coated monolith has been carried out with a gas mixture of 10000 ppm CO, 2000 ppm NO, 2000 ppm acetylene (C_2H_2) and 7000 ppm O_2. It has been observed that 100% conversion of all the pollutants occurs below 220 ^oC and CO and C_2H_2 conversion is seen before NO conversion.[170] All pollutant gases are converted to N_2, CO_2 and H_2O below 225 ^oC even with 15% excess oxygen. CO + O_2, NO + CO and three-way catalytic reactions over $Ce_{0.98}Pd_{0.02}O_{2-\delta}$ coated on cordierite monolith are displayed in Fig. 11. In an another study, three-way catalysis over noble metal ionic catalyst coated on monolith is carried out in presence of NO, CO, O_2 and a mixture of hydrocarbons such as acetylene (C_2H_2), ethylene (C_2H_4), propene (C_3H_6) and propane (C_3H_8) with a GHSV of 4523 h^{-1}. All the pollutant gases are fully converted to N_2, CO_2 and H_2O at 340 ^oC. While NO, CO and C_2H_2 go off almost at the same temperature 260 ^oC, C_2H_4, C_3H_6 and C_3H_8 convert fully at 290, 315 and 340 ^oC, respectively.[171] Thus, $Ce_{0.98}Pd_{0.02}O_{2-\delta}$ catalyst coated on cordierite monolith by novel solution combustion method demonstrates a good low temperature three-way catalytic activity. In this regard, it is to be noted that solution combustion method provides a new

technique of washcoating of high surface area oxide such as γ-Al_2O_3 and dispersing of catalyst active phase containing noble metal ion over monolith.

4.4.2.6. Hydrocarbon oxidation

Complete CH_4 oxidation occurs over $Ce_{0.99}Pt_{0.01}O_{2-\delta}$ and $Ce_{0.99}Pd_{0.01}O_{2-\delta}$ at 400 and 330 °C, respectively, whereas complete oxidation of C_3H_8 over these catalysts has been observed at 110 and 230 °C, respectively.[20] On the other hand, these reactions occur at much higher temperatures over 1% Pt/Al_2O_3 and 1% Pd/Al_2O_3 catalysts.[172] Similarly, 100% conversions of CH_4 and C_3H_8 have been noticed at much lower temperatures over $Ce_{0.99}Ag_{0.01}O_{2-\delta}$ and $Ce_{0.99}Au_{0.01}O_{2-\delta}$ catalysts in comparison with 1% Ag/Al_2O_3 and 1% Au/Al_2O_3.[45,46] Rate of C_2H_4 oxidation over bimetal ionic $Ce_{1-x}Pt_{x/2}$ $Rh_{x/2}O_{2-\delta}$ is observed to be higher than corresponding monometal ionic $Ce_{1-x}Pt_xO_{2-\delta}$ and $Ce_{1-x}Rh_xO_{2-\delta}$ catalysts.[73] $Ce_{0.84}Ti_{0.15}Pt_{0.01}O_{2-\delta}$ shows higher catalytic activity toward oxidation of C_3H_8, C_2H_4 and C_2H_2.[47] Activation energies of oxidation of C_2H_4 and C_2H_2 over $Ce_{0.98}Pd_{0.02}O_{2-\delta}$ and $Ti_{0.99}Pd_{0.01}O_{2-\delta}$ are found to be lower in comparison with the previous studies in the literature.[154,142] Oxidation reactions of several hydrocarbons over $Ce_{1-x}Ru_xO_{2-\delta}$ occur at lower temperatures and complete conversion temperatures depend on amount of Ru.[63] Hydrocarbon oxidation temperatures over $Ti_{1-x}Pd_xO_{2-\delta}$ catalysts decrease with increase in Pd content and room temperature C_2H_2 oxidation occurs over $Ti_{0.97}Pd_{0.03}O_{2-\delta}$ catalyst.[55]

5. Water gas shift reaction

The reaction of CO with steam leading to H_2 and CO_2 is generally called water gas shift reaction (WGSR). It has been used as an important step in the production of H_2 as well as bringing down CO level in the steam reformate introduced into the polymer electrolyte

fuel cells (PEMFC). Fu and Flytzani-Stephanopoulos have shown that water gas shift occurs at significantly low temperature over leached Pt/CeO_2 and Au/CeO_2 containing ionic Pt and Au compared to catalysts without leaching that contains metallic species.[90] Ionic Pt and Au species strongly associated with surface cerium-oxygen groups are responsible for the high activity. CO conversion has been found to be maximum at 200 °C over $Ce_{1-x}Pt_xO_{2-\delta}$ catalysts without any methanation.[173] However, $Ti_{0.99}Pt_{0.01}O_{2-\delta}$ shows highest activity among $Ti_{0.99}Pt_{0.01}O_{2-\delta}$, $Ce_{0.83}Ti_{0.15}Pt_{0.02}O_{2-\delta}$ and $Ce_{0.98}Pt_{0.02}O_{2-\delta}$ catalysts without deactivation.[174] There is no carbonate formation over $Ti_{0.99}Pt_{0.01}O_{2-\delta}$ due to highly acidic nature of Ti^{4+} in the catalyst and consequently, no deactivation is observed even after prolonged reaction. Pt^{2+} substituted ZrO_2 shows lowest temperature WGS reaction among Pt^{2+} and Pd^{2+} substituted ZrO_2 and $Ce_{0.85}Zr_{0.15}O_{2-\delta}$ catalysts.[175] Formation of Brønsted acid-base pairs is the main cause for high activity of ZrO_2 catalysts. $Ce_{0.78}Sn_{0.2}Pt_{0.02}O_{2-\delta}$ shows excellent CO conversion due to the presence of Ce^{4+}/Ce^{3+} and Sn^{4+}/Sn^{2+} redox couples.[176] Much higher activity of WGS reaction is noticed over $Ce_{0.65}Fe_{0.33}Pt_{0.02}O_{2-\delta}$ catalyst compared to $Ce_{0.67}Fe_{0.33}O_{2-\delta}$ due to synergistic interaction Pt^{4+} with Ce^{4+} and Fe^{3+} ions.[177] $Ce_{0.95}Ru_{0.05}O_{2-\delta}$ prepared by hydrothermal method shows low activation energy and high conversion rates at low temperature and 100% H_2 selectivity is observed over this catalyst.[178] Sonochemically synthesized $Ce_{0.65}Fe_{0.33}Pd_{0.02}O_{2-\delta}$ catalyst is highly active for water gas shift reaction with reaction rate of 27.2 μmol g^{-1} s^{-1} and 46.4 kJ mol^{-1}.[70]

6. CO-PROX reaction

Preferential oxidation of CO (CO-PROX) is widely used to reduce very trace level of CO in H_2 rich gas stream from fuel reformate that is fed to polymer electrolyte fuel cells

(PEMFC).[179] CO content above 10 ppm present in H_2 rich gas stream from fuel reformate that is fed to PEMFC deactivates platinum based electrodes in PEMFC. An effective CO-PROX catalyst show high activity and selectivity for CO oxidation. It should be active in two temperature ranges, 170–230 °C which is outlet temperature for low temperature water gas shift reaction (WGSR) and 80–100 °C which is the operation temperature for PEMFC. Therefore, wide temperature is required to avoid precise temperature controls. There have been reports of Pt/CeO_2 catalyst for PROX reaction where Pt is present in the metallic state.[180] Pt^{2+} in CeO_2 in the form of $Ce_{1-x}Pt_xO_{2-\delta}$ solid solution is more efficient catalyst than supported Pt metal catalysts and just 15% of Ti substitution in CeO_2 improves the overall PROX activity.[181] CO conversion of 100% is observed over $Ce_{0.83}Ti_{0.15}Pt_{0.02}O_{2-\delta}$ catalyst at 55 °C which is much higher conversion than $Ce_{0.98}Pt_{0.02}O_{2-\delta}$. Thus, CO-PROX temperature window is larger that $Ce_{0.98}Pt_{0.02}O_{2-\delta}$ catalyst. Higher activity of $Ce_{0.83}Ti_{0.15}Pt_{0.02}O_{2-\delta}$ is because of the higher reducibility of this catalyst in comparison with $Ce_{0.98}Pt_{0.02}O_{2-\delta}$. Lattice oxygen becomes activated because of Ti substitution and can easily be removed in reaction condition. Here, reducibility is an important factor as the reaction condition is highly reducing (35% H_2) that makes $Ce_{0.83}Ti_{0.15}Pt_{0.02}O_{2-\delta}$ more active than $Ce_{0.98}Pt_{0.02}O_{2-\delta}$. On the other hand, $Ti_{0.98}Pt_{0.02}O_{2-\delta}$ is not a good PROX catalyst for CO as it shows a good activity for H_2 + O_2 recombination reaction.

7. H_2 + O_2 reaction

H_2 + O_2 recombination is technologically a very important reaction. Keeping the H_2 concentration lower than 4.1% in nuclear power reactors is crucial for safety. Also, the catalytic combustion of H_2 by O_2 is the cleanest source of energy. Hydrogen fuel cells

also make use of a Pt/C catalyst for the overall recombination to produce power. Ever since Michael Faraday demonstrated the $H_2 + O_2$ recombination reaction over platinum metal plates, Pt nanoparticles have remained the only room-temperature recombination catalyst for this reaction. An alternative approach to achieve higher recombination rates are: 1) to design a catalyst possessing two different adsorption sites for H_2 and O_2, unlike the single Pt^0 site in Pt nanoparticles for both the molecules, 2) dissociative chemisorptions of H_2 and O_2 so that the activation energy of recombination is brought down and 3) making the catalyst more tolerant to CO to avoid CO poisoning in fuel cell applications. We have designed new catalysts such as $Ce_{1-x}Pt_xO_{2-\delta}$ and $Ti_{0.99}Pd_{0.01}O_{2-\delta}$ where Pt and Pd are present in their ionic state and they are highly active for $H_2 + O_2$ reaction.[182,183] It has been demonstrated that $Ti_{0.99}Pd_{0.01}O_{2-\delta}$ catalyst not only shows higher rates for the $H_2 + O_2$ recombination reaction, but is also more tolerant to CO than $Ce_{0.98}Pt_{0.02}O_{2-\delta}$.[183] $Ce_{0.98}Pt_{0.02}O_{2-\delta}$ has also been found to be an excellent hydrogen and oxygen recombinant catalyst at room temperature for recovery of water in sealed lead-acid batteries.[184]

8. Photocatalysis

Photocatalysis is more economical from the low energy consumption and operating cost view points. It is an alternative method of NO reduction and decomposition that has been carried out over noble metal ionic catalysts in presence of UV light in our laboratory. Optimum Pd^{2+} concentration has been found to be 1 at.% for NO reduction by CO and NO decomposition over Pd^{2+} ion substituted TiO_2 that contains Ti^{4+}, Pd^{2+}, O^{2-} and the oxide ion vacancy sites.[53] Measureable NO conversion is not observed over pure TiO_2. With increase in Pd^{2+} ion content in $Ti_{1-x}Pd_xO_{2-\delta}$, NO conversion increases with x from

0.005 to 0.01 and then it decreases with increase in Pd^{2+} concentration and for 3 at.% Pd there is no NO conversion. The highest NO conversion of 80% was observed $Ti_{0.99}Pd_{0.01}O_{2-\delta}$. This shows that there is an optimum Pd^{2+} ion concentration for NO conversion. Pd^{2+}4d band becomes broader with an increase in Pd^{2+} ion concentration and the photoluminescence decreases significantly at 2 and 3% leading to lesser conversion. Decrease in NO conversion over $Ti_{0.98}Pd_{0.02}O_{2-\delta}$ and $Ti_{0.97}Pd_{0.03}O_{2-\delta}$ catalysts can also be correlated with increase of electron density due to Pd^{2+}4d band in the band gap region (0–3 eV) of pure TiO_2. With an increase in Pd^{2+} ion concentration, increase in h+–e- pair recombination (shorting effect) should occur lowering the rate of photocatalytic reaction. Again, NO gets adsorbed over both pure TiO_2 and $Ti_{0.99}Pd_{0.01}O_{2-\delta}$, but photodissociation of NO happens only on $Ti_{0.99}Pd_{0.01}O_{2-\delta}$, not on pure TiO_2. Therefore, photodissociation of NO requires oxide ion vacancy that is present on $Ti_{0.99}Pd_{0.01}O_{2-\delta}$ and hence, NO adsorbed on oxygen vacancy sites is dissociative NO. Hence, Pd^{2+} ion for adsorption, oxide ion vacancy and UV light are essential requirements for the photo dissociation of NO.

NO conversion of 45% is seen when NO decomposition is carried out in absence of CO over $Ti_{0.99}Pd_{0.01}O_{2-\delta}$ catalyst. In contrast, there is no NO conversion over pure TiO_2. NO decomposition decreases over $Ti_{0.99}Pd_{0.01}O_{2-\delta}$ in light on/off mode. It has been demonstrated that NO_2 formed due to partial reaction between NO and evolved O_2 from NO decomposition blocks the oxide ion vacancy sites. But in presence of CO, this O_2 is getting utilized to form CO_2 and hence, high NO conversion of 80% is observed over this catalyst.

9. Hydrogenation

Hydrogenation of p-chloronitrobenzene (p-CNB) to p-chloroaniline (p-CAN) is an important reaction, because chloroanilines are key intermediates in industry for synthesis of herbicides, pesticides, pigments, pharmaceuticules, cosmetics and other organic fine chemicals. Recently, Mistri and coworkers have demonstrated hydrogenation of p-chloronitrobenzene to p-chloroaniline over $Ce_{0.98}Pd_{0.02}O_{2-\delta}$, $Ce_{0.98}Ru_{0.02}O_{2-\delta}$ and $Ce_{0.98}Pd_{0.01}Ru_{0.1}O_{2-\delta}$ catalysts.[185] It has been observed that hydrogenation is inactive over monometal ion substituted catalysts. On the other hand, hydrogenation is completed beyond 75 min over $Ce_{0.98}Pd_{0.01}Ru_{0.1}O_{2-\delta}$. A little higher activity with a lower selectivity is noticed with increase in temperature from 35 to 80 °C. Presence of Ru^{4+} together with Pd^{2+} on CeO_2 plays a crucial role towards hydrogenation of p-CNB without dechlorination indicating remarkable Ru^{4+} promotion in the bimetal ion substituted CeO_2 catalyst.

Hydrogenation of benzene to cyclohexane is an important reaction from industrial point of view. A 42% conversion of benzene to cyclohexane with 100% selectivity is observed at 100 °C over $Ce_{0.98}Pt_{0.02}O_{2-\delta}$ catalysts.[186] Turnover frequency is observed to be an order magnitude higher than those of other Pt catalysts.

10. Heck reaction

Heck coupling reaction catalyzed by Pd is well known in organic synthesis.[187,188] It is known for its high tolerance of functional groups and general applicability.[189] The Pd catalyzed coupling reaction of organic/aromatic halides with olefins allows a one-step synthesis of aromatic olefins that are used extensively as biologically active compounds, natural products, pharmaceuticals and precursors of conjugated polymers.[190,191] Heck reaction proceeds in presence of homogeneous as well as heterogeneous Pd catalysts.

$Ce_{0.98}Pd_{0.02}O_{1.98}$ synthesized by solution combustion method catalyzes C–C cross coupling of substituted iodobenzene, bromobenzene and bromoheteroaryls with alkyl acrylates and styrenes with good yields. There is no conversion when iodobenzene with methyl acrylate is carried out over pure CeO_2 indicating Pd^{2+} ions in $Ce_{0.98}Pd_{0.02}O_{1.98}$ are the active sites for Heck reaction.[192] It has been observed that C–X (X = Cl, Br, and I) bond strength influences the activity towards Heck coupling reaction as the coupling reaction follows the order: C–I > C–Br > C–Cl. Temperature also affects the conversion for the coupling of iodobenzene and methyl acrylate that is presented in Fig. 12. Around 100% conversion is observed in 30 min at 150 °C, whereas it requires nearly 1 h when temperature is 125 °C. However, reaction is very slow at 80 °C where conversion is 60% even after 7 h. $Ce_{0.98}Pd_{0.02}O_{1.98}$ catalyst could also be recycled without significant loss of catalytic activity which indicates that catalyst is stable in the reaction condition. Observed turnover frequency (TOF) value for the reaction of iodobenzene and methyl acrylate is higher than other Pd substituted ligandless heterogeneous catalysts for C–C cross coupling reactions reported in the literature.

11. Electrocatalysis and redox coupling between noble metal ions and CeO_2

Electrocatalysis studied by several electrochemical methods toward oxygen evolution, oxidation of formic acid and methanol oxidation over noble metal ionic catalysts has been carried out that provides better understanding of electronic interaction between noble metal ions and CeO_2 through electron exchange among redox ions than gas-solid interaction. In a potentiostatic experiment (chronoamperometry) combined with extensive XPS studies, pure CeO_2 electrode shows almost complete (70%) reduction when it is

subjected to oxygen evolution potential (1.2 V) for 1000 s.[193] Envelop of Ce3d core level spectrum of CeO_2 electrode looks more similar to Ce_2O_3 after the chronoamperometry experiment. In an another experiment under potentiodynamic condition (cyclic voltammetry), when CeO_2 electrode is cycled in the potential range of 0–1.2 V, Ce^{4+} gets reduced to Ce^{3+} where Ce^{3+} amount is 75%. Though fluorite structure is retained after electrochemical experiment as demonstrated by XRD patterns, this reduced CeO_2 does not oxidize back at any electrochemical condition. On the other hand, $Ce_{0.98}Pt_{0.02}O_{2-\delta}$ electrode shows partial reduction (38%) of Ce^{4+} to Ce^{3+} in a chronoamperometry experiment at oxygen evolution potential (1.2 V) for 1000 s and Pt remains in +2 and +4 oxidation states. Ce^{4+} species in $Ce_{0.98}Pt_{0.02}O_{2-\delta}$ electrode material gets reduced to 50% Ce^{3+} after stopping the cycle at 1.2 V in a cyclic voltammetry experiment. However, it returns to its initial status when $Ce_{0.98}Pt_{0.02}O_{2-\delta}$ electrode is cycled under potentiodynamic condition in the positive potential range of 0–1.2 V with a particular scan rate. Similar phenomenon is also observed for Pt component species present in the $Ce_{0.98}Pt_{0.02}O_{2-\delta}$ electrode. There are not much differences in Ce and Pt component ratios with increase in scan rates. Thus, $Ce_{0.98}Pt_{0.02}O_{2-\delta}$ electrode is stable to redox cycle in the potential range of 0–1.2 V. Similar type of direct evidence of redox reactions are observed in $Ce_{0.98}Pd_{0.02}O_{2-\delta}$.[194] The redox catalytic property of $Ce_{0.98}Pt_{0.02}O_{2-\delta}$ and $Ce_{0.98}Pd_{0.02}O_{2-\delta}$ electrodes is associated with the interaction between $Pt^{4+}/Pt^{2+}/Pt^0$ and Ce^{4+}/Ce^{3+} and Pd^{2+}/Pd^0 and Ce^{4+}/Ce^{3+} redox couples within the oxide catalysts. Redox ability of Cu^{2+}/Cu^+ and Cu^+/Cu^0 couples in Cu/CeO_2 catalysts have been studied with cyclic voltammetry in order to understand redox catalytic reactions.[195–197] Catalytic activities of

$Ti_{0.99}M_{0.01}O_{2-\delta}$ (M = Pd, Pt, Rh and Ru) catalysts are correlated with their cyclic voltammetry studies.[54]

Substitution of the Pt^{2+} and Pd^{2+} ions in CeO_2 by sonochemical method activates the lattice oxygen and hydrogen spillover or a higher H/Pt ratio ~8.1 and H/Pd ratio ~4.2 is observed. $Ce_{0.95}Pt_{0.05}O_{2-\delta}$ reversibly releases 0.203 mol of [O]/mol of compound below −15 °C and $Ce_{0.95}Pd_{0.05}O_{2-\delta}$ releases 0.105 mol of [O]/mol of compound below 55 °C. Reversible nature of higher oxygen storage capacity or higher H/Pt and H/Pd ratios is due to interaction of redox couples like Pt^{4+}/Pt^{2+} (0.91 V), Pt^{2+}/Pt^{0} (1.18 V), Pd^{2+}/Pd^{0} (0.92 V), and Ce^{4+}/Ce^{3+} (1.61 V). Because of the participation of lattice oxygen through reduction of Ce^{4+} to Ce^{3+}, $Ce_{0.95}Pt_{0.05}O_{2-\delta}$ and $Ce_{0.95}Pd_{0.05}O_{2-\delta}$ have shown higher electro-oxidation of methanol compared to the same moles of Pt in 5% Pt/C.[69]

It has been observed that Pt^{2+} ion substitution in CeO_2 and $Ce_{1-x}Ti_xO_2$ improves the electrocatalytic activity of oxygen evolution reaction.[198] In a cyclic voltammetry experiment, bubbles can be seen on $Ce_{0.98}Pt_{0.02}O_{2-\delta}$ electrode surface above 1.1 V which confirms the oxygen evolution. CeO_2 electrode shows bubbling only after 1.4 V which confirms the catalytic effect of Pt^{2+} in CeO_2. Steady state current density values obtained from chronoamperometry experiment for 1800 s are 0.09, 0.15 and 0.31 mA cm^{-2} for CeO_2, $Ce_{0.98}Pt_{0.02}O_{2-\delta}$ and $Ce_{0.83}Ti_{0.15}Pt_{0.02}O_{2-\delta}$, respectively. From XPS studies, it has been demonstrated that oxygen evolution is directly related to extent of Ce^{4+} reduction and stability of CeO_2. Oxygen evolution current increases with decrease in Ce^{4+} reduction. Pt ions in CeO_2 and $Ce_{0.83}Ti_{0.15}O_2$ control the lattice oxygen in a particular way to impart the activity in $Ce_{0.98}Pt_{0.02}O_{2-\delta}$ and $Ce_{0.83}Ti_{0.15}Pt_{0.02}O_{2-\delta}$.

Electrooxidation of formic acid has been investigated over $Ce_{0.98}Pt_{0.02}O_{2-\delta}$ and $Ce_{0.83}Ti_{0.15}Pt_{0.02}O_{2-\delta}$ catalysts and results are compared with Pt/C electrocatalyst where Pt is in metallic state. In cyclic voltammetry experiments, CO poisoning effect is observed on Pt/C which is eliminated in $Ce_{0.98}Pt_{0.02}O_{2-\delta}$ and $Ce_{0.83}Ti_{0.15}Pt_{0.02}O_{2-\delta}$ catalysts. In chronoamperometry experiments, gain in the oxidation current in the ionic catalysts is 10 times more than the corresponding Pt/C catalysts for the same amount of Pt metal.[198] Pt^{2+}/Pt^{4+} states remain same after cyclic voltammetry and chronoamperometry experiments in $Ce_{0.98}Pt_{0.02}O_{2-\delta}$ and $Ce_{0.83}Ti_{0.15}Pt_{0.02}O_{2-\delta}$ as demonstrated by XPS studies of electrode materials. Extents of reduction of Ce^{4+} are 50 and 25% in $Ce_{0.98}Pt_{0.02}O_{2-\delta}$ and $Ce_{0.83}Ti_{0.15}Pt_{0.02}O_{2-\delta}$, respectively indicating that lattice oxygen present in the ionic catalysts is utilized initially and steady state is reached with an equilibrium concentrations of Pt^{2+}/Pt^{4+} and Ce^{4+}/Ce^{3+} states. Involvement of lattice oxygen during electrooxidation of formic acid prevents CO poisoning of the catalysts. Similar behavior of $Ce_{0.98}Pt_{0.02}O_{2-\delta}$ and $Ce_{0.83}Ti_{0.15}Pt_{0.02}O_{2-\delta}$ catalysts toward methanol oxidation has been observed and their activities are much higher than the same amount of Pt^0 in Pt/C which is attributed to interaction of Pt^{2+} ion with CeO_2 and $Ce_{0.83}Ti_{0.15}O_2$ to activate their lattice oxygen.[198]

12. Mechanism of redox reactions over noble metal ionic catalysts

Employing several characterization techniques, it has been demonstrated that there are two independent sites on the noble metal ionic catalysts which adsorb reducing and oxidizing molecules, respectively during redox type of reactions such as $CO + O_2$, $NO + CO$, $NO + H_2$, $NO + NH_3$, WGS reaction, CO–PROX reaction, $H_2 + O_2$ recombination, photocatalytic reduction of NO and Heck reaction. A dual site mechanism of redox

reactions like CO + O_2 and NO + CO based on the structure of $Ce_{1-x}M_xO_{2-\delta}$ and $Ti_{1-x}M_xO_{2-\delta}$ related catalysts has been proposed that is different from Langmuir–Hinshelwood mechanism on noble metal surface. In Fig. 13, CO + O_2 reaction mechanism over Pt metal surface is compared with $Ce_{1-x}M_xO_{2-\delta}$. It is well established that CO + O_2 reaction over Pt follows Langmuir–Hinshelwood mechanism where both CO and O_2 are adsorbed on Pt metal surface. CO is a polar molecule. CO has a triple bond as it is isoelectronic to nitrogen. The third bond is a co-ordinate-covalent bond due to lone pair donation from oxygen. Thus, carbon end of CO is relatively negative. Therefore, carbon can donate electron to Pt metal. Bonding of CO with Pt is described by the σ-donation to the Pt metal atom from its 5σ orbital and back donation of Pt metal d electron to the antibonding orbital of CO. A weak chemical bond is formed between CO and Pt metal and hence CO adsorption is a chemisorption process. Thus, adsorption of CO makes Pt metal atoms negative as a whole. The electrons received by Pt atoms on the surface from CO adsorption are shared by all the atoms in the particle that is called delocalized electrons in modern scientific term. On the other hand, oxygen being electronegative, it likes to acquire electrons. O=O bond length is known to be 1.21 Å. Unlike CO, O_2 is adsorbed horizontally on the Pt surface. Pt–Pt atoms in Pt metal are at a distance of 2.74 Å and when oxygen atom aligns on top of adjacent Pt atoms the molecule needs to be stretched from 1.21 to 2.71 Å leading to weakening of O=O bond of molecular O_2. Lengthening of O–O is favored when anti-bonding orbital of O_2 molecule receives electrons from Pt atoms. Transfer of electrons by Pt is possible because the Pt atoms have received electrons from CO. In this sense, O_2 molecule is dissociatively adsorbed on Pt metal surface. This eventually leads to dissociation of O_2 into two O

atoms or partially negative ions. Once O atom is created, it combines with C end of CO forming CO_2. In contrast, on the Pt ionic catalyst surface, CO is adsorbed on the electron-deficient metal ions, whereas O_2 is adsorbed on the oxide ion vacancy because the vacancy site is activated by the electron-rich environment. The size of the oxide ion vacancy is ~2.8 Å, which can accommodate the oxygen molecule of diameter 2.42 Å. Thus, there are two distinct sites, one for reducing and another for oxidizing molecules in the Pt metal ionic catalysts which is different from Pt metal atoms. Electron transfer from reducing molecule to oxygen is facilitated by the lattice via coupling between accessible Pt^{2+}/Pt^{0} and Ce^{4+}/Ce^{3+} redox couples. The enhanced activity is due to the creation of redox sites leading to site-specific adsorption and electronic interaction between the noble metal ions and the lattice. In addition to this, the lattice oxygen is activated in the catalyst with long M–O and Ce–O bonds and CO can get oxidized through a Mars–van Krevelen mechanism whereby oxide ion is continuously consumed and formed. The difference in the rate of CO oxidation over different noble metal ion substituted catalysts is due to differences in their redox properties.

Similar explanation can be given for NO + CO reaction over noble metal ionic catalysts. NO is an electron donor as well as an acceptor molecule. Therefore, on the ionic catalysts, NO can be molecularly adsorbed on noble metal ions and dissociatively chemisorbed on the oxide ion vacant sites. Adsorption of NO over noble metal ion is facilitated by the donation of 5σ orbital electron of NO to the metal ion leading to the molecular adsorption. On the other hand, anti bonding $2\pi^*$ orbital of NO gets electron from the oxide ion vacancy site where it is adsorbed leading to the dissociation of NO. On contrary to NO, CO is specifically adsorbed on noble metal ion sites by donating its

5σ orbital electron to the metal ions. Molecularly adsorbed NO on the metal ion sites would lead to N_2O formation, whereas N_2 is formed when NO is dissociatively adsorbed NO on the oxide ion vacant sites. Therefore, N_2 selectivity is governed by dual site adsorption of NO on the catalyst. Since both NO and CO compete for metal ion sites and NO is adsorbed on oxide ion vacant sites also, overall NO reduction results in N_2 and N_2O formation. However, N_2O formed on the metal ion sites could move to oxide ion vacant sites making the way for CO adsorption on metal ion sites and $N_2O + CO \rightarrow N_2 + CO_2$ takes over leading to N_2 formation. Based on dual site adsorption (molecular adsorption on noble metal ion and dissociative adsorption on vacant oxide ion), N_2 and N_2O formation along with CO_2 over NMIC such as $Ce_{0.98}Pd_{0.02}O_{2-\delta}$ catalyst during NO + CO reaction are schematically shown in Fig. 14. Similar kind of mechanism can also be applicable for NO + CO reaction over $Ti_{0.99}M_{0.01}O_{2-\delta}$ catalysts. Again, it has been demonstrated that $Ce_{0.98}Pd_{0.02}O_{2-\delta}$ shows higher N_2 selectivity compared to $Ce_{0.98}Rh_{0.02}O_{2-\delta}$.[155] Higher N_2O formation over $Ce_{0.98}Rh_{0.02}O_{2-\delta}$ at lower temperature seems to be due to higher NO adsorption on Rh^{3+} sites. Further, Rh ion being in +3 state, there is less oxide ion vacancy in Rh^{3+} substituted CeO_2 compared to Pd^{2+} substituted CeO_2. Therefore, $NO \rightarrow N_2O$ conversion is facilitated as NO being more molecularly adsorbed on Rh^{3+} sites and less dissociatively adsorbed on the vacant sites of $Ce_{0.98}Rh_{0.02}O_{1.99}$ at low temperature. However, at higher temperature, NO as well as N_2O dissociation is more and $NO \rightarrow N_2$ takes place. In contrast, $NO \rightarrow N_2$ conversion predominates on $Ce_{0.98}Pd_{0.02}O_{1.98}$ catalyst in the entire range of temperature.

For $NO + H_2$ reaction over $Ti_{0.99}M_{0.01}O_{2-\delta}$ (M = Pd, Pt, Rh and Ru) catalysts, both NO and H_2 are adsorbed on noble metal ion sites and NO is also adsorbed on the oxide

ion vacancy sites.[54] The formation of N_2O occurs because of close proximity of N atom of adsorbed NO and the N atom of adsorbed NO on oxide ion vacancy sites. The hydrogen atom from the noble metal ion site reacts with the oxygen in oxide ion vacant site to form water. N_2O molecule dissociates directly into N_2 and O atom in oxide ion vacancy sites. NH_3 can also be formed with the combination of adsorbed H atom with adsorbed NO in oxygen vacancy sites.

NH_3-TPD demonstrates that low temperature SCR activity of $Ti_{0.9}Mn_{0.1}O_{2-\delta}$ is due to the highest Brønsted acidity seen over this catalyst, whereas highest Lewis acidity in $Ti_{0.9}Fe_{0.1}O_{2-\delta}$ corresponds to wide SCR window.[163] Therefore, NH_3 can be adsorbed on the surface as NH_4^+ or as a molecular NH_3 in the case of Brønsted acid sites and Lewis acid sites, respectively. NO can be adsorbed molecularly on the transition metal ion or it can dissociatively chemisorb in the oxide ion vacancy of the catalysts. The adsorbed NH_3 or NH_4^+ can form an adduct with the adsorbed NO and the NH_2NO adduct dissociates into N_2 and H_2O. This path of dissociation dominates in the case of $Ti_{0.9}Fe_{0.1}O_{2-\delta}$ and $Ti_{0.9}Mn_{0.05}Fe_{0.05}O_{2-\delta}$. However, NH_2NO dissociating into N_2O is more likely to be favored over $Ti_{0.9}Mn_{0.1}O_{2-\delta}$. So, a "dual site-redox" mechanism occurs on these catalysts surface. However, if the adsorbed NH_3 reacts with the oxygen to form a NH_2OO adduct, it produces NO and the SCR window becomes narrow. This seems to be the mechanism for $Ti_{0.9}Cu_{0.1}O_{2-\delta}$. Thus, it has been have showed that the SCR reaction occurs at the lowest temperature with the highest N_2 selectivity over the catalysts that have Brønsted and Lewis acid sites for NH_3 adsorption as well as oxide ion vacancies for NO dissociation.

It has been proposed for WGS reaction that CO gets adsorbed on noble metal ionic sites, whereas H_2O is dissociatively adsorbed over oxide ion vacancy sites.[199] Surface reaction between two adsorbed species results in the formation of products that restores the catalyst upon desorption. From kinetic rate expression it has been demonstrated that WGS reaction over noble metal ionic catalysts does not follow Eley–Rideal and Langmuir–Hinshelwood mechanisms. Apparent activation energies are found to be less considering dual site mechanism for WGS reaction over NMICs.

In case of photocatalytic reduction of NO over $Ti_{0.99}Pd_{0.01}O_{1.98}$, the presence of Pd^{2+} ion sites for adsorption of CO, oxide ion vacancy sites and UV light are primary requirements for the photodecomposition of NO. A detailed mechanism accounts that there is a competitive adsorption of NO and CO on Pd^{2+} sites and high rate of NO photodissociation on the vacant oxide ion site present on the catalyst surface enhances NO reduction and decomposition activity.[53]

$Ce_{0.98}Pd_{0.02}O_{1.98}$ catalyst has two distinct sites such as Pd^{2+} ions and oxide ion vacancies. Electron deficient Pd^{2+} sites are useful for adsorption of donor molecules, whereas oxide ion vacant sites next to Pd^{2+} ions act as sites for adsorption of acceptor molecules. In Heck reaction over this catalyst, olefin is adsorbed on Pd^{2+} ions, whereas oxide ion vacancies are nucleophilic sites ideal for accommodation of –Br, –I of aryl halides.[192] Elimination of HBr facilitated by the base leads to C–C coupling.

13. DFT studies of noble metal ionic catalysts for higher OSC, adsorption and catalytic properties

In last several decades, enormous amounts of works on synthesis, structure and catalytic properties of CeO_2 related materials with different aspects have been investigated. It has

been found that OSC and catalytic activities of CeO_2 based materials get enhanced when CeO_2 is substituted with several divalent, trivalent and tetravalent metal ions. Substitution of noble metal ions into CeO_2 further augments these properties. In this sense, there should have been changes in the atomic environment of parent CeO_2 structure after substitution of metal ions that leads to the enhancement of OSC and catalytic activities. OSC of CeO_2 is observed to enhance by the substitution of Zr^{4+} ion for Ce^{4+} site in CeO_2.[117,118,140,200] As ZrO_2 itself cannot be reduced by H_2, this observation is a surprising result. OSC studies demonstrate that reducilibity of CeO_2 is increased by Ti^{4+} substitution in $Ce_{1-x}Ti_xO_2$.[47] Again, Pt ion substitution in $Ce_{1-x}Ti_xO_2$ enhances its reducilibity further compared to $Ce_{1-x}Ti_xO_2$ and $Ce_{1-x}Pt_xO_2$. Rate of CO conversion in CO + O_2 reaction over Pt ion substituted $Ce_{1-x}Ti_xO_2$ is observed to be much higher than $Ce_{1-x}Pt_xO_2$.[47] Therefore, several questions can be raised naturally about these findings. In this regard, what is the structural and chemical origin of increased OSC in transition metal ion substituted CeO_2? What is the effect of noble metal substitution on structural and chemical origin for higher OSC and high catalytic activities of CeO_2? Simulation of crystal structure of CeO_2 based catalysts and probe reactions with these catalysts employing DFT calculation has provided answers to these questions.[50,51,201–223]

First conception of the activation of lattice oxygen of CeO_2 by the substitution of smaller ion has been originated from the substitution of Zr^{4+} ion into CeO_2 lattice in $Ce_{1-x}Zr_xO_2$ (x = 0.0–0.5) solid solutions.[140] Structure can be simulated by DFT calculations considering a lattice containing 32 Ce^{4+} ions and 64 O^{2-} ions in their crystal positions in a fluorite lattice. CeO_2 crystallizes in fluorite structure where Ce^{4+} ion is inside the cube formed by eight oxide ions or coordination number of Ce^{4+} is 8. Each O^{2-}

is coordinated with four Ce^{4+} ions. Because of smaller ionic radius of Zr^{4+} (0.84 Å) compared to Ce^{4+} (0.97 Å) lattice parameter decreases when Zr^{4+} ion is substituted into eO_2 lattice. Ce^{4+} and Zr^{4+} ions are occupied in the alternate cubes in $Ce_{16}Zr_{16}O_{64}$ ideal lattice. When the smaller Zr^{4+} ion is occupied in place of Ce^{4+} ion, the Zr^{4+} ion does not have complete contact with the 8 oxide ions. Accordingly, in the $[ZrO_8]$ cube, alternate four oxide ions come closer to Zr^{4+} ion forming a tetrahedron with a shortened Zr−O distance and other four oxide ions also form a tetrahedron with longer Zr−O distance. Distortion in ZrO_8 cube will induce distortion in CeO_8 cube also leading to 4+4 coordination that creates long Ce−O and short Ce−O bonds compared to 2.34 Å in pure CeO_2. Longer Ce−O bond is naturally weaker. There is a distribution of bond lengths from the mean Ce−O values when Zr^{4+} ion is substituted.[24] Longer Ce−O bonds indeed are weaker and hence they can be more easily extracted by H_2 that leads to higher OSC.[140] Similarly, XAFS studies and DFT calculations show the presence of short and long Ce–O and Ti–O bonds in $Ce_{1-x}Ti_xO_2$ which gives strong and weakly bound oxygens.[141] The stronger bonds have a valency greater than 2 and the weaker ones have a valency less than 2 and weakly bound oxygen has been found to be responsible for higher OSC in these mixed oxides.

It has been demonstrated that CeO_2 doped with several transition, noble and rare earth metals undergoes structural distortion that enhances higher oxygen storage capacity.[50,51,201–203] On the other hand, this kind of situation cannot be found in pure CeO_2 and TiO_2, thereby these pure oxides show lower OSC compared to mixed oxides. For example, structural simulations of CeO_2, $Ce_{0·8}Sn_{0·2}O_{2-\delta}$ and $Ce_{0·78}Sn_{0.2}Pd_{0·02}O_{2-\delta}$ have been carried out by DFT calculations using their respective Ce_4O_8, $Ce_{26}Sn_6O_{64}$ and

$Ce_{25}Sn_6Pd_1O_{63}$ supercells.[50] Bond length distributions of Ce_4O_8, $Ce_{26}Sn_6O_{64}$ and $Ce_{25}Sn_6Pd_1O_{63}$ supercells are shown in Fig. 15. Optimized Ce_4O_8 supercell has all Ce–O distance equal to 2.34 Å. In contrast, Ce–O bonds get distributed in shorter and longer bonds over a range of 2.16 to 2.54 Å in $Ce_{26}Sn_6O_{64}$ supercell. Sn–O and Pd–O bonds get longer in $Ce_{0·78}Sn_{0.2}Pd_{0·02}O_{2-\delta}$ with oxygen vacancy where oxygen sites are highly activated and can easily be removed from the lattice leading to higher OSC. With increase in Sn content larger number of longer Sn–O bonds is obtained in $Ce_{16}Sn_{16}O_{64}$ supercell related to $Ce_{0·5}Sn_{0·5}O_{2-\delta}$ in comparison with $Ce_{26}Sn_6O_{64}$ supercell and thus, $Ce_{0·5}Sn_{0·5}O_{2-\delta}$ shows higher OSC in relation to $Ce_{0·8}Sn_{0·25}O_{2-\delta}$. With introduction of Pd^{2+} ions in $Ce_{0·5}Sn_{0·5}O_{2-\delta}$ Ce–O and Sn–O bonds exhibit wider distribution in $Ce_{16}Sn_{15}Pd_1O_{63}$ supercell and here Pd–O bonds are longer than $Ce_{25}Sn_6Pd_1O_{63}$ supercell. Similarly, substitution of Pd^{2+} in $Ce_{1-x}Fe_xO_2$ enhances OSC and catalytic activities.[51] It has also been observed that transition metal ion substitution in CeO_2 greatly enhances its reducibility in $Ce_{1-x}M_xO_{2-\delta}$ solid solution leading to higher OSC due to longer Ce–O and M–O bonds, whereas rare earth metal ion substitution has little effect on it.[202] Substitution of noble metal ions further enhances the OSC due to presence of still longer bonds. It has also been demonstrated that Pt^{2+}, Pd^{2+} and Cu^{2+} ions are stabilized in CeO_2 matrix and CO gets adsorbed only on Pt^{2+}, Pd^{2+} and Cu^{2+} sites present on CeO_2 surface.[204]

Both structural and electronic factors help to make CeO_2 more reducible in Pd^{2+}, Pt^{2+} and Rh^{3+} doped CeO_2 than pure CeO_2 and Zr^{4+} doped CeO_2 as shown by Yang et al.[205] Wang and coworkers have proposed a model to understand the oxygen vacancy formation in a series of $Ce_{1-x}Zr_xO_2$ materials that consists bond energy (E_{bond}) and

relaxation energy (E_{relax}).[206] It has been found that relaxation energy plays a vital role in affecting the oxygen vacancy formation energy and $Ce_{0.5}Zr_{0.5}O_2$ possesses the lowest formation energy of oxygen vacancy which is the origin of its best OSC performance. Metiu and coworkers have demonstrated that doping of Pt in CeO_2 surface weakens the bond of oxygen atoms in the neighborhood as evidenced by lowering the formation energy of oxygen vacancy. The easier specific oxygen atoms are to remove, more reactive they are when exposed to a reductant.[77] Similarly, it works for other doped CeO_2 materials.[209] Au^{3+} substituted CeO_2 is more active for CO oxidation than single Au^+ species supported on stoichiometric CeO_2 as demonstrated by Camellone and Fabris with DFT studies.[210] This higher catalytic activity is due to the formation of oxygen vacancy and the interplay between reversible Au^{3+}/Au^+ and Ce^{4+}/Ce^{3+} reductions. Chen et al. have found that substitution of Fe, Ru, Os, Sm, Pu in CeO_2 results in activated oxygen in $Ce_{1-x}M_xO_2$ compared to pure CeO_2 due to its structural and electronic modifications and oxygen vacancy formation is lowered by doping of noble metals.[211] Watson group has showed with DFT calculations that increased OSC in Pt and Pd doped CeO_2 is due to a large displacement of dopant ions from Ce lattice site. Pd^{2+} and Pt^{2+} with d^8 configuration moves by ~1.2 Å to adopt a square planar coordination with four lattice oxygen due to crystal field effect.[212] This large lattice distortion leaves three oxygen atoms under-coordinated or weakly bound in the vicinity of the dopant that are more facile to remove than oxygen atom in pure CeO_2. Similarly, several divalent dopant metal ions like Be^{2+}, Mg^{2+}, Ca^{2+}, Ni^{2+}, Cu^{2+} and Zn^{2+} distort to have coordination of their own binary oxide, instead of cubically coordinated Ce in CeO_2. Depending on the electronic structure of the dopants, the different coordinations can create weakly or under-coordionated oxygen ions

that are more easily removed than in pure CeO_2.[213] Recently, Nolan has shown that divalent Pd and Ni in $CeO_2(111)$ and $CeO_2(110)$ surfaces distort the local atomic environment and most stable structure for both dopants arises through compensation of dopant +2 valency by oxygen vacancy formation.[214] Both Pd^{2+} and Ni^{2+} dopants lower the formation energy of oxygen vacancy. In an another study, it is found that strong interactions exist between the Pt and the surfaces and the Pt adsorption is stronger on the reduced surface than that on the unreduced surface.[215] Pt–O–Ce bond may be formed between Pt adatom and CeO_2 surface. Thus, DFT calculations provide local structure, metal–oxygen distances, density of valence states to understand OSC, adsorption and catalytic properties.

OSC of $Ti_{0.97}Pd_{0.03}O_{1.97}$ is as high as 5100 μmol g^{-1}. Oxygen is extracted by CO resulting in CO_2 in absence of feed oxygen even at room temperature which is more than 20 times compared to pure TiO_2. Rate of CO oxidation is 2.75 μmol g^{-1} s^{-1} at 60 °C over $Ti_{0.97}Pd_{0.03}O_{1.97}$. Such a high catalytic activity is due to activated lattice oxygen created by the substitution of Pd^{2+} ion as seen from DFT calculations with 96 atom supercells of $Ti_{32}O_{64}$, $Ti_{31}Pd_1O_{63}$, $Ti_{30}Pd_2O_{62}$ and $Ti_{29}Pd_3O_{61}$ related to TiO_2, $Ti_{0.99}Pd_{0.01}O_{2-\delta}$, $Ti_{0.98}Pd_{0.02}O_{2-\delta}$ and $Ti_{0.97}Pd_{0.03}O_{2-\delta}$, respectively.[55] Ti–O bond distribution in $Ti_{32}O_{64}$ supercell has two types of Ti–O bonds at 1.93 and 1.97 Å. Bond length of 1.93 Å corresponds to Ti ion that is coordinated with four oxygen atoms in a planar geometry and other one is related to Ti ion coordinating with two axial oxygen atoms in addition to 4 planar oxygens. Upon substitution of Pd^{2+}, there is a distortion in the structure resulting in the metal–oxygen bonds with long and short distances compared to pure TiO_2. Four Pd–O bonds in the three Pd^{2+} ion substituted compounds are in nearly square planar

geometry with Pd–O short bonds between 1.97 to 2.0 Å. Bond distributions for both Ti–O and Pd–O bonds in all the simulated compounds are given in figure 2.13. Ti–O bonds in TiO_6 are distorted with reference to pure TiO_2 by the creation of longer and shorter Ti–O bonds. Similarly, By substitution of Pt^{2+} ion in TiO_2, there is a large change in bond distribution, with short and long bond lengths of metal–oxygen compared with $Ti_{32}O_{64}$.[56] In $Ti_{31}Pt_1O_{63}$ supercell, Pt^{2+} ion is coordinated with four oxygens in a square planar geometry having two Pt–O bonds of 1.98 Å and the other two Pt–O bonds of 2.00 Å. As a result of Pt^{2+} substitution, two shorter Ti–O bonds of 1.81 Å and one longer Ti–O bond of 2.18 Å occur coordinating the same oxygen atom. In $Ti_{30}Pt_2O_{62}$, there is slightly increased in the bond length distribution as compared to that in $Ti_{31}Pt_1O_{63}$. Bond length distributions in two different configurations of $Ti_{29}Pt_3O_{61}$ are in similar trend and these have slightly more distribution as compared to that in $Ti_{30}Pt_2O_{62}$. Chrétien and Metiu have demonstrated that doping TiO_2 with Cu, Ag, Au, Ni, Pd and Pt weakens the bond of surface oxygen and oxide that makes them better oxidation catalysts.[224] Strong electron transfer from Ru to TiO_2(101) makes Ru particles positively charged that lowers activation energy for CO dissociation resulting highly catalytic activity toward CO_2 methanation.[225]

It has been established from our studies that noble metal ion substituted CeO_2 and TiO_2 catalysts show higher OSC as well as catalytic activities towards several important reactions. DFT calculations have been carried out to understand the causes behind higher OSC and catalytic properties in CeO_2 and TiO_2 based materials. From our DFT studies along with H_2-TPR and XAFS, it has been found that change of structure at the atomic level is to be the reason for higher OSC in these types of mixed oxides. Because of the

smaller size of substituent cations, surrounding oxygen ions are displaced from the original position and the oxygens at a larger distance are removed by reducing gases easily.

14. Conclusions and future outlook

Dispersion of noble metal ions over CeO_2 and TiO_2 by solution combustion method resulting in $Ce_{1-x}M_xO_{2-\delta}$, $Ce_{1-x-y}Ti_xM_yO_{2-\delta}$, $Ce_{1-x-y}Sn_xM_yO_{2-\delta}$, $Ce_{1-x-y}Fe_xM_yO_{2-\delta}$ and $Ce_{1-x-y}Zr_xM_yO_{2-\delta}$ and $Ti_{1-x}M_xO_{2-\delta}$ (M = Pd, Pt, Rh and Ru) catalysts from an entirely different view point, structure of these materials and their catalytic properties are documented here. In these materials, noble metal ions are present as ions and they are incorporated into the reducible oxide matrices like CeO_2 and TiO_2 to a certain limit as the solution combustion method is a redox reaction type of preparation procedure. Hydrothermal and sonochemical methods have also been adopted to substitute aliovalent and isovalent noble metal ions in CeO_2 and TiO_2 matrices. Extensive experimental and theoretical works done by our group and other research groups have established that these ionically dispersed noble metal catalysts are catalytically much more active than conventional finely dispersed noble metal particles toward several important reactions such as CO oxidation, NO reduction by CO, H_2 and NH_3, selective catalytic reduction of NO, hydrocarbon oxidation, water gas shift reaction, CO–PROX reaction, H_2–O_2 reaction and hydrogenation. The idea of dispersing noble metals as ions can be extended to the other reducible transition metal oxide supports such as SnO_2, V_2O_5, WO_3 and MoO_3. These catalysts can be probed for several catalytic reactions exploring more insights into the metal–support interaction, redox properties and synergistic effects. In general, extensive studies on these NMIC materials for several heterogeneous catalytic

reactions relevant to requirement for present days other than exhaust catalytic reactions are worthwhile area to carry out on the basis of solid state chemistry view point.

Acknowledgments

We thank our past and present laboratory members and collaborators for their significant contributions. We thank Department of Science and Technology (DST), Government of India for financial support. MSH is grateful to Council of Scientific and Industrial Research (CSIR), Government of India for an Emeritus Professor Fellowship.

References

1. J. T. Richardson, *Principles of Catalyst Development*, Plenum Press, New York, 1989.
2. J. M. Thomas and W. J. Thomas, *Principles and Practice of Heterogeneous Catalysis*, VCH, Weinheim, 1997.
3. I. Chorkendorff and J. W. Niemantsverdriet, *Concepts of Modern Catalysis and Kinetics*, Wiley-VCH, Weinheim, 2003.
4. J. A. Anderson and M. F. García, *Supported Metals in Catalysis*, Imperial College Press, London, 2005.
5. J. Hagen, *Industrial Catalysis*, Wiley-VCH, Weinheim, 2006.
6. G. Rothenberg, *Catalysis: Concepts and Green Applications*, Wiley-VCH, Weinheim, 2008.
7. J. R. H. Ross, *Heterogeneous Catalysis: Fundamentals and Applications*, Elsevier, Oxford, 2012.
8. G. C. Bond, *Catalysis by Metals*, Academic Press, New York, 1962.

9. J. R. Anderson, *Structure of Metallic Catalysts*, Academic Press, NY, London, 1975.

10. H. S. Gandhi, G. W. Graham and R. W. McCabe, *J. Catal.*, 2003, **216**, 433.

11. J. C. Summers and S. A. Ausen, *J. Catal.*, 1979, **58**, 131.

12. H. C. Yao, H. S. Gandhi and M. Shelef, *Metal─Support and Metal─Additive Effects in Catalysis*, Eds. B. Imelik, C. Naccache, G. Coudurier, H. Praliaud, P. Meriaudeau, P. Gallezot, G. A. Martin and J. C. Vedrine, Elsevier, Amsterdam, 1982, p. 159.

13. H. C. Yao and Y. F. Y. Yao, *J. Catal.*, 1984, **86**, 254.

14. J. T. Kummer, *J. Phys. Chem.*, 1986, **90**, 4747.

15. S. E. Oh and C. C. Eickel, *J. Catal.*, 1988, **112**, 543.

16. G. Munuera, A. Fernandez and A. R. Gonzalez-Elipe, *Stud. Surf. Sci. Catal.*, 1991, **71**, 207.

17. J. G. Nunan, H. J. Robota, M. J. Cohn and S. A. Bradley, *Stud. Surf. Sci. Catal.*, 1991, **71**, 221.

18. J. Kašpar, P. Fornasiero and N. Hickey, *Catal. Today*, 2003, **77**, 419.

19. T. X. T. Sayle, S. C. Parker and C. R. A. Catlow, *J. Phys. Chem.*, 1994, **98**, 13625.

20. P. Bera, K. C. Patil, V. Jayaram, G. N. Subbanna and M. S. Hegde, *J. Catal.*, 2000, **196**, 293.

21. M. S. Hegde, K. C. Patil and G. Madras, *Acc. Chem. Res.*, 2009, **42**, 704.

22. P. Bera and M. S. Hegde, *J. Indian Inst. Sci.*, 2010, **90**, 299.

23. P. Bera and M. S. Hegde, *Catal. Surv. Asia*, 2011, **15**, 181.

24. M. S. Hedge and P. Bera, *Catal. Today*, 2015, **253**, 40.

25. A. Corma and H. Garcia, *Chem. Soc. Rev.*, 2008, **37**, 2096.

26. J. C. Fierro-Gonzalez and B. C. Gates, *Chem. Soc. Rev.*, 2008, **37**, 2127.

27. M. Flytzani-Stephanopoulos and B. C. Gates, *Annu. Rev. Chem. Biomol. Eng.*, 2012, **3**, 545.

28. F. J. Janssen, *Handbook of Heterogeneous Catalysis*, Ed. G. Ertl, H. Knözinger and J. Weitkamp, VCH, Weinheim, 1997, Vol.1, p.191.

29. R. L. Augustine, *Heterogeneous Catalysis for the Synthetic Chemist*, Marcel Dekker, Inc., New York, 1996, p. 267.

30. M. A. Cauqui and J. M. Rodríguez-Izquierdo, *J. Non-Cryst. Solids*, 1992, **147-148**, 724.

31. P. Turlier, H. Praliaud, P. Moral, G. A. Martin and J. A. Dalmon, *Appl. Catal.*, 1985, **19**, 286.

32. A. Hadi and I. I. Yaacob, *Mater. Lett.*, 2007, **61**, 93.

33. T. Masui, K. Fujiwara, Y. Penga, T. Sakatab, K. Machida, H. Mori and G. Adachi, *J. Alloys Compd.*, 1998, **269**, 116.

34. A. Suda, T. Kandori, N. Terao, Y. Ukyo, H. Sobukawa and M. Sugiura, *J. Mater. Sci. Lett.*, 1998, **17**, 89.

35. S. Enzo, F. Delogu, R. Frattini, A. Primavera and A. Trovarelli, *J. Mater. Res.*, 2000, **15**, 1538.

36. K. C. Patil, M. S. Hegde, T. Rattan and S. T. Aruna, *Chemistry of Nanocrystalline Oxide Materials: Combustion Synthesis, Properties and Applications*, World Scientific, Singapore, 2008.

37. W. Wen and J.-M. Wu, *RSC Adv.*, 2014, **4**, 58090.

38. A. G. Merzhanov, *SHS Research and Development Handbook*, Chernogolovka, Russia, Russian Academy of Sciences, 1999.

39. K. C. Patil, S. T. Aruna and S. Ekabaram, *Curr. Opi. Solid State Mater. Sci.*, 1997, **2**, 158.

40. K. C. Patil, S. T. Aruna and T. Mimani, *Curr. Opi. Solid State Mater. Sci.*, 2002, **6**, 507.

41. S. L. González-Cortés and F. E. Imbert, *Appl. Catal. A*, 2013, **452**, 117.

42. P. Bera, K. C. Patil, V. Jayaram, M. S. Hegde and G. N. Subbanna, *J. Mater. Chem.*, 1999, **9**, 1801.

43. K. R. Priolkar, P. Bera, P. R. Sarode, M. S. Hegde, S. Emura, R. Kumashiro and N. P. Lalla, *Chem. Mater.*, 2002, **14**, 2120.

44. A. Gayen, K. R. Priolkar, P. R. Sarode, V. Jayaram, M. S. Hegde, G. N. Subbanna and S. Emura, *Chem. Mater.*, 2004, **16**, 2317.

45. P. Bera, K. C. Patil and M. S. Hegde, *Phys. Chem. Chem. Phys.*, 2000, **2**, 3715.

46. P. Bera and M. S. Hegde, *Catal. Lett.*, 2002, **79**, 75.

47. T. Baidya, A. Gayen, M. S. Hegde, N. Ravishankar and L. Dupont, *J. Phys. Chem. B*, 2006, **110**, 5262.

48. T. Baidya, A. Marimuthu, M. S. Hegde, N. Ravishankar and G. Madras, *J. Phys. Chem. C*, 2007, **111**, 830.

49. T. Baidya, A. Gupta, P. A. Deshpandey, G. Madras and M. S. Hegde, *J. Phys. Chem. C*, 2009, **113**, 4059.

50. A. Gupta, M. S. Hegde, K. R. Priolkar, U. V. Waghmare and P. R. Sarode, S. Emura, *Chem. Mater.*, 2009, **21**, 5836.

51. A. Gupta, A. Kumar, U. V. Waghmare and M. S. Hegde, *Chem. Mater.*, 2009, **21**, 4880.

52. T. Baidya, G. Dutta, M. S. Hegde and U. V. Waghmare, *Dalton Trans.*, 2009, **38**, 455.

53. S. Roy, M. S. Hegde, N. Ravishankar and G. Madras, *J. Phys. Chem. C*, 2007, **111**, 8153.

54. S. Roy, M. S. Hegde, S. Sharma, N. P. Lalla, A. Marimuthu and G. Madras, *Appl. Catal. B*, 2008, **84**, 341.

55. B. D. Mukri, G. Dutta, U. V. Waghmare and M. S. Hegde, *Chem. Mater.*, 2012, **24**, 4491.

56. B. D. Mukri, U. V. Waghmare and M. S. Hegde, *Chem. Mater.*, 2013, **25**, 3822.

57. R. M. Barrer, *Hydrothermal Chemistry of Zeolites*, Academic Press, London, 1982.

58. W.-Q. Han, L. Wu and Y. Zhu, *J. Am. Chem. Soc.*, 2005, 127, 12814.

59. Z. Y. Zhong, T.-P. Ang, J. Z. Luo, H.-C. Gan and A. Gedanken, *Chem. Mater.*, 2005, **17**, 6814.

60. W. Hung, P. Shuk and M. Greenblatt, *Chem. Mater.*, 1997, **9**, 2240.

61. P. Singh and M. S. Hegde, *J. Solid State Chem.*, 2008, **181**, 3248.

62. P Singh, M. S. Hegde and J. Gopalakrishnan, *Chem. Mater.*, 2008, **20**, 7268.

63. P. Singh and M. S. Hegde, *Chem. Mater.*, **21**, 3337 (2009).

64. L. Yin, Y. Wang, G. Pang, Y. Koltypin and A. Gedanken, *J. Colloid Interface Sci.*, 2002, **246**, 78.

65. S. Bhattacharyya and A. Gedanken, *Microporous Mesoporous Mater.*, 2008, **110**, 553.

66. R. K. Selvan, A. Gedanken, , P. Anilkumar, G. Manikandan and C. Karunakaran, *J. Cluster Sci.*, 2009, **20**, 291.

67. V. K. Rangari, D. N. Srivastava and A. Gedanken, *Mater. Lett., 2006,* **60***,* 3766.

68. S. Shanmugam and A. Gedanken, *J. Phys. Chem. C, 2009,* **113**, 18707.

69. P. Singh and M. S. Hegde, *Cryst. Growth Design*, 2010, **10**, 2995.

70. P. Singh and M. S. Hegde, *Dalton Trans.*, 2010, **39**, 10768.

71. P. Bera, A. Gayen, M. S. Hegde, N. P. Lalla, L. Spadaro, F. Frusteri and F. Arena, *J. Phys. Chem. B*, 2003, **107**, 6122.

72. P. Bera, K. R. Priolkar, A. Gayen, P. R. Sarode, M. S. Hegde, S. Emura, R. Kumashiro, V. Jayaram and G. N. Subbanna, *Chem. Mater.*, 2003, **15**, 2049.

73. A. Gayen, T. Baidya, K. Biswas, S. Roy and M. S. Hegde, *Appl. Catal. A*, 2006, **315**, 135.

74. P. Bera, S. T. Aruna, K. C. Patil and M. S. Hegde, *J. Catal.*, 1999, **186**, 36.

75. P. Bera, K. R. Priolkar, P. R. Sarode, M. S. Hegde, S. Emura, R. Kumashiro, N. P. Lalla, *Chem. Mater.* 2002, **14**, 3591.

76. G. Li, L. Li, Y. Yuan, J. Shi, Y. Yuan, Y. Li, W. Zhao and J. Shi, *Appl. Catal. B*, 2014, **158−159**, 341.

77. W. Tang, Z. Hua, M. Wang, G.D. Stucky, H. Metiu and E. W. McFarland, *J. Catal.*, 2010, **273**, 125.

78. B. Wang, D. Weng, X. Wu and J. Fan, *Catal. Today*, 2010, **153**, 111.

79. A. Bisht, B. P. Gangwar, T. Anupriya and S. Sharma, *J. Solid State Electrochem.*, 2014, **18**, 197.

80. S.-Y. Wang, N. Li, R.-M. Zhou, L.-Y. Jin, G.-S. Hu, J.-Q. Lu and M.-F. Luo, *J. Mol. Catal. A*, 2013, **374–375**, 53.

81. L. M. Misch, J. A. Kurzman, A. R. Derk, Y.-.I. Kim, R. Seshadri, H. Metiu, E. W. McFarland and G. D. Stucky, *Chem. Mater.*, 2011, **23**, 5432.

82. E. M. Slavinskaya, R. V. Gulyaev, A. V. Zadesenets, O. A. Stonkus, V. I. Zaikovskii, Yu. V. Shubin, S. V. Korenev and A. I. Boronin, *Appl. Catal. B*, 2015, **166–167**, 91.

83. G. Li, L. Li and D. Jiang, *J. Phys. Chem. C*, 2015, **119**, 12520.

84. A. V. Malyutin, A. I. Mikhailichenko, Ya. V. Zubavichus, V. Yu. Murzin, A. G. Koshkin and I. V. Sokolov, *Kinet. Catal.*, 2015, **56**, 89.

85. W. Miao, S. Meiqing, W. Jianqiang, W. Guangxi, L. Hang and W. Jun, *J. Rare Earths*, 2014, **32**, 1114.

86. R. V. Gulyaev, E. M. Slavinskaya, S. A. Novopashin, D. V. Smovzh, A. V. Zaikovskii, D. Yu. Osadchii, O. A. Bulavchenko, S. V. Korenev and A. I. Boronin, *Appl. Catal. B*, 2014, **147**, 32.

87. H.-H. Liu, Y. Wang, A.-P. Jia, S.-Y. Wang, M.-F. Luo and Z.-Q. Lu, *Appl. Surf. Sci.*, 2014, **314**, 725.

88. R. V. Gulyaev, D. Yu. Osadchii, S. V. Koscheev and A. I. Boronin, *J. Struct. Chem.*, 2015, **56**, 566.

89. F. Pilger, A. Testino, M. A. Lucchini, A. Kambolis, M. Tarik, M. E. Kazzi, Y. Arroyo, M. D. Rossell and C. Ludwig, *J. Nanosci. Nanotechnol.*, 2015, **15**, 3530.

90. Q. Fu, H. Saltsburg and M. Flytzani-Stephanopoulos, *Science*, 2003, **301**, 935.

91. X. Tang, B. Zhang, Y. Li, Y Xu, Q. Xin and W. Shen, *Catal. Lett.*, 2004, **97**, 163.

92. J. Lin, L. Zhang, Z. Wang, J. Ni, R. Wang and K. Wei, *J. Mol. Catal. A*, 2013, **366**, 375.

93. M. Kurnatowska, W. Mista, P. Mazur and L. Kepinski, *Appl. Catal. B*, 2014, **148–149**, 123.

94. L. Ge, T. Chen, Z. Liu and F. Chen, *Catal. Today*, 2014, **224**, 209.

95. A. Karpenko, R. Leppelt, V. Plzak and R. J. Behm, *J. Catal.*, 2007, **252**, 231.

96. L. Wang, H. He, Y. Yu, L. Sun, S. Liu, C. Zhang and L. He, *J. Inorg. Biochem.*, 2014, **135**, 45.

97. M. S. Chen and D. W. Goodman, *Top. Catal.*, 2007, **44**, 41.

98. T. Baidya, K. R. Priolkar, P. R. Sarode, M. S. Hegde, K. Asakura, G. Tateno and Y. Koike, *J. Chem. Phys.*, 2008, **128**, 124711.

99. T. Baidya, P. Bera, B. D. Mukri, S. K. Parida, O. Kröcher, M. Elsener and M. S. Hegde, *J. Catal.*, 2013, **303**, 117.

100. T. Baidya and P. Bera, *Catal. Struct. Reac.* (DOI: http://dx.doi.org/10.1179/2055075815Y.0000000004).

101. C. T. Driscoll, K. M. Driscoll, M. J. Mitchell and D. J. Raynal, *Environ. Pollu.*, 2008, **123**, 327.

102. K. Marilena and E. Castanas, *Environ. Pollu.*, 2008, **151**, 362.

103. A. J. Haagen-Smit, *Ind. Eng. Chem.*, 1952, **44**, 1342.

104. P. L. Magill and R. W. Benoliel, *Ind. Eng. Chem.*, 1952, **44**, 1347.

105. A. J. Haagen-Smit and M. M. Fox, *Ind. Eng. Chem.*, 1956, **48**, 1484.

106. F. E. Littman, H. W. Ford and N. Endow, *Ind. Eng. Chem.*, 1956, **48**, 1492.

107. E. R. Stephens, P. L. Hanst, R. C. Doerr and W. E. Scott, *Ind. Eng. Chem.*, 1956, **48**, 1498.

108. A. Troveralli, *Catalysis by Ceria and Related Materials*, Imperial College Press, London, 2002.

109. A. Troveralli, *Catalysis by Ceria and Related Materials*, 2nd Edition, Imperial College Press, London, 2013.

110. M. V. Twigg, *Phil. Trans. R. Soc. A*, 2005, **363**, 1013.

111. F. Klingstedt, K. Arve, K. Eränen and D. Yu. Murzin, *Acc. Chem. Res.*, 2006, **39**, 273.

112. E. S. J. Lox, *Handbook of Heterogeneous Catalysis*, 2nd Edition, Vol. 5, Eds.: G. Ertl, H. Knözinger, F. Schüth and J. Weitkamp, Wiley-VCH, Weinheim, 2008, p. 2274.

113. P. Gabrielsson and H. G. Pedersen, *Handbook of Heterogeneous Catalysis*, 2nd Edition, Vol. 5, Eds.: G. Ertl, H. Knözinger, F. Schüth and J. Weitkamp, Wiley-VCH, Weinheim, 2008, p. 2345.

114. M. Bowker, *Chem. Soc. Rev.*, 2008, **37**, 2204.

115. P. Granger and V. I. Parvulescu, *Chem. Rev.*, 2011, **111**, 3155.

116. R. J. Farrauto and R. M. Heck, *Catal. Today*, 1999, **51**, 351.

117. A. Troveralli, *Catal. Rev. Sci. Eng.*, 1996, **38**, 439.

118. A. Troveralli, *Comments Inorg. Chem.*, 1999, **20**, 263.

119. P. Bera, Ph. D. Thesis, Indian Institute of Science, Bangalore, India, 2002.

120. T. P. Kobylinski and B. W. Taylor, *J. Catal.*, 1974, **33**, 376.

121. G. L. Bauerle, S. C. Wu and K. Nobe, *Ind. Eng. Chem. Prod. Res. Dev.*, 1975, **14**, 123.

122. J. T. Kummer, *J. Phys. Chem.*, 1986, **90**, 4747.

123. H. Bartholomew, *Ind. Eng. Chem. Prod. Res. Dev.*, 1975, **14**, 29.

124. G. L. Bauerle and K. Nobe, *Ind. Eng. Chem. Prod. Res. Dev.*, 1974, **13**, 185.

125. M. Iwamoto, *Stud. Surf. Sci. Catal.*, 1994, **84**, 1395.

126. T. Seiyama, T. Arakawa, T. Matsuda, Y. Takita and N. Yamazoe, *J. Catal.*, 1977, **48**, 1.

127. T. Komatsu, M. Nunokawa, I. S. Moon, T. Takahara, S. Namba and T. Yashima, *J. Catal.*, 1998, **148**, 427.

128. R. T. Yang, T. J. Pinnavaia, W. Li and W. Zhang, *J. Catal.*, 1997, **172**, 488.

129. E. Ito, Y. J. Mergler, B. E. Nieuwenhuys, H. P. A. Calis, H. van Bekkum and C. M. van den Bleek, *J. Chem. Soc., Faraday Trans.*, 1996, **92**, 1799.

130. J. A. Martens, A. Cauvel, A. Francis, C. Hermans, F. Jayat, M. Remy, M. Keung, J. Lievens and P. A. Jacobs, *Angew. Chem. Int. Ed.*, 1998, **37**, 1901.

131. W. Fu, X.-H. Li, H.-L. Bao, K.-X. Wang, X. Wei, Y.-Y. Cai and J.-S. Chen, *Sci. Rep.*, 2013, **3**, 2349.

132. W. F. Libby, *Science*, 1971, **176**, 499.

133. R. J. H. Voorhoeve, J. P. Remeika, P. E. Freeland and B. T. Matthias, *Science*, 1973, **177**, 353.

134. R. Zhang, A. Villanueva, H. Alamdari and S. Kaliaguine, *J. Catal.*, 2006, **237**, 368.

135. F. Severino, J. L. Brito, J. Laine, J. L. G. Fierro and A. L. Agudo, *J. Catal.*, 1998, **177**, 82.

136. R. K. Herz, J. B. Klela and J. A. Sell, *Ind. Eng. Chem. Prod. Res. Dev.*, 1983, **22**, 387.

137. M. C. Kung, K. A. Bethke, J. Yan, J.-H. Lee and H. H. Kung, *Appl. Surf. Sci.*, 1997, **121-122**, 261.

138. R. Burch, *Pure Appl. Chem.*, 1996, **68**, 377.

139. G. Kim, *Ind. Eng. Chem. Prod. Res. Dev.*, 1982, **21**, 267.

140. G. Dutta, U. V. Waghmare, T. Baidya, M. S. Hegde, K. R. Priolkar and P. R. Sarode, *Catal. Lett.*, 2006, **108**, 165.

141. G. Dutta, U. V. Waghmare, T. Baidya, M. S. Hegde, K. R. Priolkar and P. R. Sarode, *Chem. Mater.*, 2006, **18**, 3249.

142. S. Roy, A. Marimuthu, M. S. Hegde and G. Madras, *Appl. Catal. B*, 2007, **73**, 300.

143. M. E. Grass, Y. Zhang, D. R. Butcher, J. Y. Park, Y. Li, H. Bluhm, K. M. Bratlie, T. Zhang and G. A. Somorjai, *Angew. Chem. Int. Ed.*, 2008, **47**, 8893.

144. D. A. J. M. Ligthart, R. A. van Santen and E. J. M. Hensen, *Angew. Chem. Int. Ed.*, 2011, **50**, 5306.

145. I. Manuel, C. Thomas, C. Bourgeois, H. Colas, N. Matthess and G. Djéga-Mariadassou, *Catal. Lett.*, 2001, **77**, 193.

146. S. Carrettin, A. Corma, M. Iglesis and F. Sánchez, *Appl. Catal. A*, 2005, **291**, 247.

147. A. M. Venezia, G. Pantaleo, A. Longo, G. Di Carlo, M. P. Casaletto, F. L. Liotta and G. Deganello, *J. Phys. Chem. B*, 2005, **109**, 2821.

148. N. W. Cant, P. C. Hicks and B. S. Lennon, *J. Catal.*, 1978, **54**, 372.

149. Y.-F. Yu Yao, *J. Catal.*, 1984, **87**, 152.

150. S. H. Oh and C. C. Eickel, *J. Catal.*, 1988, **112**, 543.

151. E. Bekyarova, P. Fornasiero, J. Kašpar and M. Graziani, *Catal. Today*, 1998, **45**, 179.

152. A. M. Venezia, L. F. Liotta, G. Pantaleo, V. L. Parola, G. Deganello, A. Beck, Zs. Koppány, K. Frey, D. Horváth and L. Guczi, *Appl. Catal. A*, 2003, **251**, 359.

153. Y. Park, S. K. Kim, D. Pradhan and Y. Sohn, *Reac. Kinet. Mech. Catal.*, 2014, **113**, 85.

154. S. Roy, A. Marimuthu, M. S. Hegde and G. Madras, *Appl. Catal. B*, 2007, **71**, 23.

155. S. Roy and M. S. Hegde, *Catal. Commun.*, 2008, **9**, 811.

156. P. Granger, C. Dathy, J. J. Lecomte, L. Leclercq, M. Prigent, G. Mabilon and G. Leclercq, *J. Catal.*, 1998, **173**, 304.

157. P. Granger, J. J. Lecomte, C. Dathy, L. Leclercq and G. Leclercq, *J. Catal.*, 1998, **175**, 194.

158. P. Granger, L. Delannoy, J. J. Lecomte, C. Dathy, H. Praliaud, L. Leclercq and G. Leclercq, *J. Catal.*, 2002, **207**, 202.

159. J. H. Holles, M. A. Switzer and R. J. Davis, *J. Catal.*, 2000, **190**, 247.

160. D. R. Rainer, S. M. Vesecky, M. Koranne, W. S. Oh and D. W. Goodman, *J. Catal.*, 1997, **167**, 234.

161. M. Schmal, M. A. S. Baldaza and M. A. Vannice, *J. Catal.*, 1999, **185**, 138.

162. S. Roy, A. Marimuthu, M. S. Hegde and G. Madras, *Catal. Commun.*, 2008, **9**, 101.

163. S. Roy, B. Viswanath, M. S. Hegde and G. Madras, *J. Phys. Chem. C*, 2008, **112**, 6002.

164. S. Roy S, A. Marimuthu, P. A. Deshpande, M. S. Hegde and G. Madras, *Ind. Eng. Chem. Res.*, 2008, **47**, 9240.

165. M. V. Twigg, *Appl. Catal. B*, 2007, **70**, 2.

166. P. Avila, M. Montes and E. E. Miró, *Chem. Eng. J.*, 2005, **109**, 11.

167. V. Tomašić, *Catal. Today*, 2007, **119**, 106.

168. T. A. Nijhuis, A. E. W. Beers, T. Vergunst, I. Hoek, F. Kapteijn and J. A. Moulijn, *Catal. Rev. Sci. Eng.*, 2001, **43**, 345.

169. P. Jiang, G. Lu, Y. Guo, Y. Guo, S. Zhang and X. Wang, *Surf. Coat. Technol.*, 2005, **190**, 314.

170. S. Sharma and M. S. Hegde, *Catal. Lett.*, 2006, **112**, 69.

171. S. Sharma, M. S. Hegde, R. N. Das and M. Pandey, *Appl. Catal. A*, 2008, **337**, 130.

172. P. Bera, K. C. Patil and M. S. Hegde, *Phys. Chem. Chem. Phys.*, 2000, **2**, 273.

173. P. Bera, S. Malwadkar, A. Gayen, C. V. V. Satyanarayana, B. S. Rao and M. S. Hegde, *Catal. Lett.*, 2004, **96**, 213.

174. S. Sharma, P. A. Deshpande, M. S. Hegde and G. Madras, *Ind. Eng. Chem. Res.*, 2009, **48**, 6535.

175. P. A. Deshpande, M. S. Hegde and G. Madras, *Appl. Catal. B*, 2010, **96**, 83.

176. A. Gupta and M. S. Hegde, *Appl. Catal. B*, 2010, **99**, 279.

177. N. Mahadevaiah, P. Singh, B. D. Mukri, S. K. Parida and M. S. Hegde, *Appl. Catal. B*, 2011, **108−109**, 117.

178. P. Singh, N. Mahadevaiah, S. K. Parida and M. S. Hegde, *J. Chem. Sci.*, 2011, **123**, 577.

179. A. Martínez-Arias, D. Gamarra, M. Fernández-García, A. Hornés, P. Bera, Zs. Koppány and Z. Scahy, *Catal. Today*, 2009, **143**, 211.

180. D. Teschner, A. Wootsch, O. Pozdnyakova-Tellinger, J. Kröhnert, E. M. Vass, M. Hävecker, S. Zafeiratos, P. Schnörch, P. C. Jentoft, A. Knop-Gericke and R. Schlögl, *J. Catal.*, 2007, **249**, 318.

181. S. Sharma, A. Gupta and M. S. Hegde, *Catal. Lett.*, 2010, **134**, 330.

182. P. Bera, M. S. Hegde and K. C. Patil, *Curr. Sci.*, 2001, **80**, 1576.

183. S. Sharma and M. S. Hegde, *Chem Phys Chem*, 2009, **10**, 637.

184. B. Hariprakash, P. Bera, S. K. Martha, S. A. Gaffoor, M. S. Hegde and A. K. Shukla, *Electrochem. Solid-State Lett.*, 2001, **4**, A23.

185. R. Mistri, J. Llorca, B. C. Ray and A. Gayen, *J. Mol. Catal. A*, 2013, **376**, 111.

186. K. Nagaveni, G. Sivalingam, A. Gayen, G. Madras and M. S. Hegde, *Catal. Lett.*, 2003, **88**, 73.

187. A. de Meijere A and F. E. Meyer, *Angew. Chem. Int. Ed.*, 1995, **33**, 2379.

188. A. P. Beletskaya and V. Cheprakov, *Chem. Rev.*, 2000, **100**, 3009.

189. G. T. Crisp, *Chem. Soc. Rev.*, 1998, **27**, 427

190. J. G. de Vries, *Can. J. Chem.*, 2001, **79**, 1086.

191. T. R. Burke, D. G. Liu and Y. J. Gao, *J. Org. Chem.*, 2000, **65**, 6288.

192. S. R. Sanjaykumar, B. D. Mukri, S. Patil, G. Madras and M. S. Hegde, *J. Chem. Sci.*, 2011, **123**, 47.

193. S. Sharma and M. S. Hegde, *J. Chem. Phys.*, 2009, **130**, 114706.

194. S. Sharma, B. D. Mukri and M. S. Hegde, *Dalton Trans.*, 2011, **40**, 11480.

195. P. Bera, S. Mitra, S. Sampath and M. S. Hegde, *Chem. Commun.*, 2001, 927.

196. X. Tang, B. Zhang, Y. Li, Y. Xu, Q. Xin and W. Shen, *Catal. Today*, 2004, **93–95**, 191.

197. L. Li, Y. Zhan, Q. Zheng, Y. Zheng, X. Lin, D. Li and J. Zhu, *Catal. Lett.*, 2007, **118**, 91.

198. S. Sharma, P. Singh and M. S. Hegde, *J. Solid State Electrochem.*, 2011, **15**, 2185.

199. P. A. Deshpande, M. S. Hegde and G. Madras, *AIChE J.*, 2010, **56**, 1315.

200. R. Di Monte, P. Fornasiero, M. Graziani and J. Kašpar, *J. Alloys Compd.*, 1998, **275**, 877.

201. G. Dutta, U. V. Waghmare, T. Baidya and M. S. Hegde, *Chem. Mater.*, 2007, **19**, 6430.

202. A. Gupta, U. V. Waghmare and M. S. Hegde, *Chem. Mater.*, 2010, **22**, 5184.

203. A. Gupta, A. Kumar, U. V. Waghmare and M. S. Hegde, *J. Chem. Phys.*, 2010, **132**, 194702.

204. G. Dutta, A. Gupta, U. V. Waghmare and M. S. Hegde, *J. Chem. Sci.*, 2011, **123**, 509.

205. Z. Yang, G. Luo, Z. Lu, T. K. Woo and K. Hermansson, *J. Phys.: Condens. Mater.*, 2008, **20**, 035210.

206. H.-F. Wang, X.-Q. Gong, Y.-L. Guo, Y. Guo, G. Z. Lu and P. Hu, *J. Phys. Chem. C*, 2009, **113**, 10229.

207. V. Shapovalov and H. Metiu, *J. Catal.*, 2007, **245**, 205.

208. Z. Hu and H. Metiu, *J. Phys. Chem. C*, 2011, **115**, 17898.

209. E. W. McFarland and H. Metiu, *Chem. Rev.*, 2013, **113**, 4391.

210. M. F. Camellone and S. Fabris, *J. Am. Chem. Soc.*, 2009, **131**, 10473.

211. H.-L. Chen, J.-G. Chang and H.-T. Chen, *Chem. Phys. Lett.*, 2011, **502**, 169.

212. D. O. Scanlon, B. J. Morgan and G. W. Watson, *Phys. Chem. Chem. Phys.*, 2011, **13**, 4279.

213. A. B. Kehoe, D. O. Scanlon and G. W. Watson, *Chem. Mater.*, 2011, **23**, 4464.

214. M. Nolan, *J. Mater. Chem.*, 2011, **21**, 9160.

215. Y. Zhao, B.-T. Teng, X.-D. Wen, Y. Zhao, L.-H. Zhao and M.-F. Luo, *Catal. Commun.*, 2012, **27**, 63.

216. H.-T. Chen, *J. Phys. Chem. C*, 2012, **116**, 6239.

217. Z. Yang, Z. Lu and G. Luo, *Phys. Rev. B*, 2007, **76**, 075421.

218. Z. Lu and Z. Yang, *J. Phys.: Condens. Mater.*, 2010, **22**, 475003.

219. A. Bruix, K. M. Neyman and F. Illas, *J. Phys. Chem. C*, 2010, **114**, 14202.

220. W. Song, C. Popa, A. P. J. Jansen and E. J. M. Hensen, *J. Phys. Chem. C*, 2010, **116**, 22904.

221. J. Paier, C. Penschke and J. Sauer, *Chem. Rev.*, 2013, **113**, 3949.

222. X.-Q. Gong, L.-L. Yin, J. Zhang, H.-F. Wang, X.-M. Cao, G. Lu and P. Hu, *Adv. Chem. Eng.*, 2014, **44**, 1.

223. A. D. Mayernick and M. J. Janik, *J. Catal.*, 2011, **278**, 16.

224. S. Chrétien and H. Metiu, *Catal. Lett.*, 2006, **107**, 143.

225. F. Wang, S. Zhang, C. Li, J. Liu, S. He, Y. Zhao, H. Yan, M. Wei, D. G. Evans and X. Duan, *RSC Adv.*, 2014, **4**, 10834.

Table 1. Various metal ions substituted CeO_2 and TiO_2 catalysts prepared in our laboratory. Reprinted from [24] with permission of Elsevier B. V.

Metal ions	Support oxides					
	CeO_2	$Ce_{1-x}Ti_xO_{2-\delta}$	$Ce_{1-x}Sn_xO_{2-\delta}$	$Ce_{1-x}Fe_xO_{2-\delta}$	$Ce_{1-x}Zr_xO_{2-\delta}$	TiO_2
Pd^{2+}	$Ce_{1-x}Pd_xO_{2-\delta}$ (x = 0.01, 0.02) (20,43)	$Ce_{0.75-x}Ti_{0.25}Pd_xO_{2-\delta}$ (x = 0.01, 0.02) (48)	$Ce_{0.78}Sn_{0.2}Pd_{0.02}O_{2-\delta}$ (49,50)	$Ce_{1-x-y}Fe_xPd_yO_{2-\delta}$ (x = 0.1–0.45, y = 0.02) (51,70)	$Ce_{1-x-y}Zr_xPd_yO_{2-\delta}$ (x = 0.25, y = 0.02) (52)	$Ti_{1-x}Pd_xO_{2-\delta}$ (x = 0.01, 0.03) (54,55)
Rh^{3+}	$Ce_{1-x}Rh_xO_{2-\delta}$ (x =0.005, 0.01) (44)					$Ti_{1-x}Rh_xO_{2-\delta}$ (x = 0.01) (54)
Pt^{2+}, Pt^{4+}	$Ce_{1-x}Pt_xO_{2-\delta}$ (x = 0.01, 0.02) (20,69,71,72)	$Ce_{0.85-x}Ti_{0.15}Pt_xO_{2-\delta}$ (x = 0.01, 0.02) (47)				$Ti_{1-x}Pt_xO_{2-\delta}$ (x = 0.01) (54)
Pt^{2+}, Rh^{3+}	$Ce_{1-x}Rh_{x/2}Pt_{x/2}O_{2-\delta}$ (x = 0.01, 0.02) (73)					
Ru^{4+}	$Ce_{1-x}Ru_xO_{2-\delta}$ (x =0.05, 0.1) (63)					$Ti_{1-x}Ru_xO_{2-\delta}$ (x = 0.01) (54)
Cu^{2+}	$Ce_{1-x}Cu_xO_{2-\delta}$ (x = 0.01–0.1) (74,75)					
Ag^{+}	$Ce_{1-x}Ag_xO_{2-\delta}$ (x = 0.01) (45)					
Au^{3+}	$Ce_{1-x}Au_xO_{2-\delta}$ (x = 0.01) (46)					
Cr^{4+}, Cr^{6+}	$Ce_{1-x}Cr_xO_{2+\delta}$ (x = 0.01–0.2) (62)					

Table 2 Oxygen storage capacities (OSC) of CeO_2 and TiO_2 based materials studied in our laboratory.

Materials	OSC (μmol g^{-1})	References
CeO_2	174	52
$Ce_{0.98}Rh_{0.02}O_{1.99}$	244	44
$Ce_{0.75}Zr_{0.25}O_2$	1900	140
$Ce_{0.6}Zr_{0.4}O_2$	2429	52
$Ce_{0.5}Zr_{0.5}O_2$	2900	140
$Ce_{0.9}Ti_{0.1}O_2$	740	47
$Ce_{0.85}Ti_{0.15}O_2$	880	47
$Ce_{0.8}Ti_{0.2}O_2$	1110	47
$Ce_{0.75}Ti_{0.25}O_2$	1340	141
$Ce_{0.7}Ti_{0.3}O_2$	1590	47
$Ce_{0.6}Ti_{0.4}O_2$	2000	47
$Ce_{0.99}Pt_{0.01}O_{1.99}$	290	47
$Ce_{0.84}Ti_{0.15}Pt_{0.01}O_{1.99}$	1570	47
$Ce_{0.83}Ti_{0.15}Pt_{0.02}O_{1.98}$	2320	47
$Ce_{0.73}Ti_{0.25}Pd_{0.02}O_{1.98}$	1286	52
$Ce_{0.75}Hf_{0.25}O_2$	714	52
$Ce_{0.73}Hf_{0.25}Pd_{0.02}O_{1.98}$	1121	52
$Ce_{0.58}Hf_{0.4}Pd_{0.02}O_{1.98}$	804	52
$Ce_{0.98}Pd_{0.02}O_{1.98}$	232	52
$Ce_{0.83}Zr_{0.15}Pd_{0.02}O_{1.98}$	638	52
$Ce_{0.73}Zr_{0.25}Pd_{0.02}O_{1.98}$	1509	52
$Ce_{0.58}Zr_{0.4}Pd_{0.02}O_{1.98}$	1612	52
$Ce_{0.78}Zr_{0.2}Pd_{0.02}O_{1.98}$	620	50
$Ce_{0.9}Sn_{0.1}O_2$	980	49
$Ce_{0.8}Sn_{0.2}O_2$	1650	49
$Ce_{0.7}Sn_{0.3}O_2$	2100	49

$Ce_{0.6}Sn_{0.4}O_2$	2545	49
$Ce_{0.5}Sn_{0.5}O_2$	2780	49
$Ce_{0.78}Sn_{0.2}Pd_{0.02}O_{1.98}$	1650	50
$Ce_{0.5}Sn_{0.48}Pd_{0.02}O_{1.98}$	1330	50
$Ce_{0.95}Ru_{0.05}O_{1.97}$	1335	63
$Ce_{0.9}Ru_{0.1}O_{1.94}$	2513	63
$Ce_{0.9}Fe_{0.1}O_{1.88}$	665	51
$Ce_{0.89}Fe_{0.1}Pd_{0.01}O_{1.84}$	780	51
$Ce_{0.67}Cr_{033}O_{2.11}$	2513	62
TiO_2	250	55
$Ti_{0.99}Pd_{0.01}O_{1.99}$	1240	55
$Ti_{0.98}Pd_{0.02}O_{1.98}$	2220	55
$Ti_{0.97}Pd_{0.02}O_{1.97}$	5100	55
$Ti_{0.97}Pt^{2+}{}_{0.03}O_{1.97}$	2010	56
$Ti_{0.97}Pt^{4+}{}_{0.02}O_{1.97}$	2315	56

Table 3 Comparison of CO conversion rates and activation energies (E_a) for CO + O_2 reaction over noble metal ionic catalysts with supported nano metal catalysts.

Catalysts	Rate (μmol g^{-1} s^{-1})	E_a (kJ mol^{-1})	References
5 wt.% Ru/SiO_2	1.0 (110 °C)	94	148
5 wt.% Rh/SiO_2	0.0251 (110 °C)	103	148
5 wt.% Pd/SiO_2	0.316 (143 °C)	103	148
5 wt.% Ir/SiO_2	0.26 (180 °C)	105	148
5 wt.% Pt/SiO_2	0.32 (115 °C)	56	148
$Pd/CeO_2/Al_2O_3$	38 (250 °C)	84	149
0.014 wt.% Rh/Al_2O_3	0.6 (196 °C)	115.5	150
0.014 wt.% Rh/9 wt.% Ce/Al_2O_3	0.95 (196 °C)	90.3	150
0.5 wt.% $Pd/CeO_2–ZrO_2$	0.7 (220 °C)	175	151
1.53% Pd/SiO_2	0.155 (140 °C)	–	152
25Au75Pd/SiO_2	0.128 (140 °C)	–	152
50Au50Pd/SiO_2	0.06 (140 °C)	–	152
5% Au/CeO_2	0.77 (300 °C)	80.3	153
5% Pd/CeO_2	0.76 (300 °C)	76.9	153
$Ce_{0.98}Pd_{0.02}O_{2-\delta}$	7.0 (130 °C)	67.2	48
1 at.% Pd/Al_2O_3 (Impregnated)	2.73 (200 °C)	86.88	142
1 at.% Pd/TiO_2 (Impregnated)	0.758 (100 °C)	75.25	142
$Ce_{0.99}Pt_{0.01}O_{2-\delta}$	0.6 (155 °C)	55.4	47
$Ce_{0.84}Ti_{0.15}Pt_{0.01}O_{2-\delta}$	28.0 (155 °C)	82.3	47
$Ce_{0.73}Ti_{0.25}Pd_{0.02}O_{2-\delta}$	18.0 (120 °C)	54.6	48
2% $Pd/Ce_{0.75}Ti_{0.25}O_{2-\delta}$	–	132.3	48
$Ce_{0.78}Sn_{0.2}Pd_{0.02}O_{2-\delta}$	1.9 (50 °C)	84	49
$Ce_{0.95}Ru_{0.05}O_{2-\delta}$	2.05 (100 °C)	94.5	63
$Ce_{0.9}Ru_{0.1}O_{2-\delta}$	3.3 (100 °C)	44.8	63
$Ce_{0.89}Fe_{0.1}Pd_{0.01}O_{2-\delta}$	–	52.5	51

$Ce_{0.9}Fe_{0.1}O_{2-\delta}$	–	46.2	51
$Ce_{0.99}Pd_{0.01}O_{2-\delta}$	–	63	51
$Ce_{0.65}Fe_{0.33}Pd_{0.02}O_{2-\delta}$	4.1 (80 °C)	38	70
0.74% Pd/CeO_2	–	42	82
2% $Pt/Ce_{0.72}Zr_{0.18}Pr_{0.1}O_2$	1.6 (61 °C)	–	84
2% $Pd/Ce_{0.72}Zr_{0.18}Pr_{0.1}O_2$	1.6 (130 °C)	–	84
2% $Ru/Ce_{0.72}Zr_{0.18}Pr_{0.1}O_2$	1.6 (150 °C)	–	84
2% Pt/CeO_2	2.89 (40 °C)	51	87
$Ti_{0.99}Pd_{0.01}O_{1.99}$	13.83 (120 °C)	53.13	142
$Ti_{0.97}Pd_{0.03}O_{1.97}$	2.75 (60 °C)	17	55
$Ti_{0.97}Pt^{2+}_{0.03}O_{1.97}$	0.76 (60 °C)	33.6	56
$Ti_{0.97}Pt^{4+}_{0.02}O_{1.97}$	0.08 (60 °C)	16.8	56

Table 4 Comparison of NO conversion rates, activation energies (E_a) and selectivities (S_{N_2} and S_{N_2O}) for NO + CO reaction over noble metal ionic catalysts with supported nano metal catalysts.

Catalysts	Rate (μmol g^{-1} s^{-1})	E_a (kJ mol^{-1})	S_{N_2}	S_{N_2O}	References
1 wt.% Pt/Al_2O_3	0.1 (300 °C)	92.4	27	73	156
0.2 wt.% Rh/Al_2O_3	7.2 (300 °C)	184.8	32	68	157
1 wt.% Pt-0.02 wt.% Rh/Al_2O_3	0.58 (300 °C)	126	39	61	158
Pt-Rh/Al_2O_3-CeO_2	0.54 (300 °C)	84	33	67	158
Rh/Al_2O_3	0.58 (227 °C)	86.6	45	55	159
$Pd/Rh/Al_2O_3$	0.11 (227 °C)	100	43	57	159
Pd/Al_2O_3	0.83 (227 °C)	59.8	36	64	159
$Pd/La_2O_3/Al_2O_3$	4.3 (227 °C)	100	30	70	159
1% Pd/γ-Al_2O_3	0.75 (287 °C)	158	34	66	160
$Pd8Mo/Al_2O_3$	2.0 (300 °C)	84	39	61	161
$Ce_{0.98}Pd_{0.02}O_{2-\delta}$	0.242 (175 °C)	70.2	75	25	154
$Ce_{0.73}Ti_{0.25}Pd_{0.02}O_{2-\delta}$	2.0 (180 °C)	52.9	–	–	48
$Ce_{0.99}Pt_{0.01}O_{2-\delta}$	0.2 (135 °C)	100.8	–	–	47
$Ce_{0.84}Ti_{0.15}Pt_{0.01}O_{2-\delta}$	0.2 (135 °C)	96.6	–	–	47
$Ce_{0.78}Sn_{0.2}Pd_{0.02}O_{2-\delta}$	5.0 (150 °C)	105.4	100	–	49
$Ce_{0.89}Fe_{0.1}Pd_{0.01}O_{2-\delta}$	3.8 (220 °C)	–	56	44	51
$Ce_{0.95}Ru_{0.05}O_{2-\delta}$	3.8 (200 °C)	41	100	–	63
$Ce_{0.9}Ru_{0.1}O_{2-\delta}$	3.4 (200 °C)	53.2	100	–	63
$Ti_{0.99}Pd_{0.01}O_{2-\delta}$	1.47 (175 °C)	64.1	70	30	142
1% Pd/Al_2O_3 (impregnated)	0.05 (240 °C)	86.6	59	41	142

Figure captions

Fig. 1 Sequences of solution combustion synthesis: initial solution of precursors, flame during combustion and final product. Reprinted from [21] with permission of American Chemical Society.

Fig. 2 Rietveld refined XRD patterns of (a) $Ce_{0.99}Pt_{0.01}O_{2-\delta}$ and (b) $Ti_{0.99}Pd_{0.01}O_{2-\delta}$. Reprinted from [71] with permission of American Chemical Society and from [142] with permission of Elsevier B. V.

Fig. 3 Top panel: HRTEM image of $Ce_{0.73}Ti_{0.25}Pd_{0.02}O_{2-\delta}$ (A) and ED patterns of $Ce_{0.73}Ti_{0.25}Pd_{0.02}O_{2-\delta}$ (B) and impregnated 2 at.% $Pd/Ce_{0.73}Ti_{0.25}Pd_{0.02}O_{2-\delta}$ (C); Bright field TEM image of $Ti_{0.97}Pd_{0.03}O_{2-\delta}$ and its ED pattern (inset), (b) HRTEM image of $Ti_{0.97}Pd_{0.03}O_{2-\delta}$ and (c) EDXS of $Ti_{0.97}Pd_{0.03}O_{2-\delta}$ from the image. Reprinted from [48] and [55] with permission of American Chemical Society.

Fig. 4 Left panel: XPS of Pt4f core levels of (a) Pt metal, (b) $(NH_3)_4Pt(NO_3)_2$, (c) PtO_2, (d) $Ce_{0.99}Pt_{0.01}O_{2-\delta}$ and (e) $Ce_{0.84}Ti_{0.15}Pt_{0.01}O_{2-\delta}$; Right panel: XPS of Rh3d core levels of (a) Rh metal, (b) Rh_2O_3, (c) $Ce_{0.99}Rh_{0.01}O_{2-\delta}$ and (d) $Ce_{0.98}Rh_{0.02}O_{2-\delta}$. Reprinted from [24] with permission of Elsevier B. V. and from [44] with permission of American Chemical Society.

Fig. 5 XPS of (a) Pd3d in $Ti_{0.99}Pd_{0.01}O_{2-\delta}$, (b) Pt4f in $Ti_{0.99}Pt_{0.01}O_{2-\delta}$, (c) Rh3d in $Ti_{0.99}Rh_{0.01}O_{2-\delta}$ and (d) Ru3p in $Ti_{0.99}Ru_{0.01}O_2$. Reprinted from [54] with permission of Elsevier B. V.

Fig. 6 Left panel: Valence band XPS of CeO_2, $Ce_{0.9}Pd_{0.1}O_{2-\delta}$, PdO, Pd metal and difference spectrum of $Ce_{0.9}Pd_{0.1}O_{2-\delta}$ and CeO_2 valence bands showing Pd^{2+}4d band position, Reprinted from [23] with permission of Springer; Right panel: Valence band

XPS of TiO_2, $Ti_{0.97}Pd_{0.03}O_{2-\delta}$ and difference spectrum of $Ti_{0.97}Pd_{0.03}O_{2-\delta}$ and TiO_2 valence bands showing Pd^{2+}4d band position.

Fig. 7 Left panel: Fourier Transformed XAFS of Pt metal, PtO_2, $Ce_{0.99}Pt_{0.01}O_{2-\delta}$ and $Ce_{0.98}Pt_{0.02}O_{2-\delta}$, Reprinted from [23] with permission of Springer; Right panel: Rh metal, Rh_2O_3, $Ce_{0.99}Rh_{0.01}O_{2-\delta}$ and $Ce_{0.98}Rh_{0.02}O_{2-\delta}$.

Fig. 8 DRIFT spectra of (a) NO adsorption and (b) followed by CO adsorption over $Ce_{0.98}Pd_{0.02}O_{2-\delta}$. Reprinted from [99] with permission of Elsevier B. V.

Fig. 9 H_2-TPR profiles of (a) $Ce_{0.99}Pt_{0.01}O_{2-\delta}$, (b) $Ce_{0.84}Ti_{0.15}Pt_{0.01}O_{2-\delta}$ and $Ce_{0.83}Ti_{0.15}Pt_{0.02}O_{2-\delta}$.

Fig. 10 Top panel: CO oxidation over Pt substituted CeO_2 and TiO_2 based catalysts; Bottom panel: CO oxidation over Rh metal and oxidized Rh species. Reprinted from [47] with permission of American Chemical Society and from [145] with permission of Springer.

Fig. 11 Catalytic reactions over $Ce_{0.98}Pd_{0.02}O_{2-\delta}$ coated on cordierite monolith: (a) CO + O_2, (b) NO + CO and (c) three-way catalysis. Reprinted from [170] with permission of Springer.

Fig. 12 Conversion efficiency of reaction of iodobenzene and methyl acrylate at different temperatures. Reprinted from [192] with permission of Springer.

Fig. 13 CO + O_2 reaction: (a) Langmuir–Hinshelwood mechanism on Pt metal and (b) dual site mechanism on $Ce_{1-x}Pt_xO_{2-\delta}$. Reprinted from [21] with permission of American Chemical Society.

Fig. 14 Mechanism of N_2, N_2O and CO_2 formations during NO + CO reaction over $Ce_{1-x}Pd_xO_{2-\delta}$. Reprinted from [23] with permission of Springer.

Fig. 15 Bond length distributions in (a) Ce_4O_8, (b) $Ce_{26}Snd_6O_{64}$ and (c) $Ce_{25}Sn_6Pd_1O_{63}$ supercells from DFT calculations. Reprinted from [50] with permission of American Chemical Society.

Fig. 1 Sequences of solution combustion synthesis: initial solution of precursors, flame during combustion and final product. Reprinted from [21] with permission of American Chemical Society.

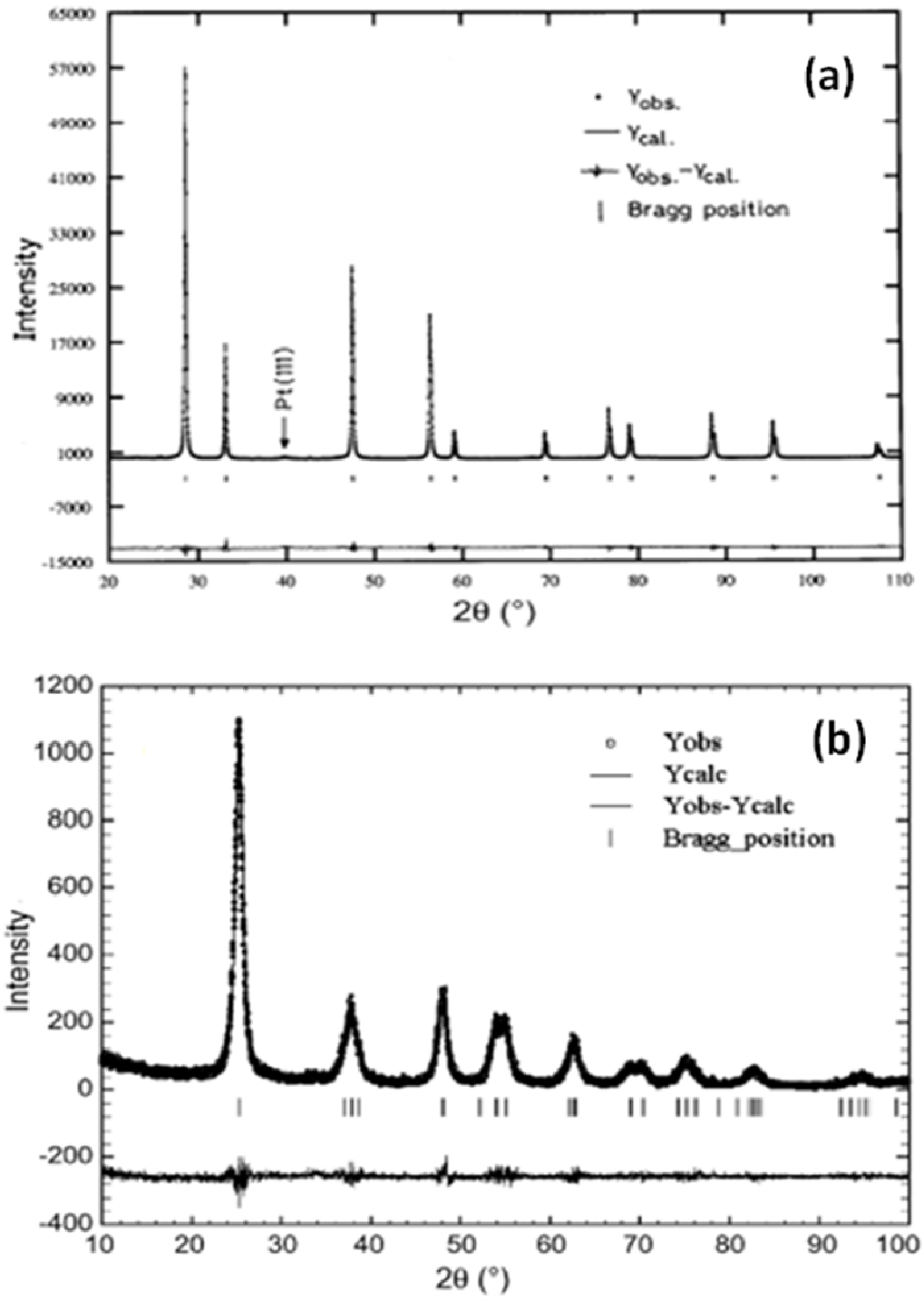

Fig. 2 Rietveld refined XRD patterns of (a) $Ce_{0.99}Pt_{0.01}O_{2-\delta}$ and (b) $Ti_{0.99}Pd_{0.01}O_{2-\delta}$. Reprinted from [71] with permission of American Chemical Society and from [142] with permission of Elsevier B. V.

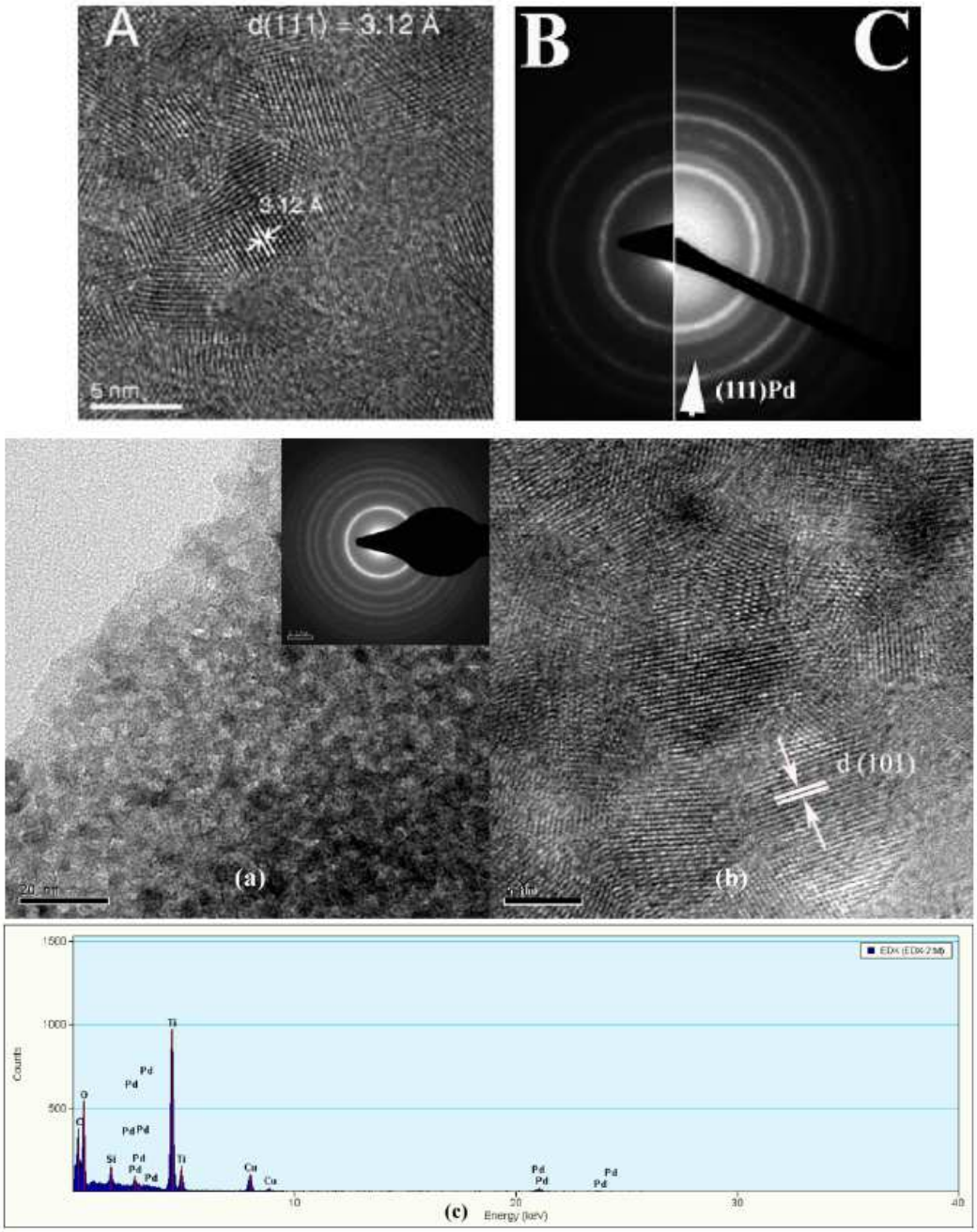

Fig. 3 Top panel: HRTEM image of $Ce_{0.73}Ti_{0.25}Pd_{0.02}O_{2-\delta}$ (A) and ED patterns of $Ce_{0.73}Ti_{0.25}Pd_{0.02}O_{2-\delta}$ (B) and impregnated 2 at.% $Pd/Ce_{0.73}Ti_{0.25}Pd_{0.02}O_{2-\delta}$ (C); Bright field TEM image of $Ti_{0.97}Pd_{0.03}O_{2-\delta}$ and its ED pattern (inset), (b) HRTEM image of $Ti_{0.97}Pd_{0.03}O_{2-\delta}$ and (c) EDXS of $Ti_{0.97}Pd_{0.03}O_{2-\delta}$ from the image. Reprinted from [48] and [55] with permission of American Chemical Society.

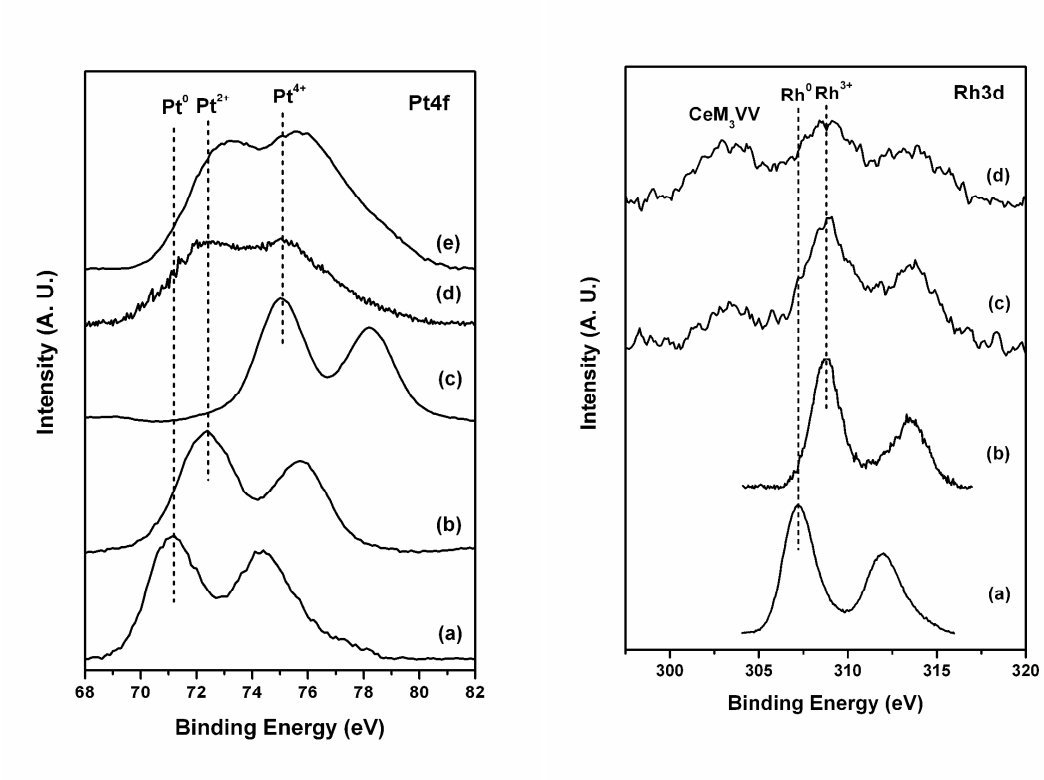

Fig. 4 Left panel: XPS of Pt4f core levels of (a) Pt metal, (b) $(NH_3)_4Pt(NO_3)_2$, (c) PtO_2, (d) $Ce_{0.99}Pt_{0.01}O_{2-\delta}$ and (e) $Ce_{0.84}Ti_{0.15}Pt_{0.01}O_{2-\delta}$; Right panel: XPS of Rh3d core levels of (a) Rh metal, (b) Rh_2O_3, (c) $Ce_{0.99}Rh_{0.01}O_{2-\delta}$ and (d) $Ce_{0.98}Rh_{0.02}O_{2-\delta}$. Reprinted from [24] with permission of Elsevier B. V. and from [44] with permission of American Chemical Society.

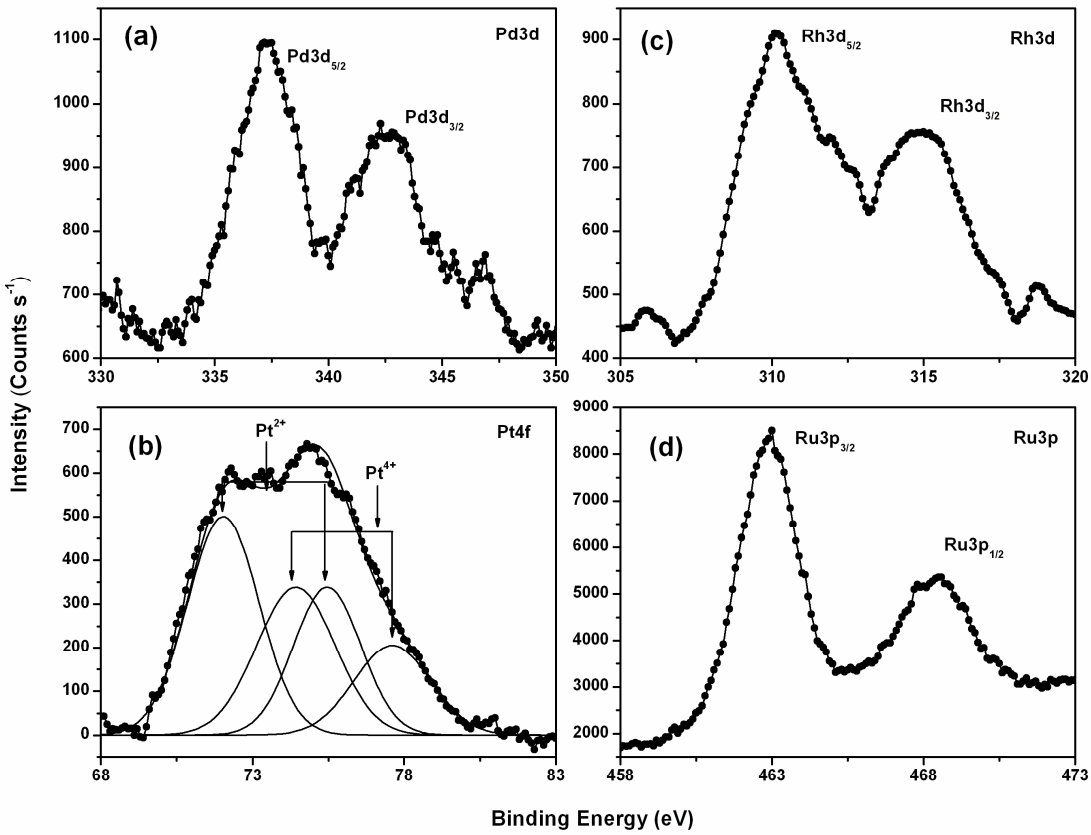

Fig. 5 XPS of (a) Pd3d in $Ti_{0.99}Pd_{0.01}O_{2-\delta}$, (b) Pt4f in $Ti_{0.99}Pt_{0.01}O_{2-\delta}$, (c) Rh3d in $Ti_{0.99}Rh_{0.01}O_{2-\delta}$ and (d) Ru3p in $Ti_{0.99}Ru_{0.01}O_2$. Reprinted from [54] with permission of Elsevier B. V.

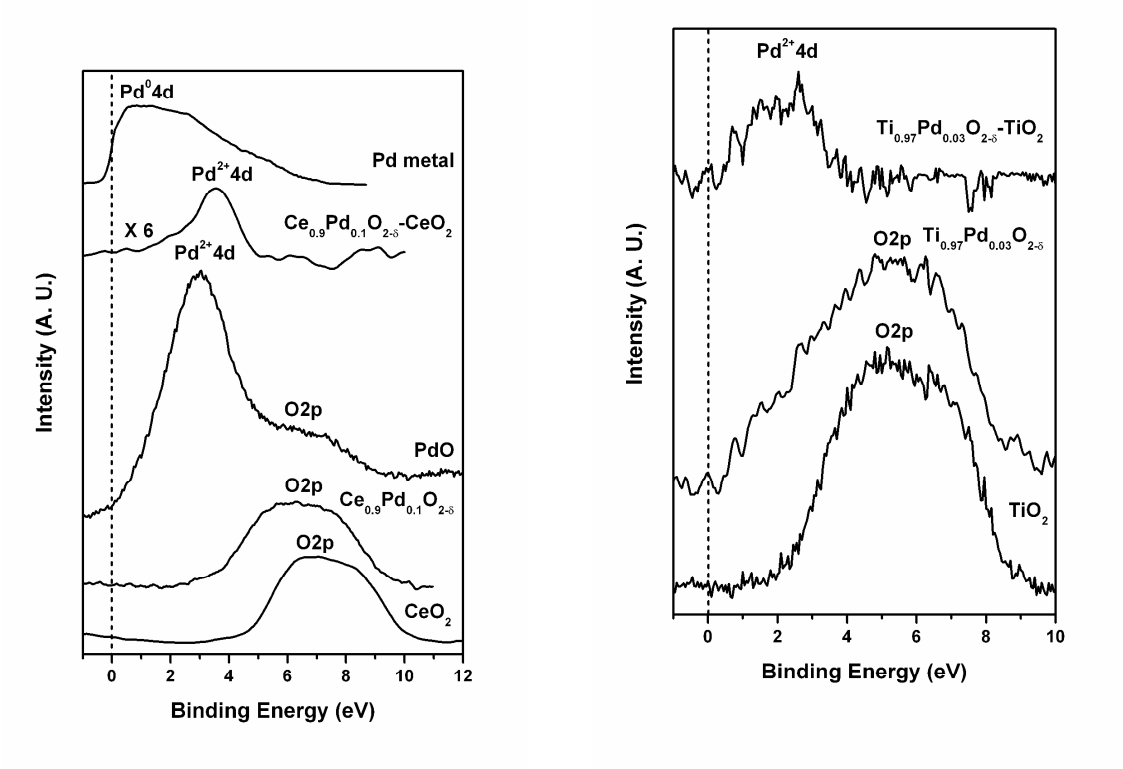

Fig. 6 Left panel: Valence band XPS of CeO_2, $Ce_{0.9}Pd_{0.1}O_{2-\delta}$, PdO, Pd metal and difference spectrum of $Ce_{0.9}Pd_{0.1}O_{2-\delta}$ and CeO_2 valence bands showing $Pd^{2+}4d$ band position, Reprinted from [23] with permission of Springer; Right panel: Valence band XPS of TiO_2, $Ti_{0.97}Pd_{0.03}O_{2-\delta}$ and difference spectrum of $Ti_{0.97}Pd_{0.03}O_{2-\delta}$ and TiO_2 valence bands showing $Pd^{2+}4d$ band position.

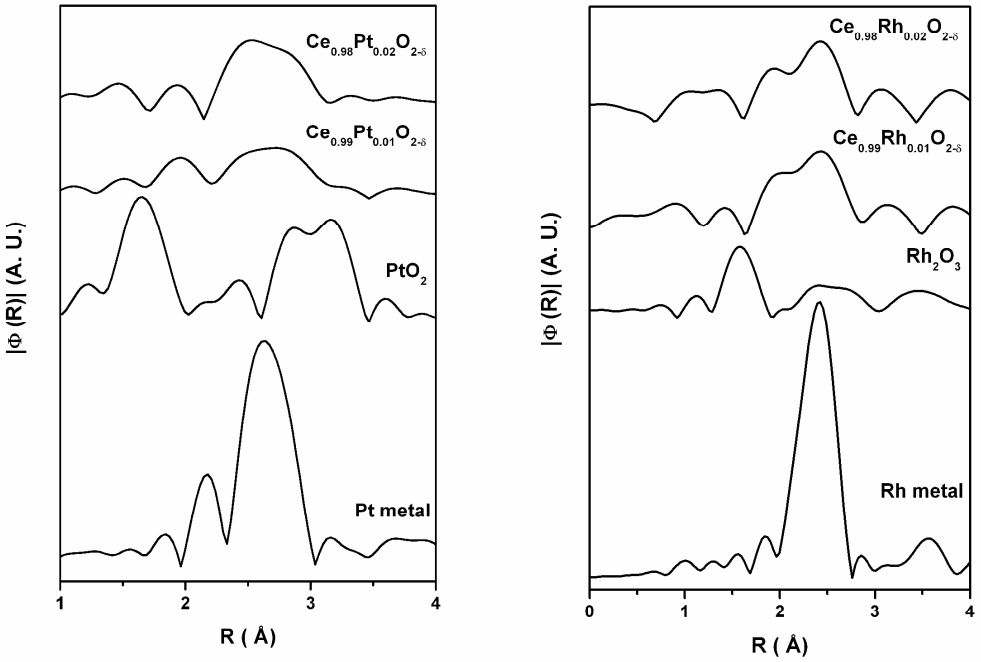

Fig. 7 Left panel: Fourier Transformed XAFS of Pt metal, PtO_2, $Ce_{0.99}Pt_{0.01}O_{2-\delta}$ and $Ce_{0.98}Pt_{0.02}O_{2-\delta}$, Reprinted from [23] with permission of Springer; Right panel: Rh metal, Rh_2O_3, $Ce_{0.99}Rh_{0.01}O_{2-\delta}$ and $Ce_{0.98}Rh_{0.02}O_{2-\delta}$.

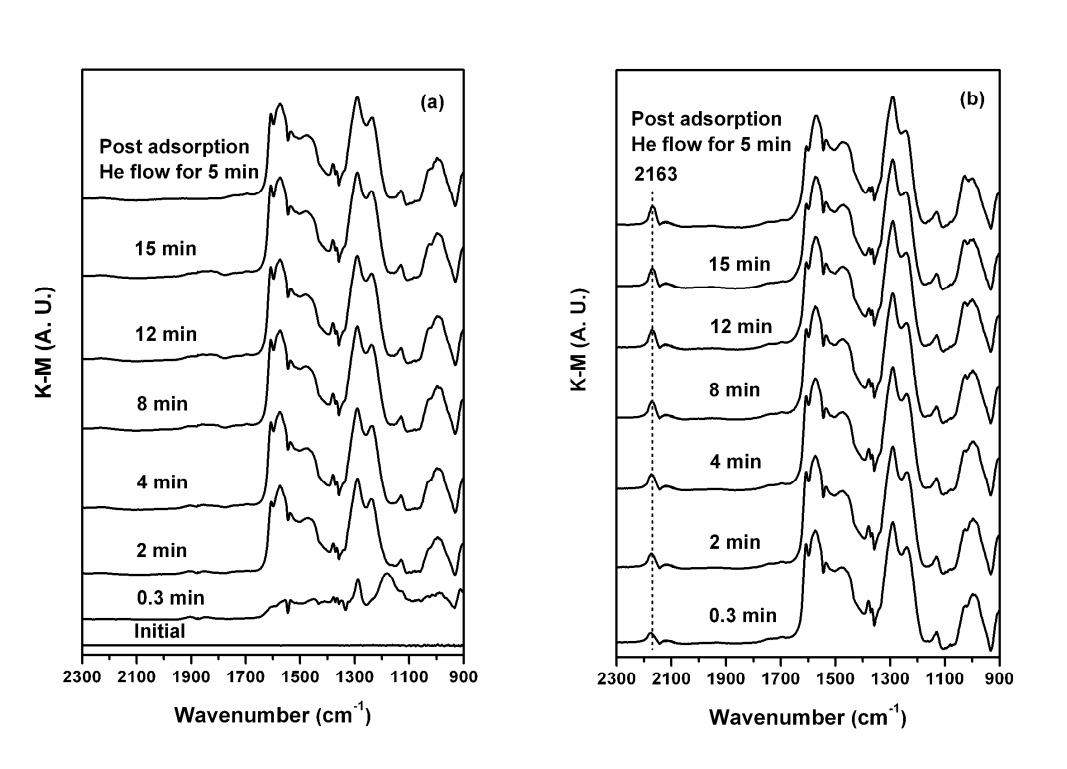

Fig. 8 DRIFT spectra of (a) NO adsorption and (b) followed by CO adsorption over $Ce_{0.98}Pd_{0.02}O_{2-\delta}$. Reprinted from [99] with permission of Elsevier B. V.

.

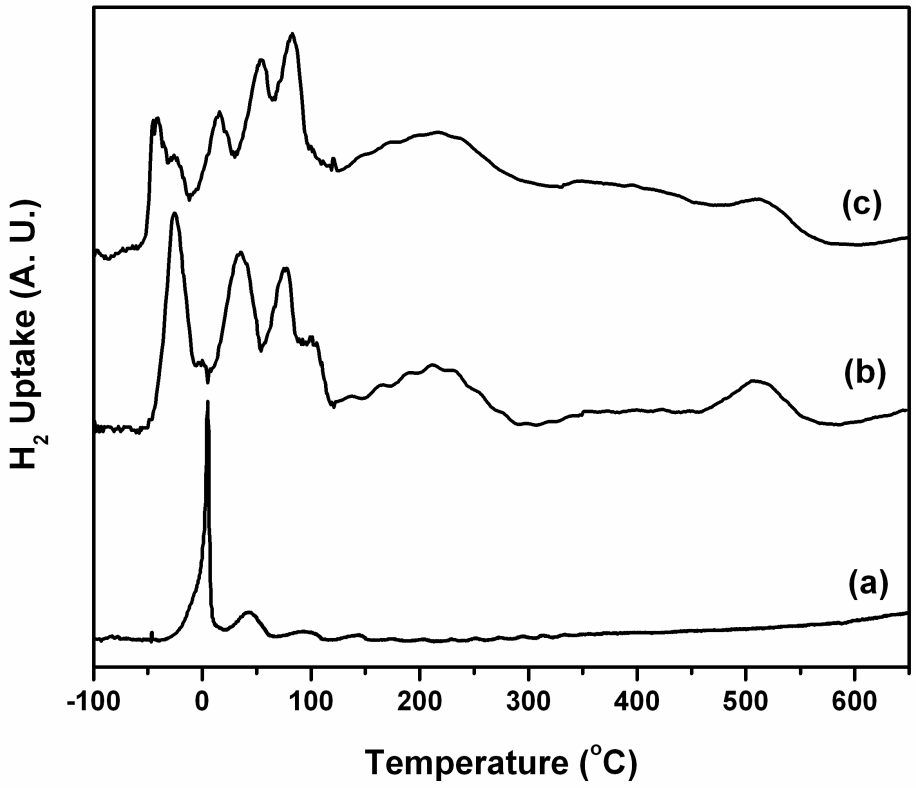

Fig. 9 H_2-TPR profiles of (a) $Ce_{0.99}Pt_{0.01}O_{2-\delta}$, (b) $Ce_{0.84}Ti_{0.15}Pt_{0.01}O_{2-\delta}$ and $Ce_{0.83}Ti_{0.15}Pt_{0.02}O_{2-\delta}$.

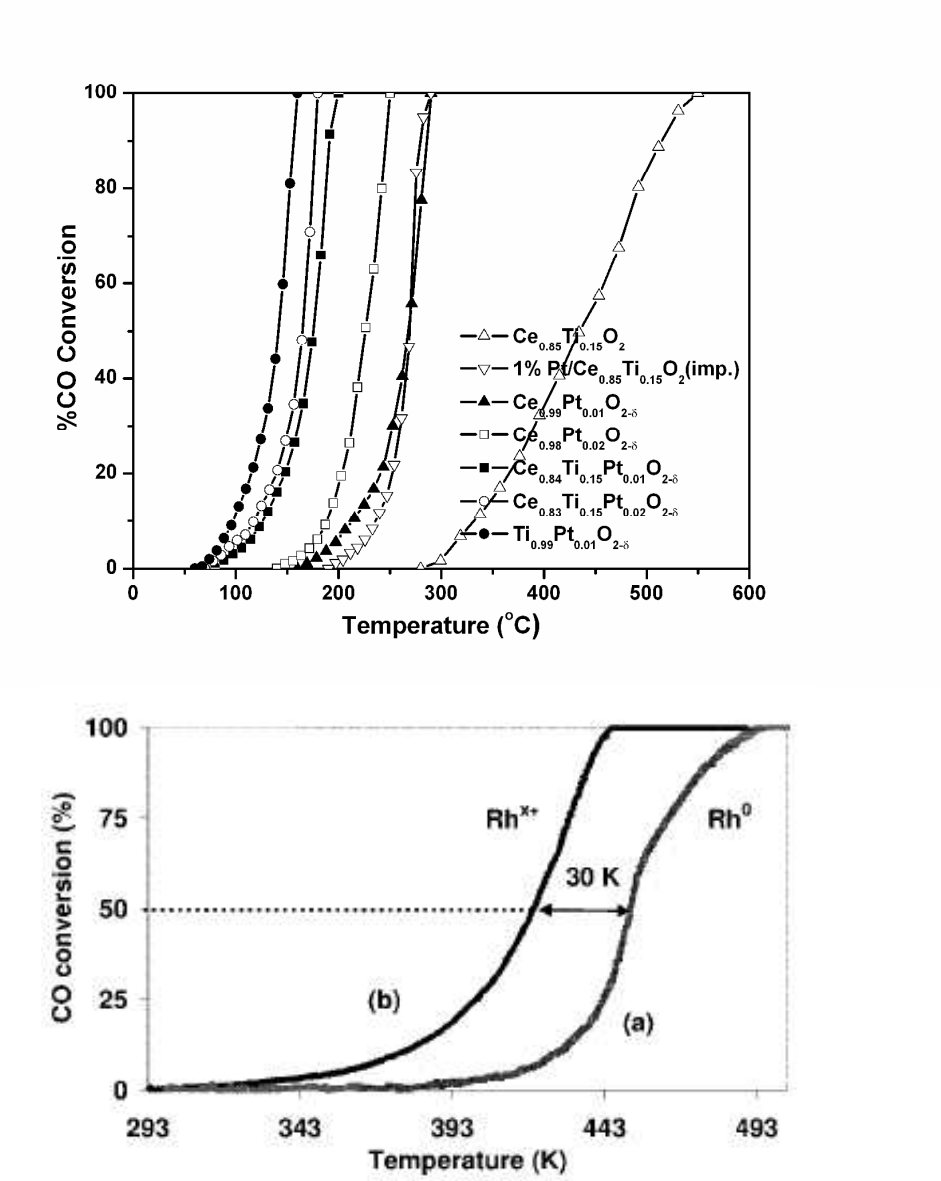

Fig. 10 Top panel: CO oxidation over Pt substituted CeO_2 and TiO_2 based catalysts; Bottom panel: CO oxidation over Rh metal and oxidized Rh species. Reprinted from [47] with permission of American Chemical Society and from [145] with permission of Springer.

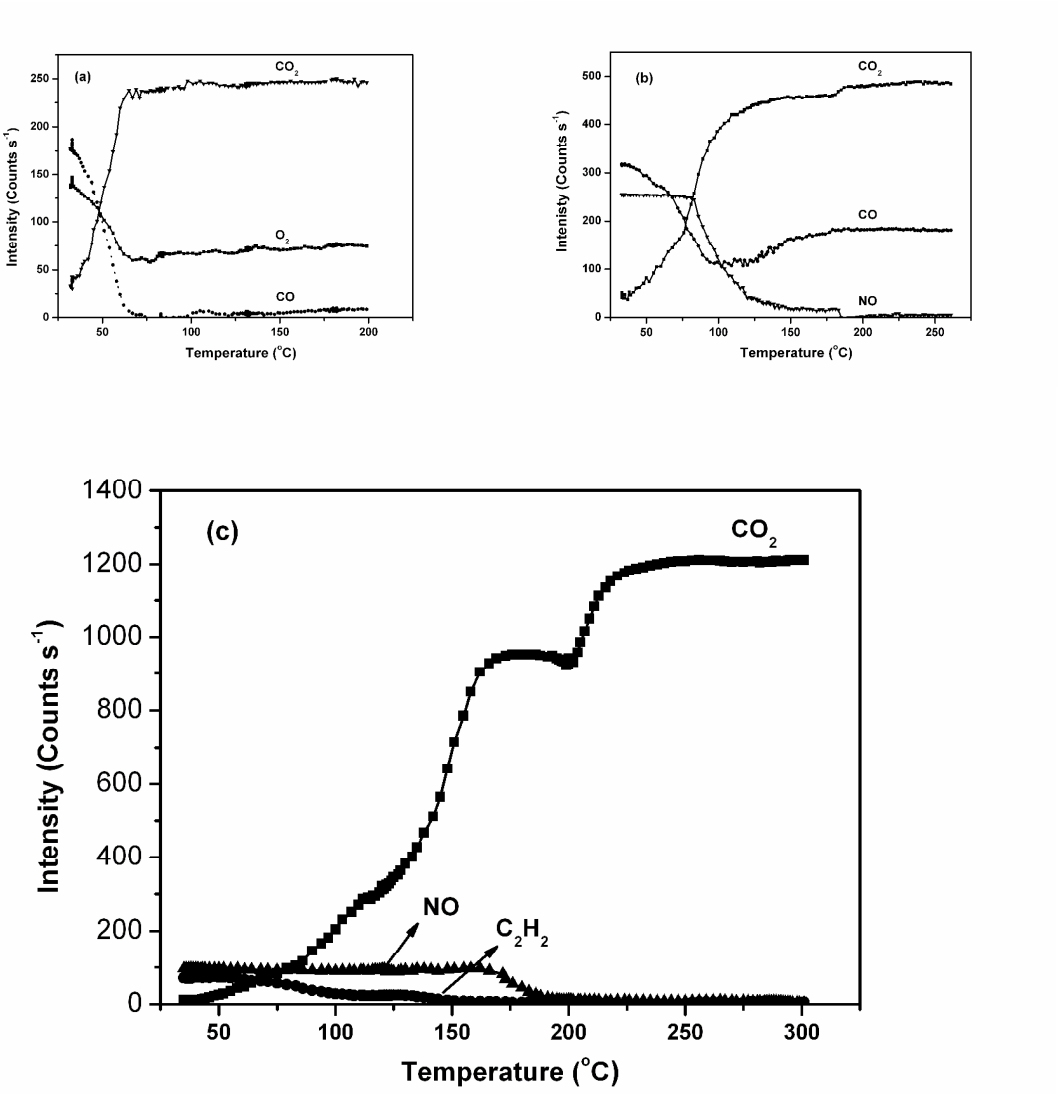

Fig. 11 Catalytic reactions over $Ce_{0.98}Pd_{0.02}O_{2-\delta}$ coated on cordierite monolith: (a) CO + O_2, (b) NO + CO and (c) three-way catalysis. Reprinted from [170] with permission of Springer.

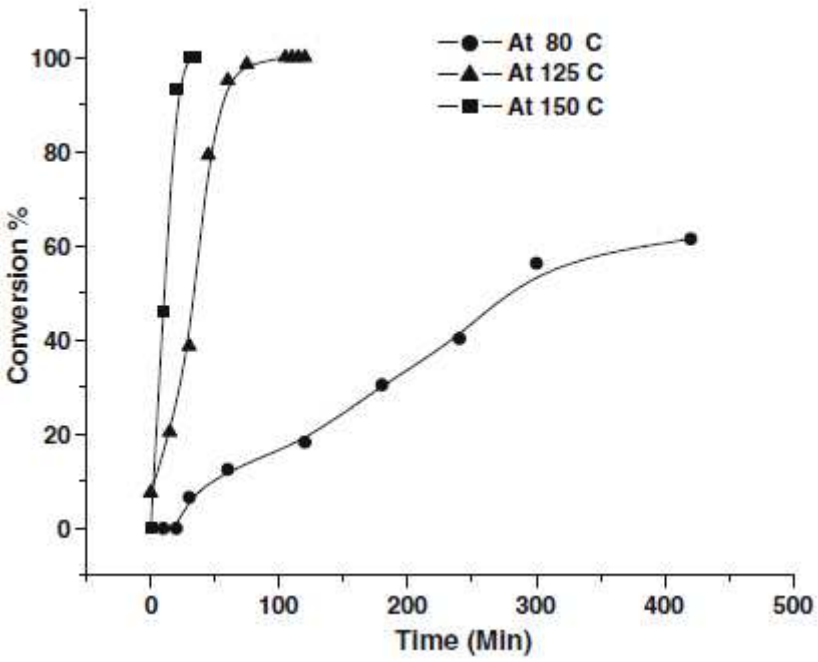

Fig. 12 Conversion efficiency of reaction of iodobenzene and methyl acrylate at different temperatures. Reprinted from [192] with permission of Springer.

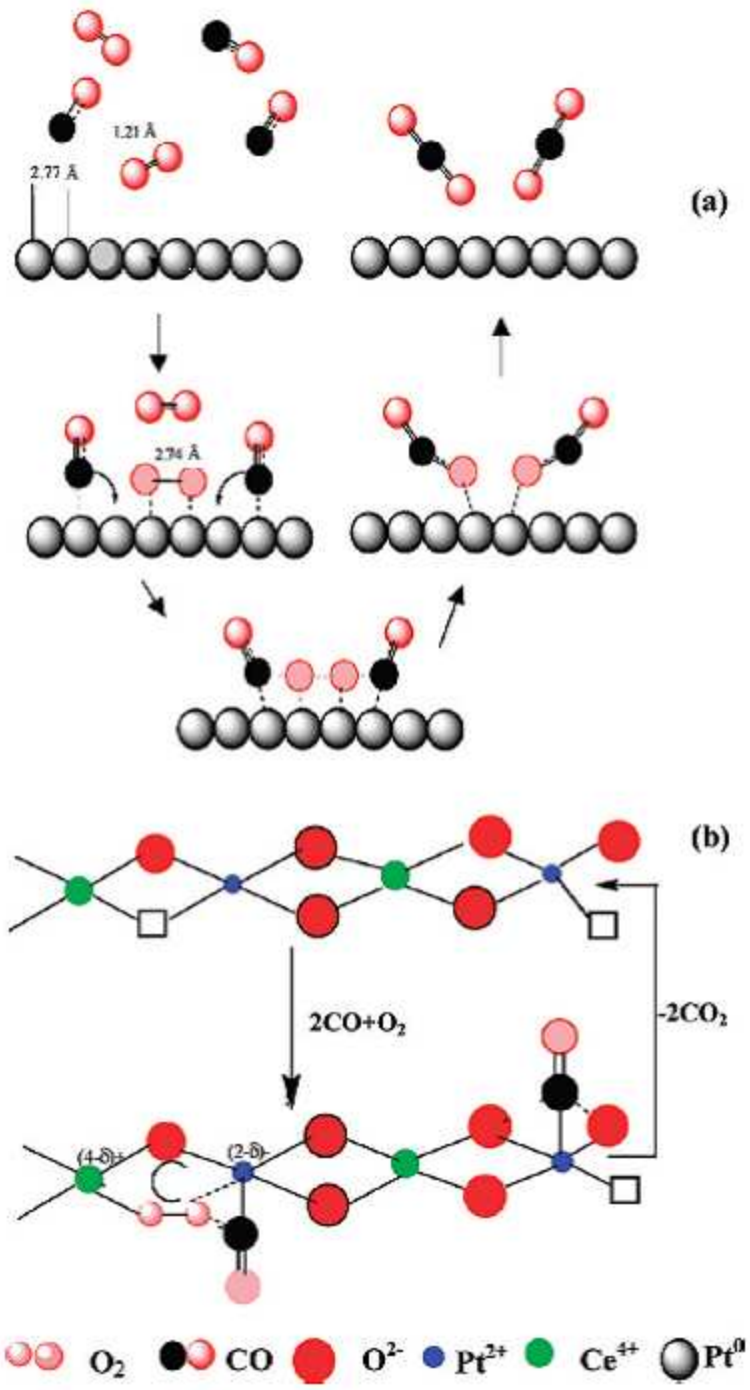

Fig. 13 CO + O_2 reaction: (a) Langmuir–Hinshelwood mechanism on Pt metal and (b) dual site mechanism on $Ce_{1-x}Pt_xO_{2-\delta}$. Reprinted from [21] with permission of American Chemical Society.

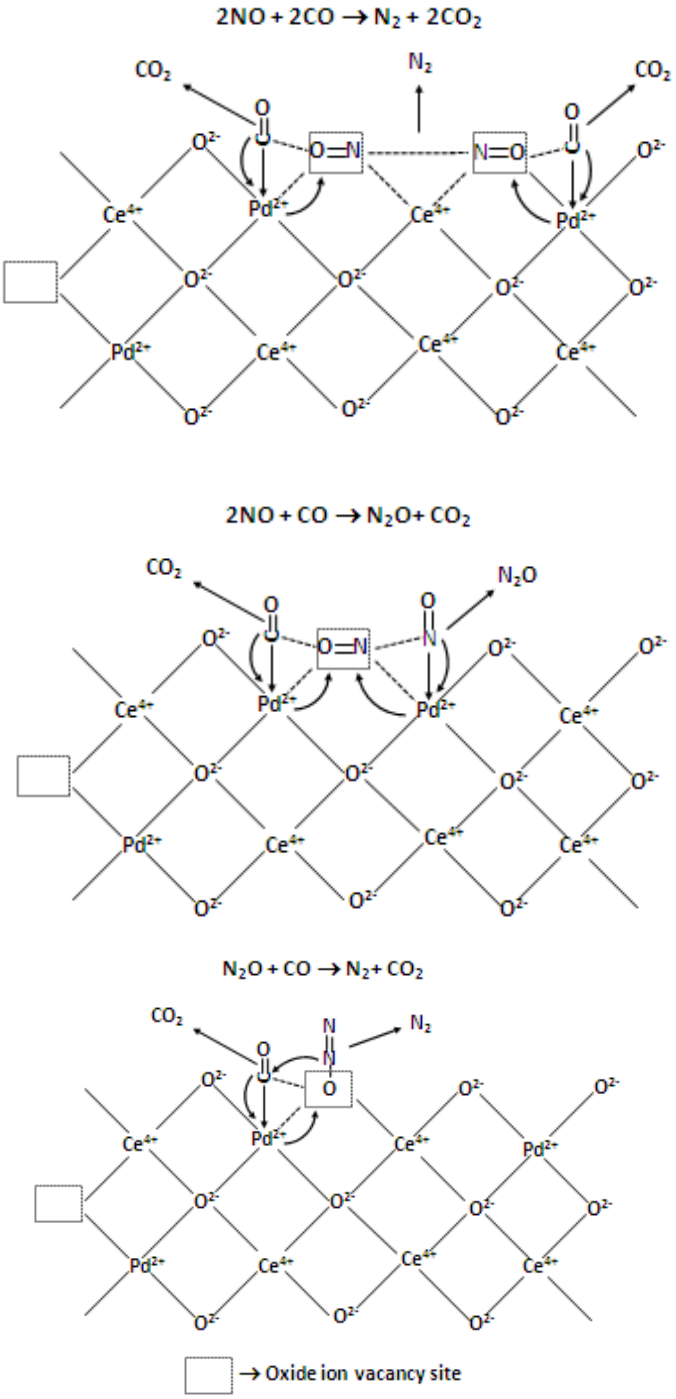

Fig. 14 Mechanism of N_2, N_2O and CO_2 formations during NO + CO reaction over $Ce_{1-x}Pd_xO_{2-\delta}$. Reprinted from [23] with permission of Springer.

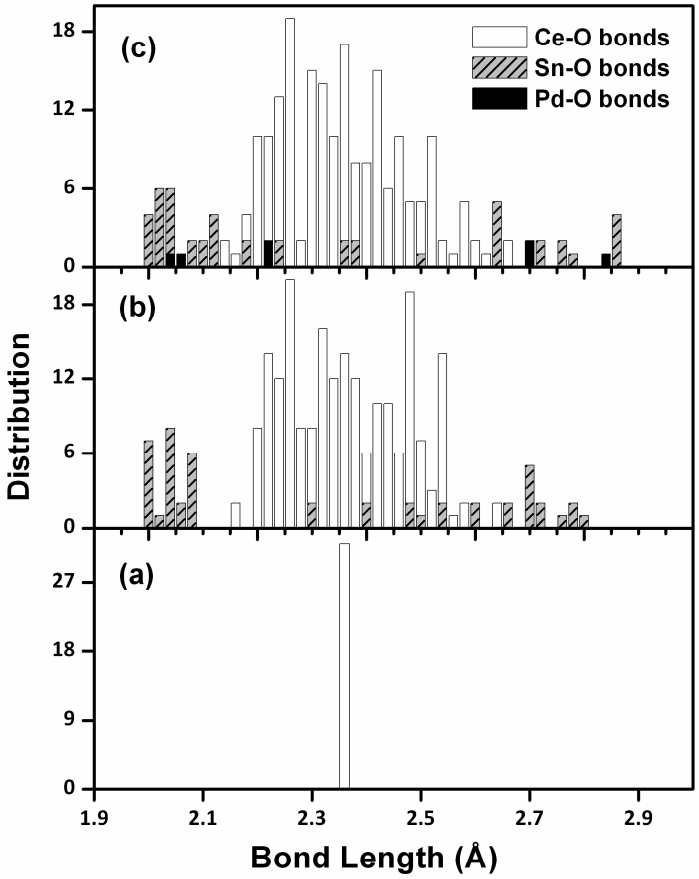

Fig. 15 Bond length distributions in (a) Ce_4O_8, (b) $Ce_{26}Snd_6O_{64}$ and (c) $Ce_{25}Sn_6Pd_1O_{63}$ supercells from DFT calculations. Reprinted from [50] with permission of American Chemical Society.

Parthasarathi Bera was born and raised at Moyna in Purba Medinipur district of West Bengal, India. He obtained his B. Sc and M. Sc. in Chemistry from Jadavpur University, Kolkata and earned his Ph. D. in Heterogeneous Catalysis from Indian Institute of Science, Bangalore under the supervision of Professor M. S. Hegde. He worked as a Post Doctoral Fellow at University of Washington, Seattle, USA with Professor Charles T. Campbell and University of Pennsylvania, Philadelphia, USA with Professor John M. Vohs. He was a Marie Curie Fellow at Instituto de Catálisis y Petroleoquímica, CSIC, Madrid, Spain under Professor Arturo Martínez-Arias. He joined CSIR–National Aerospace Laboratories, Bangalore in January 2010. Presently, he is a Senior Scientist in CSIR–National Aerospace Laboratories. His main research interests include heterogeneous catalysis for green energy and environment, in-situ catalysis, surface science and materials science.

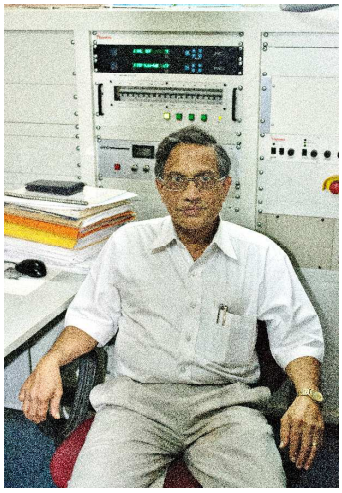

M. S. Hegde received his Ph.D. from Indian Institute of Technology Kanpur in 1976 and joined Solid State and Structural Chemistry Unit, Indian Institute of Science, Bangalore in 1977. In the initial stages of his career, he worked mainly on surface science employing XPS, UPS, AES and thermal desorption techniques. Then he moved to areas like solid state chemistry, epitaxial oxide thin films and finally to heterogeneous catalysis. During the last 15 years he and his colleagues have developed 'Noble Metal Ionic Catalysts' where noble metal ions substituted in reducible oxide supports creating oxide ion vacancies are observed to show higher catalytic activities compared to supported noble metal nanoparticles. Presently, he is an Emeritus Professor in Solid State and Structural Chemistry Unit, Indian Institute of Science and is engaged in training of science teachers from schools, colleges and universities in the newly created Talent Development Centre of Indian Institute of Science in its second campus at Kudapura.